Biophysical Studies to Elucidate Structure-Activity Relationships in β-Defensins

Martin De Cecco

Ph.D.

The University of Edinburgh

2011

"There are known knowns:

these are things we know that we know.

There are known unknowns:

that is to say, there are things that we now know we don't know.

But there are also unknown unknowns:

these are things we do not know we don't know."

Donald H. Rumsfeld
Former United States Secretary of Defense
12th February 2002

Declaration

This thesis is submitted in part fulfilment of the requirements for the degree of Doctor of Philosophy at the University of Edinburgh. Unless otherwise stated, this work is my own and has not been submitted for any other degree or professional qualification.

_____

Martin De Cecco

Acknowledgments

First I would like to thank my supervisor, Perdita Barran, for her guidance, enthusiasm and respect. It has been a great experience working with an academic who is "not shy of a spanner"!

The interdisciplinary work presented in this thesis would not be possible without collaboration. I am grateful to Derek Macmillan and Emily Seo for providing me with peptides, to Dušan Uhrín and Haris Panagos for oligosaccharides and to Natalie Reynolds and Kirsty Tyrrell for their biological data. Thanks also go to the other members of 'Team Defensin', especially Julia Dorin, Dominic Campopiano and Gareth Morrison, for their insights.

I have been lucky to have shared my time in Edinburgh with an excellent group of lab-mates: Pete, Jason, Stefan, Fiona, Roland, Hattie, Yana, Jude, Ewa and Luiz. Thank you all for your help and friendship.

I wish to acknowledge the technical support staff in both the Schools of Chemistry and Physics for helping to solve a wide variety of instrumental problems!

Finally, thank you to Eilidh, my friends and family for their continuing love and support.

Abstract

β-defensins are a class of mammalian defence peptides with therapeutic potential because of their ability to kill bacteria and attract host immune cells. In order to realise this potential, it is necessary to understand how the functions of these peptides are related to their structures. This thesis presents biophysical analysis of β-defensins and related peptides in conjunction with biological assays. These studies provide new insights into the structure-activity relationships of β-defensins.

Ion mobility-mass spectrometry (IM-MS) is used throughout this thesis to probe the tertiary structure of peptides *in vacuo* and, by inference, make conclusions about their conformations in solution prior to ionisation. Where appropriate, IM-MS is complemented by other techniques, including high performance liquid chromatography and circular dichroism spectroscopy.

First, the importance of a C-terminal cysteine residue within the murine β-defensin Defb14 is investigated. The functional and structural implications of chemically modifying the cysteine residue are examined. Second, the N-terminal region of Defb14 is modified by the substitution and deletion of amino acids. Again, the effects on biological activity and structure are discussed.

Finally, the functional and structural overlap of β-defensins with another family of proteins – the chemokines – is considered. The oligomerisation of β-defensins and their interaction with glycosaminoglycans is of particular interest: structural data for human β-defensins 2 and 3 in the absence and presence of polysaccharides are presented.

Contents

Abbreviations

ANOVA	analysis of variance
ATD	arrival time distribution
BBD	bovine β-defensin
CCL	CC chemokine ligand
CCR	CC chemokine receptor
CD	circular dichroism
cGMP	cyclic guanosine monophosphate
CPK	Corey Pauling Koltun (colouring convention)
CXCL	CXC chemokine ligand
DC	direct current
dp	degree of polymerisation
DTT	dithiothreitol
EHSS	exact hard-sphere scattering
ESI	electrospray ionisation
FAIMS	field-asymmetric waveform ion mobility spectrometry
GAG	glycosaminoglycan
GPCR	G-protein coupled receptor
HBD	human β-defensin
HEK	human embryonic kidney
HPF	high power field
HPLC	high performance liquid chromatography
i.d.	internal diameter
IM-MS	ion mobility-mass spectrometry
IMS	ion mobility spectrometry
LC	liquid chromatography
MALDI	matrix-assisted laser desorption ionisation
MBC	minimum bactericidal concentration
MBD	murine β-defensin
MoQToF	mobility quadrupole time-of-flight
mRNA	messenger ribonucleic acid

MS	mass spectrometry
nESI	nano-electropray ionisation
NMR	nuclear magnetic resonance
PA	projection approximation
PDB	Protein Data Bank
PKG	protein kinase G
Q-ToF	quadrupole time-of-flight
RF	radio frequency
RPMI	Roswell Park Memorial Institute (medium)
tBD	template β-defensin
TFE	2,2,2-trifluoroethanol
TM	trajectory method
ToF	time-of-flight
TWIMS	travelling wave ion mobility spectrometry
UV	ultraviolet

Physical quantities and symbols

d	distance
e	elementary charge (= $1.6021765 \times 10^{-19}$ C)
E	electric field strength
E_k	kinetic energy
K	(ion) mobility
k_B	Boltzmann constant
K_d	dissociation constant
m	mass
m/z	mass-to-charge ratio
N	number density
p	probability
P	pressure
q	net charge
r	relative retention time
r_g	van der Waals radius of buffer gas
t	time
T	temperature
Td	Townsend (unit), defined as 1 Td = 10^{-17} V cm^2
U	DC potential
v	velocity;
	RF frequency
V	electrical potential difference;
	peak amplitude of RF potential
z	nominal charge
Φ_0	total electric potential
μ	reduced mass
ρ	density
ω	angular frequency
Ω	momentum transfer integral (collision cross-section)

1 Introduction

1.1 Antimicrobial peptides

1.1.1 Therapeutic potential

Antimicrobial resistance is, according to the World Health Organization, *"a global problem that needs urgent action"*.[1] The inevitability that bacteria will develop resistance to an antibiotic in clinical use means that there is a continual requirement for the discovery of new drugs. However, there is a dearth of such compounds in the pharmaceutical pipeline,[2] resulting in a decreasing number of treatments available for serious bacterial infections.[3] As such, there is a clear need to develop new classes of antibiotics with novel modes of action.

Antimicrobial peptides are a relatively untapped source of molecules with therapeutic potential. In nature, almost every organism uses cationic antimicrobial peptides as part of its arsenal to combat infection.[4, 5] These peptides comprise part of the innate immune system: a series of non-specific mechanisms to overcome invasion by microorganisms. The antibiotics polymixin B and gramicidin S are antimicrobial peptides derived from bacteria and have been in clinical use for many years.[6] Antibiotics from the antimicrobial peptides of higher organisms have yet to be used.

The interest in antimicrobial peptides stems from their broad-spectrum of antimicrobial activities and their rapid action. Conventional drug development generally favours the concept of a single drug for an individual target.[3] In contrast, within a given mammal, a number of antimicrobial peptides often have overlapping activities and may interact with different biological processes.[7] As a result, it is more difficult for bacteria to develop resistance.[8, 9]

The greatest obstacle to the development of antimicrobial peptides as drugs is their high cost of manufacture by solid-phase chemical synthesis.[7] Recombinant expression methods may be less expensive but, thus far, few of these systems have generated peptides at a sufficient quantity and purity for commercial use.[10] It is therefore desirable to design shorter, functional analogues of wild-type peptides that

are cheaper to produce. This requires identifying which parts of the structure are important to its biological activity.

1.1.2 General structure

Antimicrobial peptides are short proteins of approximately 10 – 50 amino acids.[4, 5] There is a high degree of variation in the primary structure of these peptides: rapid evolution is believed to occur as a result of selective pressure to contend with the development of bacterial resistance.[8] Most sequences comprise a large number of basic residues, giving the peptide an overall positive charge, in addition to a significant number of hydrophobic amino residues. In three dimensional space the peptide may adopt an amphipathic structure, such that distinct regions of high positive charge and high hydrophobicity are formed. Antimicrobial peptides can be loosely classified according to their secondary structure content (Figure 1.1): the main categories being those consisting mainly of β-sheet (including defensins) and those that are predominantly α-helical (including cathelicidins and magainins).

1.1.3 Modes of action

The first step in the mechanism of antimicrobial action involves the accumulation of the peptides at the microbial surface.[11] This occurs *via* electrostatic attraction of the cationic peptides to the negatively-charged components of the outer bacterial cell wall: lipopolysaccharides in Gram-negative bacteria and teichoic acids in the Gram-positive bacteria (Figure 1.2). Thereafter the peptides may kill the bacteria either: by permeation through the membrane (without inducing permanent damage) and subsequent action upon an intracellular target; or by lysis of the cell membrane.[11] There are two major theories as to how the latter may occur: the pore model[12] and the carpet model.[13] In both the pore and carpet models, bacterial death results through leakage of the cytoplasmic contents from the cell.

Figure 1.1 Secondary structure motifs

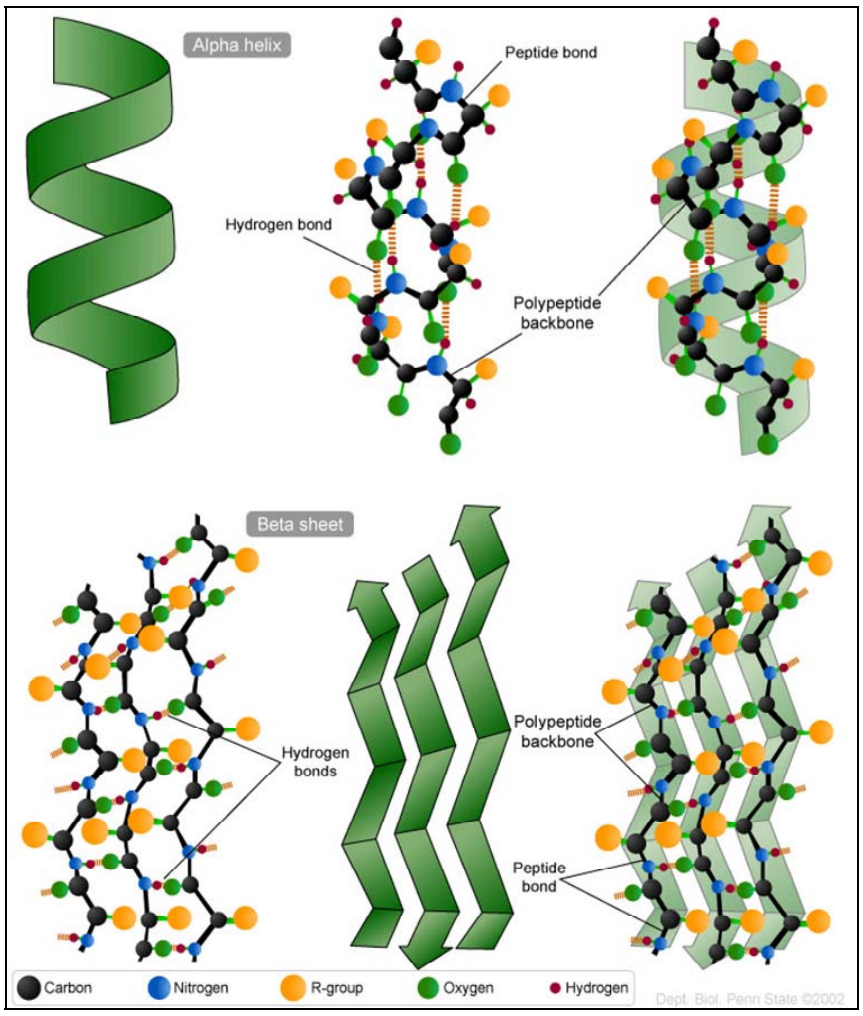

Reproduced with permission from The Pennsylvania State University.

In the pore model (Figure 1.3a), a series of peptides insert into the bacterial membrane and re-orientate themselves perpendicular to the phospholipid bilayer. These peptides group together to form an oligomer that forces each phospholipid layer to bend until a toroidal pore is formed. In the carpet model (Figure 1.3b), peptides accumulate at the surface of the membrane, weakening the integrity of the bilayer. The peptides act like surfactant molecules: once a critical concentration is reached the membrane is broken down and solubilised with the formation of micelles.

Figure 1.2 Schematic of the cell walls of Gram-negative and Gram-positive bacteria

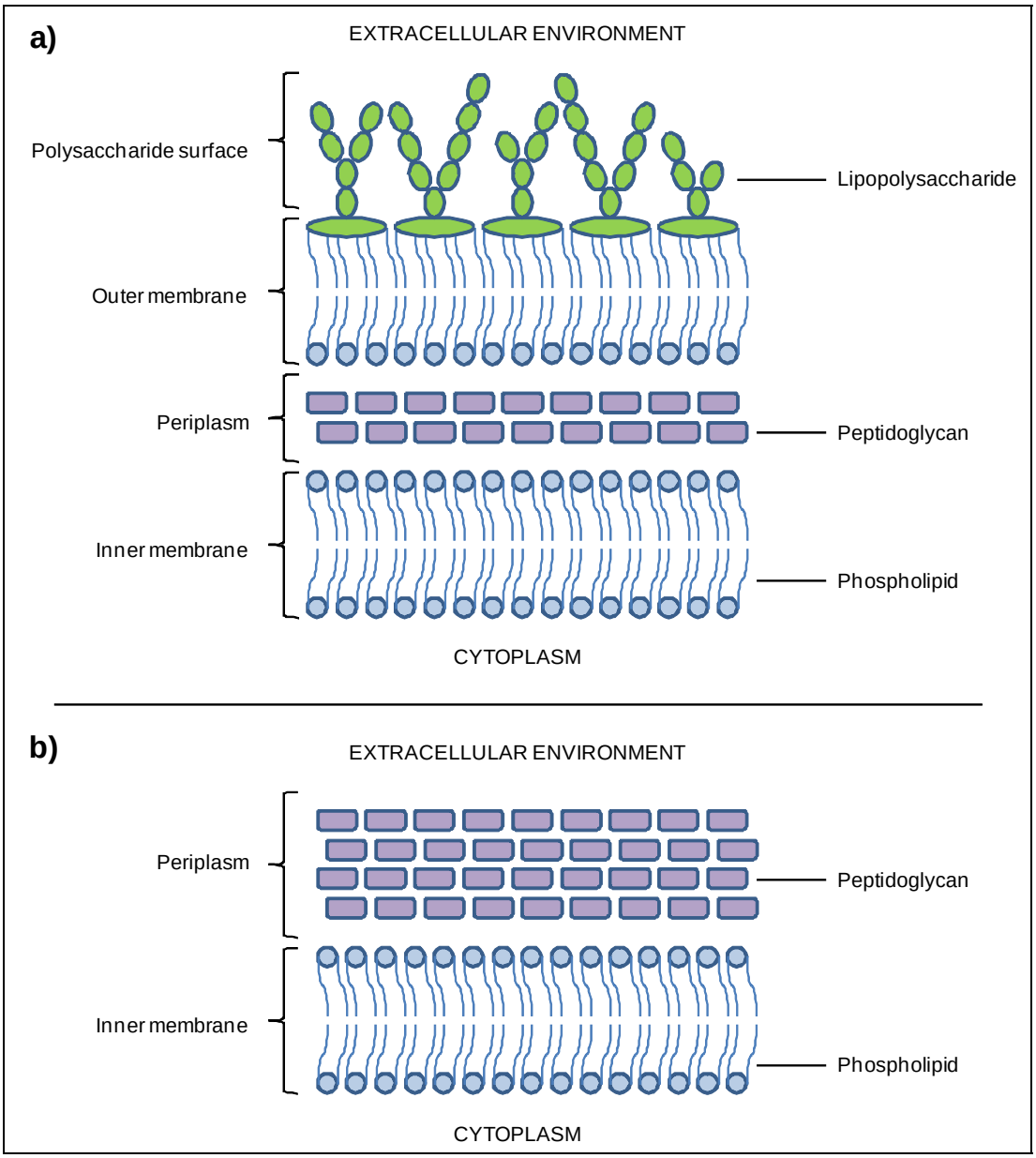

The above schematic illustrates the cell walls of (a) Gram-negative and (b) Gram-positive bacteria. The Gram-positive bacterial cell wall consists of only two layers: the inner membrane and a thicker peptidoglycan layer. Teichoic acids protrude from the outer surface of Gram-positive bacteria, similar to the lipopolysaccharides in Gram-negative bacteria.

Figure 1.3 Models of antimicrobial action

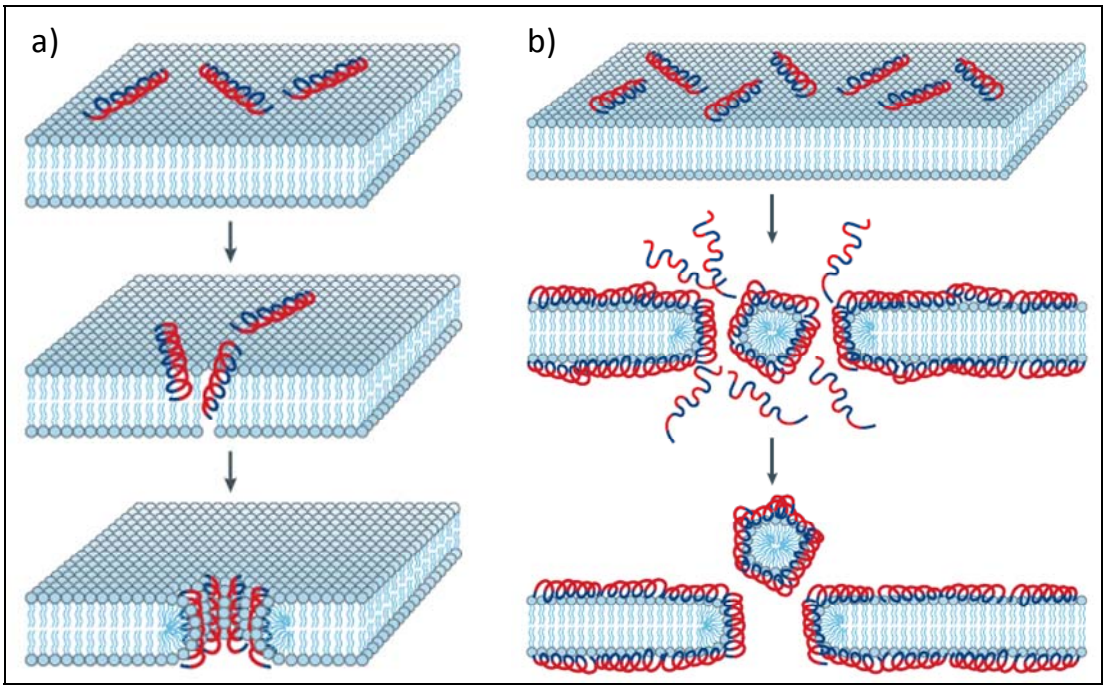

The above schematic shows: (a) the toroidal pore model; and (b) the carpet model. Hydrophilic regions of the peptide are coloured red, hydrophobic regions are coloured blue. Images are taken from ref (11).

1.2 Defensins

1.2.1 Classification and expression

Defensins are an important class of antimicrobial peptides found in plants and animals that have therapeutic potential on account of their broad-spectrum activity towards Gram-positive and Gram-negative bacteria, fungi and viruses.[14-16] Defensins contain six highly-conserved cysteine residues and are classified into α, β or θ sub-families according to the pattern of disulfide bonding that occurs between these amino acids (Table 1.1).

Table 1.1 Classification of defensins

Sub-family	Cysteine connectivity		
α	Cys^{I}-Cys^{VI}	Cys^{II}-Cys^{IV}	Cys^{III}-Cys^{V}
β	Cys^{I}-Cys^{V}	Cys^{II}-Cys^{IV}	Cys^{III}-Cys^{VI}
θ	Cys^{I}-Cys^{VI}	Cys^{II}-Cys^{V}	Cys^{III}-Cys^{IV}

Both α- and β-defensins are found in humans, with θ-defensins being expressed only in a number of monkey and ape species.[17] Interestingly, humans do contain genes that code for θ-defensins but these contain mutations that introduce stop codons in the mRNA, terminating peptide translation.[18] This thesis focuses entirely on the β-defensin class of antimicrobial peptides.

In mammals, β-defensins are expressed mainly in epithelial cells and leukocytes.[15] To date, three human β-defensins (HBDs) have been isolated: HBD1 from blood filtrate,[19] HBD2 and HBD3 from psoriatic scales.[20, 21] The sequences of several more have been predicted from computational searching of the human genome.[22] HBD1 is present at nanomolar levels in human plasma and is expressed constitutively: that is to say that the peptide is always present at a constant concentration. In contrast, the production of HBD2 and HBD3 is induced upon bacterial challenge and during inflammation.[14]

1.2.2 Structure

Like many other antimicrobial peptides, β-defensins are small (3 – 6 kDa), cationic and amphipathic.[14, 16, 23] As shown in Figure 1.4, there is very little sequence homology between the different β-defensins, except for the six highly-conserved cysteine residues and two or three glycines, whose flexibility is important in an otherwise rigid three-dimensional fold.[24]

Despite the variation in primary structure, analysis by NMR spectroscopy and X-ray crystallography reveals a remarkable similarity in tertiary structure.[25-28] β-defensins contain a β-sheet region consisting of three anti-parallel strands, in addition to a short α-helical section near the N-terminus (Figure 1.5). The three disulfide bonds help to stabilise the three-dimensional fold. This compact geometry results in the peptide being more resistant to digestion by proteolytic enzymes.

Figure 1.4 Sequence homology of β-defensins

```
HBD1:   ......DHYNCVSSGGQCLYSACPIFTKIQGTCYRGKAKCCK...
HBD2:   ...GIGDPVTCLKSGAICHPVFCPRRYKQIGTCGLPGTKCCKKP.
HBD3:  GIINTLQKYYCRVRGGRCAVLSCLPKEEQIGKCSTRGRKCCRRKK
MBD1:   ......DQYKCLQHGGFCLRSSCPSNTKLQGTCKPDKPNCCKS..
MBD2:   .....AELDHCHTNGGYCVRAICPPSARRPGSCFPEKNPCCKYMK
MBD3:   ....INNPVSCLRKGGRCWN.RCIGNTRQIGSCGVPFLKCCKRK.
BBD2:   ......NHVTCRINRGFCVPIRCPGRTRQIGTCFGPRIKCCRSW.
BBD12:  ......GPLSCGRNGGVCIPIRCPVPMRQIGTCFGRPVKCCRSW.
```

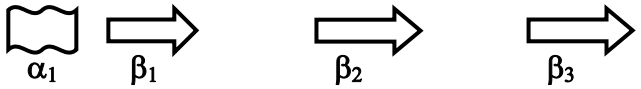

Shown are the amino acid sequences for a range of human (HBD), mouse (MBD) and bovine (BBD) β-defensins. Highly conserved residues are shaded black, moderately conserved residues are shaded grey. Regions of secondary structure (α-helix and β-strand) are indicated beneath the sequences. Figure modified from ref (24).

Figure 1.5 Tertiary structure of a β-defensin

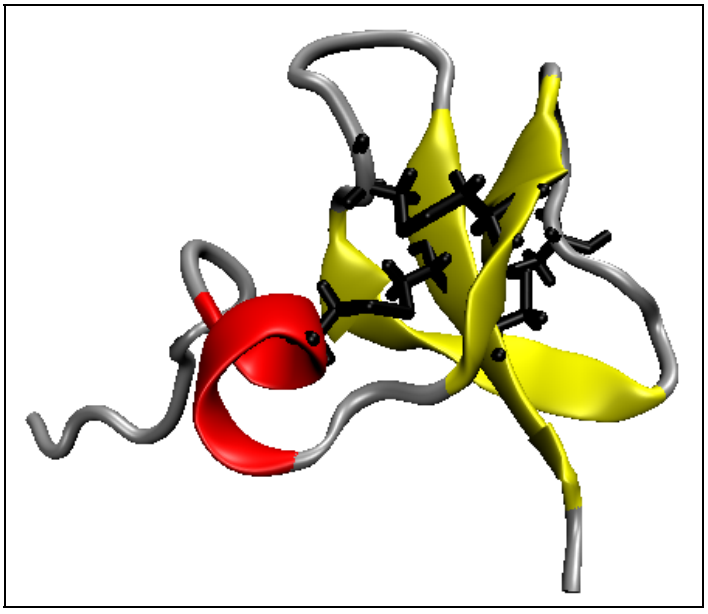

Shown above is a cartoon of HBD3 (ref 28), whose three-dimensional structure is typical of the β-defensin family of peptides. The α-helical region is coloured red; the three β-strands are coloured yellow. The six cysteine residues are shown in black.

At sub-millimolar concentrations, most β-defensins are present as monomers in solution.[24, 27, 28] In the crystal structure, however, HBD2 is observed as a dimer and an octamer (effectively a tetramer of dimers).[26] Several solution-phase methods have

determined that HBD3 exists as a dimer, although the structure of this oligomer has yet to be solved.[28] The formation of multimers may offer the peptide greater protection against proteolysis as well as helping to increase the local concentration of the peptide at the bacterial membrane. In addition, the oligomerisation of β-defensins could be important to the mechanism of antimicrobial action, since the pore model involves the formation of a higher order structure.[12] Defr1 is a β-defensin related peptide that exists as a covalently-linked dimer.[29] The antimicrobial activity of this peptide is diminished upon modification to prevent the formation of a covalent dimer.[30]

1.2.3 Antimicrobial activity

Human β-defensins 1 and 2 are potent towards Gram-negative bacteria, including *Escherichia coli* and *Pseudomonas aeruginosa*, and fungi such as *Candida albicans*.[20] In contrast, they possess only weak activity versus Gram-positive bacteria. HBD3 is active against both Gram-negative and Gram-positive bacteria, including multi-drug resistant *Staphylococcus aureus*.[21] In addition, unlike the other human β-defensins, the antimicrobial activity of HBD3 is insensitive to salt.[31, 32] The action of some antimicrobial peptides, including HBD1 and HBD2, is attenuated by physiological concentrations of salt that weaken the electrostatic attraction of the peptide to the membrane.[4] This is not the case for HBD3, perhaps because of its increased charge.[21]

The potency of a cationic antimicrobial peptide depends greatly on its overall charge. For example, reduction of the positive charge in human α-defensin 5 by the mutation of arginine to alanine resulted in a loss of activity.[33] In addition, antimicrobial activity is strongly influenced by hydrophobicity, which affects the ability of the peptide to solubilise, permeate, or insert into the bacterial membrane, depending on the mechanism. This was demonstrated in a study by Taylor *et al.*, who divided a β-defensin inspired peptide into two halves of similar charge.[34] They observed that the hydrophobic, N-terminal fragment was much more active than the hydrophilic, C-terminal fragment.

1.2.4 Modes of action

The mechanism by which defensins kill bacteria is complicated and has yet to be fully resolved. Not only do different peptides possess distinct modes of action against the same bacterium, but each peptide may act in a variety of ways against different organisms.[35] The α-defensin sub-family has been the most studied to date and have been shown to form ion channels,[36] larger pores,[37] as well as completely lyse membranes.[38] It has been proposed that, rather than being entirely different processes, each of these mechanisms are related and merely represent varying degrees of membrane impairment.[11, 39] In addition, α-defensins have also been shown to act against intracellular targets, inhibiting nucleotide and protein synthesis in *E. coli*.[40]

Sahl and co-workers have recently investigated the killing of *S. aureus* by a number of β-defensins: HBD3, plectasin (a fungal β-defensin) and 'tBD' (a synthetic peptide based on a β-defensin template).[41-43] In each case, only partial efflux of cellular metabolites was observed and the ingress of impermeant molecules was slow. This implied that cell lysis was not the dominant mechanism of antimicrobial action. Instead, these peptides are believed to interfere with biosynthesis of the cell wall in *S. aureus*. This is supported by the finding that plectasin binds Lipid II, a cell wall precursor.[42]

One concern surrounding the clinical use of β-defensins is their potential toxicity: some antimicrobial peptides can interact with the membrane of human cells as well as those of microorganisms.[7] Interactions with cells of higher organisms are usually weaker due to differences in the composition of the membrane, including a lack of negatively-charged surface lipids. HBD3 has been shown to break down red blood cells in dilute medium, but not under physiological conditions.[21] Several studies have described how it is possible to 'tune' the activity of HBD3 and other peptides, such that cytotoxicity is minimised whilst retaining antimicrobial activity.[44, 45] A decreased number of hydrophobic residues within the peptide leads to a reduction in the lysis of non-target cells.

1.2.5 Bacterial resistance to defensins

Despite the broad-spectrum activity of β-defensins in general, and HBD3 in particular, the Gram-negative bacterium *Burkholderia cepacia* is highly resistant to these peptides.[46] It is believed that this is a result of a modification in its lipopolysaccharide: the addition of aminoarabinose molecules helps to lower its net negative charge and so diminishes the electrostatic attraction of the cationic peptide to the bacterial membrane.[47]

This strategy of membrane charge reduction has been employed in various ways by other microorganisms and represents a possible method by which bacteria could potentially acquire resistance to β-defensins.[48] These concerns are mitigated to some extent by the fact that antimicrobial peptides are "dirty drugs", acting with a variety of mechanisms.[7, 8] Furthermore, β-defensins possess a number of other significant biological functions that may prove to be more important than their antimicrobial activity.

1.2.6 Chemotaxis

In addition to their ability to kill bacteria directly, β-defensins can also recruit host immune cells to fight incoming pathogens.[15] This occurs through the process of chemotaxis, whereby cells are attracted towards sites of increased β-defensin concentration.[49] Thus, β-defensins can be considered to provide a bridge between innate and acquired immunity: their inherent antimicrobial activity provides an immediate response to counter infection, whilst the modulation of the immune system offers a longer-lasting response.[15, 50] Given the poor antimicrobial activity of some β-defensins in physiological concentrations of salt, it has been suggested that the immunomodulatory properties of β-defensins may be more important to the host defense system.[7]

Each of the human β-defensins isolated to date has been shown to recruit memory T cells and immature dendritic cells.[50] The movement of these cells is believed to occur *via* an interaction between the β-defensin and the chemokine receptor CCR6, a G-protein coupled receptor on the surface of some cells. In 1999, Yang *et al.* demonstrated that human embryonic kidney cells transfected with CCR6 migrated towards HBD3.[51] Upon the addition of an antibody that blocked CCR6, chemotaxis

was inhibited. In addition to memory T cells and immature dendritic cells, HBD3 also chemoattracts monocytes.[50] In this case chemotaxis must be mediated by an alternative, as yet unknown, receptor since monocytes do not express functional CCR6.[52]

Whilst net charge and hydrophobicity are generally accepted to be factors that influence antimicrobial activity, the structural criteria for chemotactic activity are less clear. Lu and collaborators found that the migration of immune cells in response to HBD3 was clearly affected by the connectivities of the six cysteine residues.[53] This result appeared to explain why the characteristic pattern of disulfide bonds is so highly conserved in β-defensins, since these intramolecular bonds are not essential to the antimicrobial activity of these peptides.[53] However, this rationalisation is complicated by the discovery of HBD3 analogues that contain only a single cysteine residue but are equally potent chemoattractants.[34] In another study, mutations of the N-terminal sequence of HBD1 were found to significantly decrease the peptide's affinity for the receptor.[54]

1.2.7 *Other roles of β-defensins* in vivo

Stimulation of the immune response by chemotactic β-defensins represents a powerful defense mechanism, but overstimulation can result in potentially harmful proinflammatory responses. Various inflammatory diseases have been linked with increased levels of β-defensins, including mastitis (inflammation of the mammary gland) and psoriasis (skin).[55] Interestingly, the elevated concentration of β-defensins means that psoriatic lesions seldom become infected. Conversely, atopic dermatitis, another inflammatory skin condition, is associated with a decreased number of β-defensins and is susceptible to infection.[56]

Undoubtedly the biological activity of β-defensins is not limited to their function as antimicrobials. In 2007, Barsh and colleagues discovered that β-defensins even affect the hair colour of dogs! The canine orthologue of HBD3 was found to bind a melanocortin receptor and therefore influences pigmentation.[57] It is worth noting that melanocortin receptors have a range of other functions, including the suppression of inflammation.[58]

1.3 Investigating peptide structure-activity relationships

As the understanding of the roles of β-defensins develops, it is apparent that much more work is required to fully understand the biological activity of these peptides and determine how that activity is related to their structure. Studies of peptide structure-activity relationships broadly adopt one of two strategies: the modification of an existing peptide sequence or the design of a completely new peptide.[59] Following the generation of modified or novel peptides, biological testing and structural analysis is performed.

1.3.1 Sequence modification

In this type of approach, the peptide of interest is altered by the addition, deletion or substitution of one or more amino acids. In order to make the synthesis of these new peptides practical, modification of the sequence will often be limited: either with regard to the number of residues that are mutated, or by the number of different substitutions at each position. In an illustration of the former, Beuerman and co-workers synthesised a range of human β-defensin 3 analogues in which only the cysteine residues were modified: these were replaced by amino acids of varying hydrophobicity.[45] They observed a general correlation between greater hydrophobicity and increased cytotoxicity, although other factors such as the three-dimensional structure of the peptide were also pertinent. A recent investigation by Wei *et al.*, in which each residue within human α-defensin 1 was mutated successively to alanine, is an example of the latter methodology.[60] Such an approach is known as 'alanine scanning': alanine is chosen as the replacement amino acid because its methyl side-chain is small and generally inert.[61] In that particular study, the tryptophan residue at residue 26 was found to be especially important to the antimicrobial and antiviral activities of human α-defensin 1.

Another peptide modification used is truncation: the deletion of amino acids from either the N- or C-terminus. In addition to identifying regions of the peptide that are key to its function, this approach has the additional potential benefit of discovering analogues that work but which are shorter and therefore cheaper to produce. For instance, Park *et al.* found that the first four residues of the peptide buforin II were dispensable for its antimicrobial activity.[62] Removal of further amino acids resulted

in a loss of activity due to the impairment of a helical region crucial to cell penetration.

1.3.2 New peptide design

Structure-activity relationships may also be elucidated by the design of peptides *de novo*. Sometimes a minimalist strategy will be employed, where very few types of amino acid are used – typically a mix of basic and hydrophobic residues.[63] This can be useful in identifying the minimum requirements for activity. Alternatively, the peptide sequence can be based on a template, constructed following a comparison of homologous peptides.[64] For example, Tossi and co-workers synthesised a peptide with defensin-like properties using a sequence obtained by identifying the most frequently occurring amino acids in β-defensins.[43] With this approach, the aim is to find arrangements of amino acids that confer particular structures or properties important to a particular function.[59]

1.4 Biophysical techniques for studying peptide structure

1.4.1 High resolution techniques

Of the biophysical techniques available to study peptides and proteins, X-ray crystallography and nuclear magnetic resonance (NMR) spectroscopy offer the highest degree of structural information. Crystallographers obtain an electron density map from the X-ray diffraction of highly ordered crystals, which is then used to build a model structure of the protein, whose sequence has been determined by other means.[65] In NMR spectroscopy, the nuclear Overhauser effect between different nuclear spins is used to identify hydrogen atoms in proximity to each other, either due to primary structure or as a result of the protein's three-dimensional fold.[66] This yields a series of constraints to the possible distances and angles between atoms, from which a model can be constructed.

Both techniques offer unparalleled structural resolution and NMR spectroscopy has the additional advantage of being able study proteins in their 'natural state', in solution. However, each method also has its drawbacks.[67] Both require a relatively large quantity of protein: typically ~1 mM solutions for NMR. The resolution of X-ray diffraction data is highly dependent on the formation of well ordered crystals and

some proteins are particularly resistant to crystallisation. In addition, the static nature of crystallography is not applicable to the measurement of dynamic processes. NMR is routinely used to monitor such processes, but spectra reveal only the average state of a protein complex.

1.4.2 Circular dichroism and other spectroscopies

In addition to the techniques described above, a range of low-resolution spectroscopic methods are available for the study of peptide structure, including: infrared,[68] fluorescence,[69] Raman[70] and circular dichroism (CD)[71] spectroscopies. Whilst none of these techniques provides the same level of detail as NMR or X-ray crystallography, they can be useful in identifying changes in protein structure that occur in response to an external stimulus.[72]

CD spectroscopy has the advantage of being relatively simple to perform and is used in this thesis as a probe of secondary structure. Circular dichroism is the differential absorption of left and right circularly polarised light and is observed when a chromophore is chiral – either intrinsically or as a result of its three-dimensional environment within the molecule.[71] The peptide bond is a UV chromophore with a weak, $n \rightarrow \pi^*$ transition at ~220 nm and a more intense $\pi \rightarrow \pi^*$ transition at ~190 nm. In proteins, the distinct environments created by different types of secondary structure result in different CD signals. Given that these absorptions are broad and proteins generally contain a mix of structural elements, exact quantification of the structural composition from the CD spectrum is difficult. Instead, an estimation of the secondary structure content can be obtained by using various algorithms that compare the CD spectrum to those whose structure has been solved by crystallography.[73]

1.4.3 Mass spectrometry

Principles

Mass spectrometry (MS) is a powerful tool for the study of protein and peptide structure because of its sensitivity, speed and specificity.[67, 74-77] The ability to gain useful structural information from a few picomoles of an analyte is a major advantage where the molecule of interest is particularly valuable or in short supply.

Furthermore, MS can be used to examine dynamic mixtures and so complements higher resolution techniques such as NMR and crystallography, which are not suited to such analyses.

Mass spectrometry involves the measurement of gaseous ions according to their mass-to-charge ratio (*m/z*). As such, in an MS experiment there is a requirement for: (i) the conversion of solution-phase molecules to gas-phase ions; (ii) the separation of these ions based on their *m/z*; and (iii) the recording of the separated ions. These functions are carried out respectively by the ion source, the mass analyser and the detector of the mass spectrometer.

Ionisation

Ionisation is the critical step in preserving a conformation in the gas-phase that is representative of the protein's structure in solution and is discussed below. Mass analysers and detectors are described only briefly in this thesis but a more thorough explanation of their operation can be found in references (78) and (79).

In the field of protein mass spectrometry, currently the two most commonly employed methods of ionisation are electrospray ionisation (ESI)[80, 81] and matrix-assisted laser desorption/ionisation (MALDI).[82, 83] These ionisation techniques have found widespread application because in each case the ionisation process occurs with minimal fragmentation of the analyte in the ion source. In MALDI, the protein sample is generally co-crystallised with an organic acid. Consequently, MALDI is generally less suited to the study of natively-folded proteins and complexes since the low pH can result in denaturation. In this thesis only ESI will be discussed.

In ESI, the sample is delivered through a metal capillary to which a high electric potential is applied. Either positive or negative ions can be generated; the applied potential generally being of the order of ± 2 to 5 kV. In the case of positive ion formation, the positively-charged particles are drawn towards the end of the capillary to form a so-called Taylor cone,[84, 85] from which a fine spray of highly charged droplets is produced (Figure 1.6).

Figure 1.6 Mechanism of electrospray ionisation

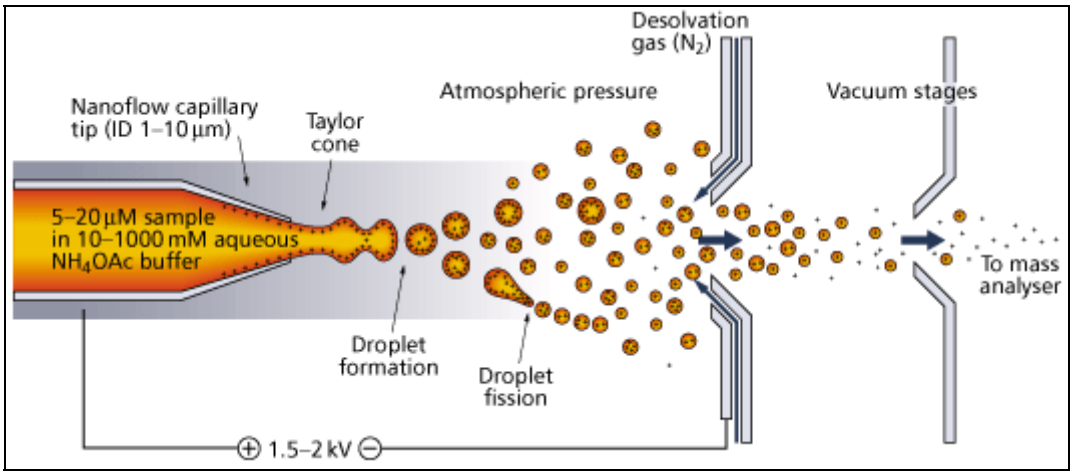

Illustration of Taylor cone formation and subsequent desolvation to gaseous ions, adapted from ref (85). Note that the source shown above is a nano-electrospray ionisation source (see page 17).

Evaporation of the solvent, facilitated by heat and the flow of a nebulising gas, leads to a decrease in the size of the droplets and an increase in the density of charge at the surface. Eventually the Coulombic repulsion between like charges at the surface becomes sufficiently large so as to overcome surface tension and cause fission of the droplet. This process continues, producing sequentially smaller droplets until a desolvated ion is formed. Decreasing potential and pressure gradients, from the tip of the capillary to the interface with the mass analyser, propel the ions into the spectrometer.

The mechanism of the final step in which a solvent-free ion is formed from a charged droplet has been the subject of much debate. There are two major theories: the charged residue model, proposed by Dole,[80] and the ion evaporation model, put forward by Iribarne and Thomson.[86] In the former model, droplet fission (as described above) continues until a single analyte ion remains within a droplet. Total desolvation of this droplet leaves the gaseous "charged residue". The latter (ion evaporation) model states that, before complete evaporation of the solvent occurs, the analyte ion is expelled from the droplet when Coulombic repulsion exceeds the forces of solvation. Whilst it appears that the majority of ions are not formed exclusively by a single mechanism, there is evidence to support the premise that Dole's charged residue model is the most relevant for large biomolecules such as proteins.[87]

During the electrospray ionisation of large molecules, multiply-charged analyte species are created. In the positive ionisation of proteins, this often corresponds to the addition of a proton (or another positive ion, such as Na^+) to some or all of the basic amino acid side-chains within the molecule. Given that, in MS, it is the mass-to-charge ratio that is measured, this inherent feature of ESI means that even very large molecules can be detected within the range of common mass analysers (*m/z* = 100 – 2000).

Although various different solvents can be used in ESI-MS, ESI is most efficient when volatile, protic co-solvents such as methanol are used. ESI of samples in aqueous solution is possible and is routinely performed for the study of natively folded proteins but the comparatively low vapour pressure of water means that sensitivity is reduced. Volatile buffers such as ammonium acetate are preferred to those which are less volatile such sodium and potassium phosphate for the reasons discussed above.

The ESI process was improved by Wilm and Mann with the development of nano-electrospray ionisation (nESI).[88] Similar to ESI, ions are formed by a sequential fission of charged droplets as described previously, however a finely-tipped glass capillary with a micron-wide internal diameter is used in nESI rather than the metal capillary (i.d. ~ 0.1 mm) employed in ESI. In nESI, the voltage (± 1 to 2 kV) is applied either to a metal coating on the inside of the glass capillary, or to an inert metal wire inserted into the sample solution. The result is that the droplets formed by nESI are an order of magnitude smaller than those generated in conventional ESI.[89, 90]

The low flow rates utilised in nESI (~20 nl/min, compared to 1-1000 μl/min in ESI) have the advantage of decreased sample consumption as well as improved sensitivity since the smaller droplet size means that salts and other impurities, which are detrimental to ionisation of the analyte, are less concentrated. An excellent example of this is described by Benesch *et al.*, who observed a remarkable improvement in the resolution of an 800 kDa tetradecameric complex when nESI was used rather than conventional ESI (Figure 1.7).[77] Since less energy is required for the

desolvation of smaller droplets, some protein ions formed by nESI may be more 'native-like' than those produced by ESI.

Figure 1.7 Comparison of nESI and ESI spectra for the $GroEL_{14}$ complex

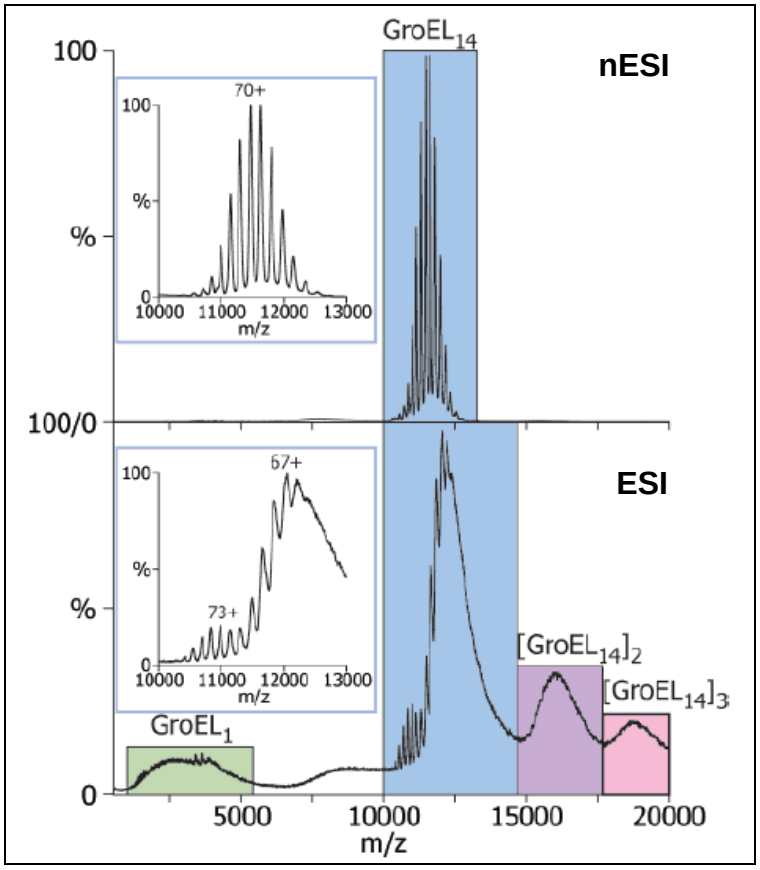

The upper spectrum, obtained using nESI, shows excellent resolution of the 14-mer. The lower (ESI) spectrum shows poor resolution and non-specific oligomerisation. Image taken from reference (77).

Mass analysis and detection

This thesis employs a Q-ToF mass spectrometer, featuring quadrupole (Q) and time-of-flight (ToF) mass analysers, which are introduced below. A more detailed description of these and other types of mass analyser can be found elsewhere, including references (78) and (79).

A quadrupole comprises four parallel rods, with opposite rods paired electronically.[91] An alternating RF potential plus a fixed DC voltage are applied to the rods such that when one pair of rods is in-phase (*e.g.* positive) the other pair is completely out of phase (*i.e.* negative). The total electric field experienced by ions passing through the quadrupole is given by:

{ 1.1 } $$\Phi_0 = +(U - V\cos\omega t) \text{ and } -\Phi_0 = -(U - V\cos\omega t)$$

where Φ_0 is the total potential on the rods, U is the DC potential, V is the peak amplitude of the RF potential and ω is the angular frequency (equal to $2\pi\nu$, where ν is the RF frequency). Upon entering the quadrupole, a positively-charged ion will be attracted towards a negative rod. As shown in equation {1.1}, the potential on this rod is a cosine function of time, t. Thus, the trajectory of the ion will change if the potential changes sign before the ion collides with the rod.

Ions of a given *m/z* have certain values of U, V and ω that generate a stable trajectory for transmission (Figure 1.8). Ions of different *m/z* values can be transmitted by scanning the RF amplitude: upon detection, a mass spectrum can be generated by determining the *m/z* from the detection time and the potential applied. Alternatively, the quadrupole can be used as a mass filter, whereby only ions of a particular *m/z* range are transmitted. This method of operation is commonly employed when the quadrupole is used in tandem with other mass analysers.

Figure 1.8 Quadrupole mass analyser

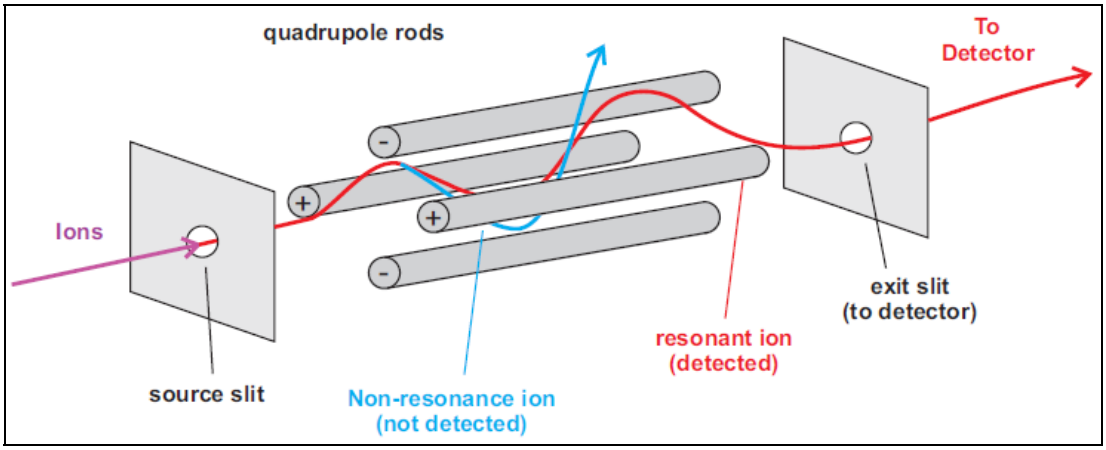

Opposite rods have the same sign, adjacent rods have the opposite sign. The red ion has a stable trajectory and is transmitted, the blue ion has an unstable trajectory and is discharged as it collides with the rod. Image adapted from ref (92).

In the time-of-flight mass analyser, packets of ions are accelerated by a potential (V) into a field-free drift tube.[93] As shown in equations {1.2} to {1.4}, the time taken for an ion to travel a fixed distance (d) is related to its *m/z*:

{ 1.2 } $$E_k = \frac{1}{2}mv^2$$

{ 1.3 } $$E_k = qV = zeV$$

{ 1.4 } $$t = \frac{d}{v} = \sqrt{\left(\frac{m}{z}\right)\left(\frac{d^2}{2eV}\right)}$$

where E_k is kinetic energy, q is charge and e is the charge on an electron.

The mass resolution of ToF analysers is improved by the use a reflectron.[94] A reflectron is a series of grids and ring electrodes that creates a retarding field, deflecting the ions back along the drift tube. In addition to increasing the effective drift length, the reflectron refocuses ions of the same *m/z* that have small differences in kinetic energy (Figure 1.9).

Figure 1.9 Schematic of a ToF analyser equipped with a reflectron

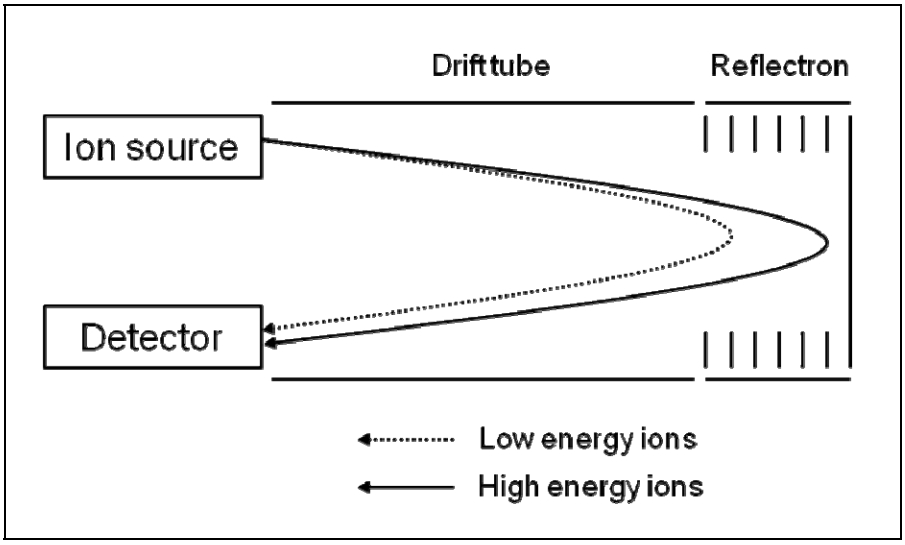

Ions of the same m/z but greater kinetic energy penetrate the retarding field of the reflectron more deeply. Thus more energetic ions spend longer in the reflectron and ultimately arrive at the detector at the same time as less energetic ions.

ToF instruments commonly use microchannel plate detectors.[78] These contain an array of electron multiplier channels, each coated with a semiconductor. An ion entering a channel will strike the semiconductor surface, releasing secondary electrons. This process continues, creating a cascade of electrons that are then measured as a current.

Relevance of gas-phase measurements to protein studies

A major issue surrounding the analysis of proteins by mass spectrometry is the extent to which the gas-phase structures of proteins resemble their solution-phase counterparts.[95] Clearly there must be some correlation with the situation *in vivo* for a mass spectrometry experiment to be of relevance in a biological context.

Modern ionisation techniques such as ESI, allow specific, non-covalent interactions to be preserved without molecular fragmentation. As a result, a multitude of non-covalent protein complexes have been observed with MS, including enzyme-substrate,[96] receptor-ligand,[97] antibody-antigen[98] and protein-protein (*i.e.* quaternary structure) aggregates.[76, 77, 99, 100] An elegant illustration of the use of ESI-MS to determine the stoichiometry of the constituent parts of a protein complex is described by Medalia *et al*.[101] Analysis of a nucleotidase by size-exclusion chromatography implied that the enzyme had a molecular mass of around 600 kDa and therefore existed as a dodecameric complex. However, the ESI-MS spectrum indicated the presence of hexamer, not a dodecamer. The MS data was validated by electron microscopy which confirmed that the complex was a hexamer containing a large cavity. The hollow space gives the complex results in an unusually large diameter and so the protein exhibits a deceptively short elution time in size-exclusion chromatography.

When considering likely protein conformations, it is worth noting that the energy of a particular protein fold is partly dependent on the non-bonded interactions within the molecule.[102] Protein folding is typically driven by a combination of the following non-covalent interactions: hydrogen bonding, van der Waals forces, electrostatic interactions and the hydrophobic effect. Given that in the mass spectrometer there is no solvent with which the protein complex can interact, it is likely that ionic interactions become reinforced upon transfer of the protein complex to the gas-phase. For instance, the binding of an acidic peptide to a (basic) polyamine is much stronger in the gas-phase than in solution.[103] Conversely, the strength of hydrophobic interactions diminishes when removed from the solvent. For example, Robinson *et al*. observed that various protein-coenzyme complexes had different solution-phase dissociation constants but similar gas-phase stabilities.[103, 104]

One variable in the estimation of the energy of these interactions is the dielectric constant of the medium, $\varepsilon/\varepsilon_o$. It has been calculated that proteins typically have $\varepsilon/\varepsilon_o$ values in the range 2-6.[105] The dielectric constant of water is 78,[106] whereas that of a vacuum is 1 by definition. Thus, in this regard the immediate environment of a cellular protein, especially those which are in the vicinity of membranes, can be said to be better represented by the gas-phase than by dilute aqueous solution.

The single most important factor which affects a protein's gas-phase structure is that of its solution-phase conformation prior to ionisation.[107, 108] ESI mass spectra of denatured proteins tend to exhibit more highly charged species than those of natively folded species (Figure 1.10). In addition, a broader distribution of charge states may be observed for denatured proteins. This is partly as a result of the increased number of basic sites which become available for protonation when a protein is unfolded. Accordingly, ESI-MS can be used to evaluate the degree to which a protein is folded in solution.

Figure 1.10: Mass spectra of lysozyme under buffered and denaturing conditions

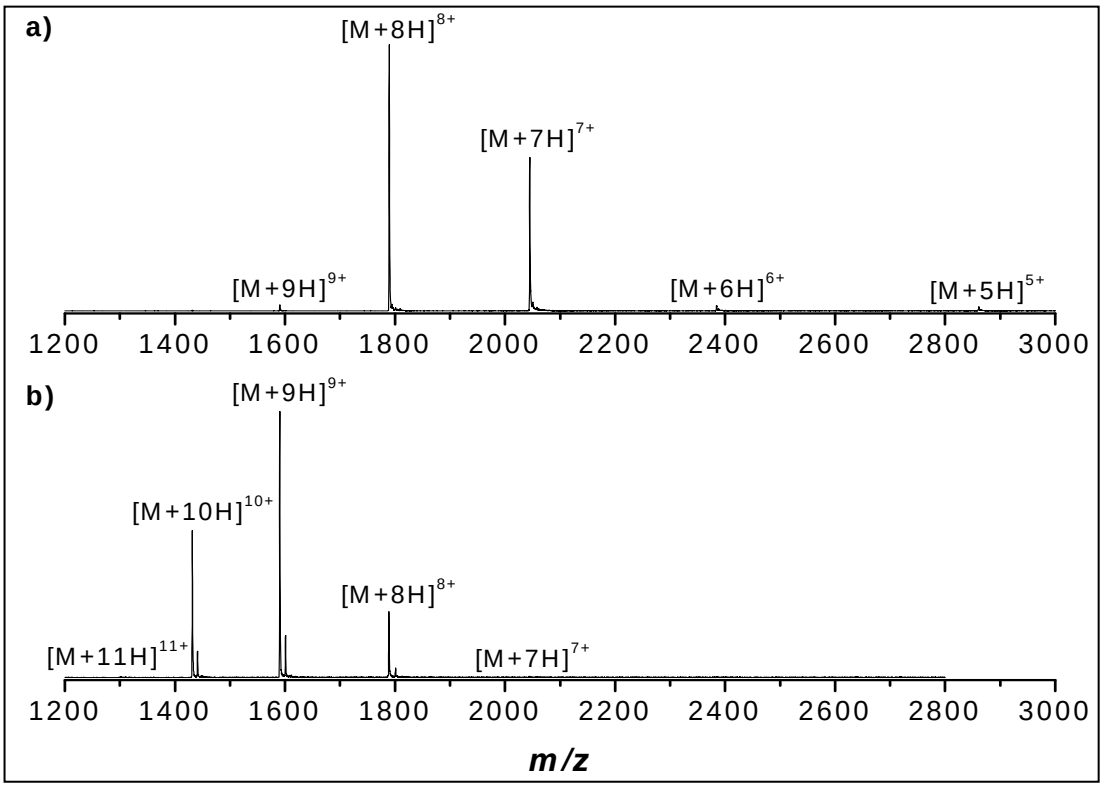

ESI mass spectra of a 10 mM solution of lysozyme in (a) 10 mM ammonium acetate buffer and (b) 49.5% water, 49.5% methanol, 1.0% formic acid. Ions of lower charge are observed for the buffered protein solution, indicating that the addition of acid and organic solvent denatures the protein to some extent. Spectra were acquired on an LCQ Classic (Finnigan).

Perhaps one of the most attractive features of mass spectrometry is its ability to be used in combination with other methods of analysis. In this way, it is possible to gain a greater degree of structural information than would be possible from MS alone. Discussed below is the utility of the mass spectrometer as a detector for ion mobility spectrometry, which is a useful technique for probing the tertiary structures of proteins in the gas-phase.

1.4.4 Ion mobility-mass spectrometry

Ion mobility spectrometry (IMS) is the separation of gaseous ions on the basis of their charge and average size.[109-111] A variety of different IMS set-ups exist[112, 113]: the only method that allows the direct calculation of the size of an ion is known as drift-time IMS and this method is used in this thesis. Other commonly employed IMS methods include travelling-wave IMS (TWIMS) and field-asymmetric waveform IMS (FAIMS).

Drift-time IMS

In a drift-time IMS experiment, pulses of gaseous ions are introduced to a drift cell containing an inert buffer gas and to which a uniform electric field is applied. The ions are accelerated through the cell by the potential gradient, but decelerated by collisions with the buffer gas. Thus, the ions traverse the cell with a constant drift velocity, v_D, which is determined by measuring the drift time. The mobility (K) of an ion is defined as the ratio of its drift velocity (v_d) to the electric field strength (E):

$$\{ 1.5 \} \qquad K = \frac{v_d}{E}$$

The energy of an ion in such a system is given by the electric field strength divided by the number density of the buffer gas, N. When operating in the so-called 'low-field limit' (*i.e.* below ~10 Td, where 1 Td = 10^{-17} V cm^2) there is no alignment of the ions in the electric field and v_d is independent of E. Under these conditions, the mobility of the ion can be described by:[114]

{ 1.6 } $$K = \frac{3ze}{16N}\left(\frac{2\pi}{\mu k_B T}\right)^{1/2}\frac{1}{\Omega}$$

Where μ is the reduced mass of the analyte and the buffer gas, k_B is the Boltzmann constant, T is the temperature in Kelvin and Ω is the momentum transfer integral (effectively the rotationally-averaged collision cross-section: a measure of the size and shape of the ion). For ease of comparison, often mobility is quoted in terms of the reduced mobility, K_o, which accounts for experimental variances in temperature and pressure:

{ 1.7 } $$K_0 = \left(\frac{P}{P^\circ}\right)\left(\frac{T^\circ}{T}\right)K$$

where $P°$ and $T°$ are the standard pressure (760 Torr) and temperature (273.15 K) respectively.

As shown in equation {1.6}, the mobility of an ion is inversely related to its rotationally-averaged collision cross-section. In other words, a more compact ion will undergo fewer collisions with the buffer gas and hence travels faster through the drift cell than a more extended ion (Figure 1.11). This phenomenon can therefore be used to separate ions of the same *m/z* but of different conformations: for example a folded protein versus a denatured protein.[115, 116]

Figure 1.11 Separation of protein conformations by drift-time IMS

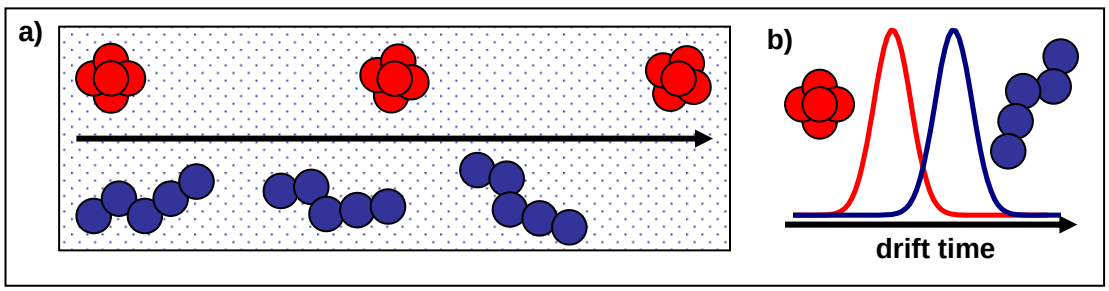

In this schematic, two ions of the same mass and charge are resolved by IMS. In (a) the more extended (blue) protein conformer takes longer to traverse the drift cell because it collides more often with the buffer gas than the compact (red) protein conformer. This gives rise to the arrival time distribution (b). Graphic based on that from ref (77).

Ion mobility spectrometry and mass spectrometry are extremely complementary given that both methods involve the analysis of gas-phase ions. IMS drift times are approximately three orders of magnitude greater than flight times in ToF MS (ms

versus μs) and so it is possible to 'nest' mass spectra within ion mobility spectra.[117-119] Combination of the two techniques (IM-MS) allows for the separation of ions firstly on the basis of their size/charge and then according to their mass/charge.

TWIMS

Travelling-wave IMS is a different mode of ion mobility separation that has been successfully integrated into a commercially available IM-MS instrument.[120] Separation occurs in one of three stacked ring ion guides (the others being used for the accumulation and transfer of ions). The ion guide consists of a sequence of ring electrodes, ordered so that opposite phases of an RF voltage are applied to neighbouring electrodes.[121] A sequence of transient DC voltages applied to adjacent electrodes generates a 'travelling wave' for the propulsion of ions through the apparatus (Figure 1.12). Although the net movement of ions is in the direction of the wave, frictional forces at typical operating pressures (> 0.2 mbar) result in ions periodically slipping behind the wavefront.

Since ions of greater mobility fall behind the wave less often than those of lesser mobility, separation of ions on the basis of their mobility results. Unlike drift-time IMS, in TWIMS the drift time of the ion is not directly proportional to its collision cross-section.[122] To derive this information from TWIMS data, a calibration of drift time to cross-section is performed using standards whose cross-section has been determined by drift-time IMS previously.[123] For accurate results, this approach requires a calibration set that encompasses the size of the analyte of interest. Furthermore, in the case of proteins and peptides, it is important that the 'standard' proteins exhibit the same conformations in both drift time and TWIMS instruments.

Figure 1.12 Propulsion of ions through a stacked ring ion guide by a travelling wave

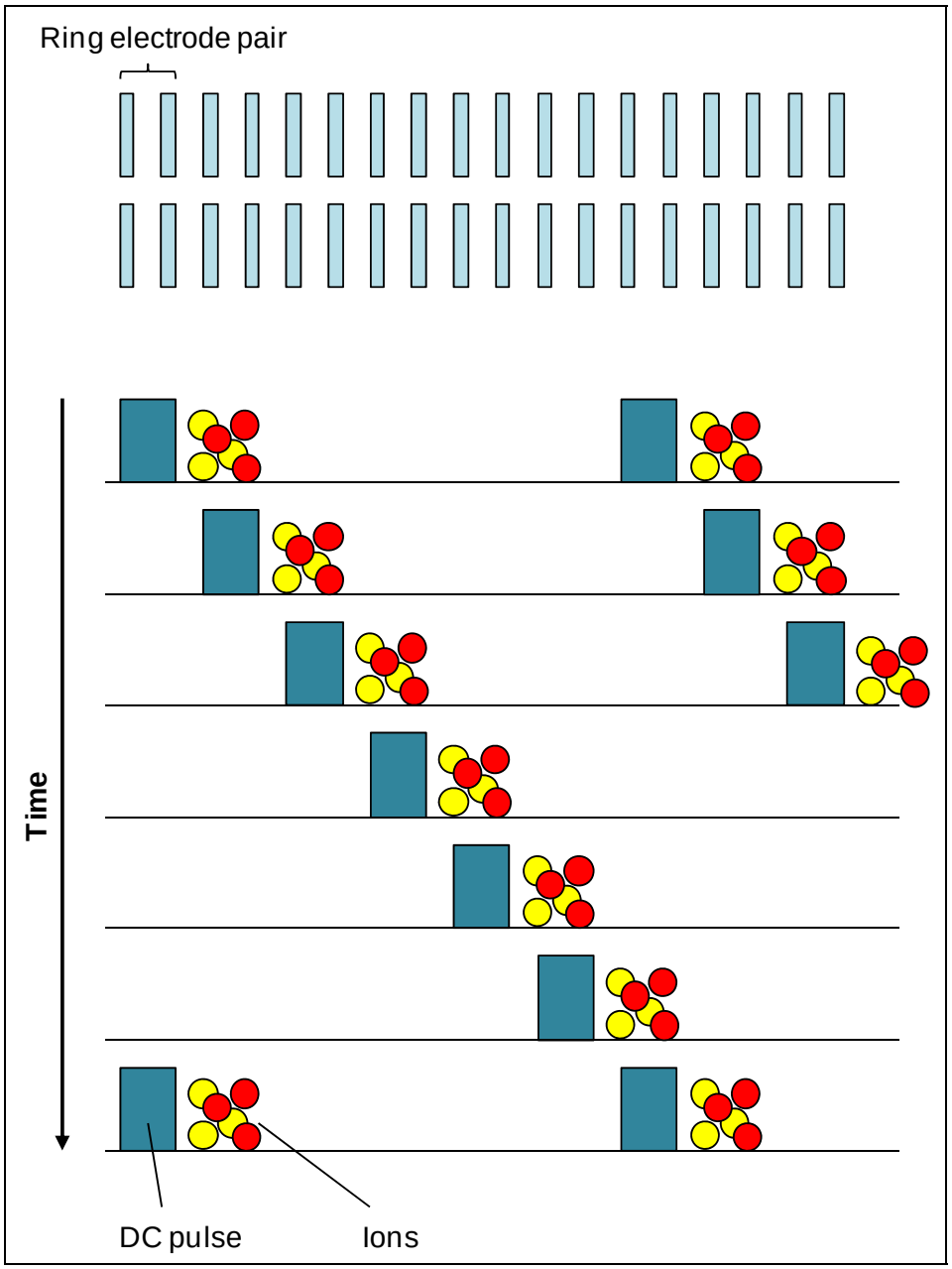

Image based on that given in reference (120).

FAIMS

Also referred to as differential mobility spectrometry, field-asymmetric waveform IMS represents an alternative technique for the separation of ions on the basis of their mobility.[124, 125] In FAIMS ions pass between two electrodes, which are either planar and parallel or cylindrical and concentric. An alternating electric field, perpendicular to the gas flow, is applied such that the ions oscillate between the two electrodes and disperse according to their difference in mobilities (Figure 1.13).

Superimposition of a DC 'compensation voltage' allows ions to traverse the device: scanning this voltage allows ions of varying mobility to be detected.

Figure 1.13 Principle of FAIMS separations

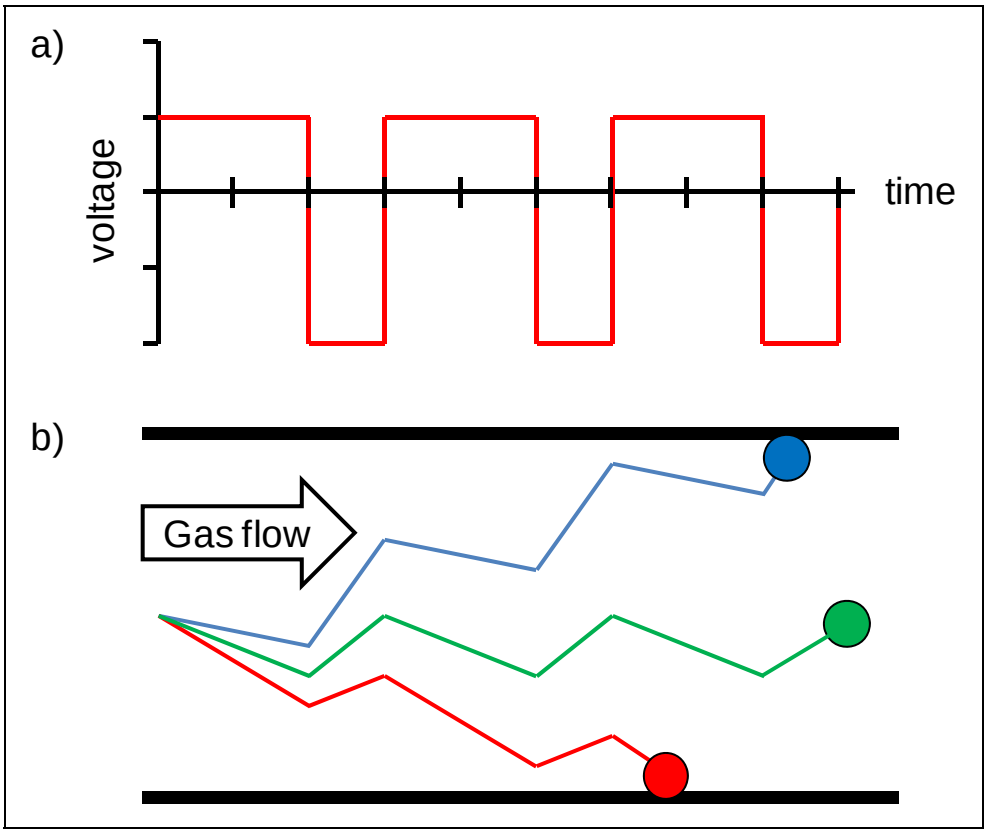

(a) The field applied is twice as strong in one direction as the in the other but is applied for only half as long. (b) The red ion has higher mobility at low field than high field and so it moves towards and collides with the bottom electrode. The blue ion has higher mobility at high field and so strikes the top electrode. The mobility of the green ion in high and low fields is balanced such that the net displacement from the centre is zero and so is transmitted. Image modified from reference (125).

Unlike drift-time IMS, a high electric field is used and so mobility (and therefore collision cross-section) is not independent of electric field strength. In some cases, the heating of ions in high electric fields can induce protein unfolding.[126] Nonetheless, FAIMS has proven to be useful in the separation of complex biological mixtures.[127, 128]

Applications

Particularly in recent years with the advent of commercially available ion mobility-mass spectrometers,[120, 129] an increasing number of researchers are using IM-MS in the study of biomolecules.[130] IM-MS can provide useful insights into protein

structure, especially when analysis by traditional methods is problematic. Examples include the investigation of large, multi-protein complexes,[123, 131] and the analysis of dynamic mixtures of proteins that aggregate.[132-134]

In a study in 2007, Ashcroft and co-workers used IM-MS to investigate the structure of β_2-microglobulin, a peptide known to form amyloid fibrils.[135] They reported that a greater percentage of a mutant was in a more unfolded conformation when compared to the unmodified peptide, as indicated by its greater collisional cross-section. Since fibril formation is a result of protein misfolding, the authors propose that this may explain the increased amyloidogenicity of the mutant.

In another example, Heck and colleagues presented interesting IM-MS data in their study of PKG, a protein kinase activated by the binding of cyclic guanosine monophosphate (cGMP).[136] Although the crystal structure of this enzyme has yet to be reported, it is believed that PKG expands upon activation by cGMP. Two aspects of the IM-MS data support this theory. First, comparison of the ESI mass spectra of PKG before and after binding of cGMP shows that the charge state distribution of the activated complex is centred around a higher charge, relative to that of the free PKG. This suggests that, as cGMP binds to PKG, the conformation of PKG changes such that more residues are available for protonation in ESI. Second, the drift times of each cGMP-bound PKG ion are longer than those of the cGMP-free ions of the same charge state, indicating that the activated PKG complex has a more extended structure. Together, the MS and ion mobility data confirm that PKG adopts a more open conformation when bound to cGMP.

Evaluation of ion mobility data

Ion mobility data can be compared to those from other techniques by calculating the theoretical collision cross-section of a protein structure obtained by molecular modelling, NMR spectroscopy or X-ray crystallography. Structures obtained by the latter two methods are available from an online repository known as the Protein Data Bank (PDB), run by the Research Collaboratory for Structural Bioinformatics.[137] There are three different methods of calculating the rotationally-averaged collision cross-section: the projection approximation (PA), the exact hard-sphere scattering (EHSS) model and the trajectory method (TM).

In the projection approximation the average cross-section is calculated for each possible orientation of the molecule, with each atom within the molecule assumed to be a hard-sphere. In the original iteration of the PA, the interaction between the ion and the buffer gas was considered simply as a hard-sphere collision.[138] This model was improved by von Helden *et al.*, who allowed for the variation in atomic radii with temperature.[139]

The PA only holds for molecular surfaces that are perfectly convex. In reality, the irregular surface of a protein molecule means that multiple collisions may occur at some regions, whilst parts of the molecule may be protected from collisions by another. This lead to the development of the EHSS model by Shvartsburg and Jarrold to account for such phenomena.[140] A further refinement, known as the trajectory method, also considers long-range interactions between the ion and the buffer gas.[141]

In their 1997 review, Clemmer and Jarrold compared these various methods.[109] They demonstrated that for molecules of >200 atoms, the PA significantly underestimates the collision cross-section, whilst the EHSS and TM values are similar. For bovine pancreatic trypsin inhibitor (a peptide of similar size to defensins), the cross-section obtained by the PA was ~17% smaller than the EHSS and TM values; for larger molecules this deviation increases. The EHSS and TM methods are therefore the most suitable for calculating the collision cross-sections of biomolecules.

1.5 Summary

In this thesis, ion mobility-mass spectrometry is employed to examine the conformations of β-defensins. Structure-activity relationships of the murine β-defensin Defb14 are interrogated using a sequence modification approach. In addition, the interactions of human β-defensins 2 and 3 with oligosaccharides are studied. It is hoped that a greater understanding of the structures of β-defensins, and how they relate to their biological functions, will be useful in the quest to develop new antibiotics.

1.6 References

1. World.Health.Organization, *WHO Global Strategy for Containment of Antimicrobial Resistance*, 2001.
2. S. J. Projan and P. A. Bradford, *Curr. Opin. Microbiol.*, 2007, **10**, 441-446.
3. D. Bumann, *Curr. Opin. Microbiol.*, 2008, **11**, 387-392.
4. T. Ganz and R. I. Lehrer, *Mol. Med. Today*, 1999, **5**, 292-297.
5. M. Zasloff, *Nature*, 2002, **415**, 389-395.
6. T. Mogi and K. Kita, *Cell. Mol. Life Sci.*, 2009, **66**, 3821-3826.
7. R. E. W. Hancock and H. G. Sahl, *Nat. Biotechnol.*, 2006, **24**, 1551-1557.
8. A. Peschel and H. G. Sahl, *Nat. Rev. Microbiol.*, 2006, **4**, 529-536.
9. G. G. Perron, M. Zasloff and G. Bell, *Proc. Biol. Sci.*, 2006, **273**, 251-256.
10. P. H. Mygind, R. L. Fischer, K. M. Schnorr, M. T. Hansen, C. P. Sonksen, S. Ludvigsen, D. Raventos, S. Buskov, B. Christensen, L. De Maria, O. Taboureau, D. Yaver, S. G. Elvig-Jorgensen, M. V. Sorensen, B. E. Christensen, S. Kjaerulff, N. Frimodt-Moller, R. I. Lehrer, M. Zasloff and H. H. Kristensen, *Nature*, 2005, **437**, 975-980.
11. K. A. Brogden, *Nat. Rev. Microbiol.*, 2005, **3**, 238-250.
12. H. W. Huang, F. Y. Chen and M. T. Lee, *Phys. Rev. Lett.*, 2004, **92**, 198304.198301–198304.198304.
13. Z. Oren and Y. Shai, *Biopolymers*, 1998, **47**, 451-463.
14. R. I. Lehrer, *Nat. Rev. Microbiol.*, 2004, **2**, 727-738.
15. M. E. Selsted and A. J. Ouellette, *Nat. Immunol.*, 2005, **6**, 551-557.
16. E. Kluver, K. Adermann and A. Schulz, *J. Peptide Sci.*, 2006, **12**, 243-257.
17. T. X. Nguyen, A. M. Cole and R. I. Lehrer, *Peptides*, 2003, **24**, 1647-1654.
18. A. M. Cole, T. Hong, L. M. Boo, T. Nguyen, C. Q. Zhao, G. Bristol, J. A. Zack, A. J. Waring, O. O. Yang and R. I. Lehrer, *Proc. Natl. Acad. Sci. U.S.A.*, 2002, **99**, 1813-1818.
19. K. W. Bensch, M. Raida, H. J. Magert, P. Schulzknappe and W. G. Forssmann, *FEBS Lett.*, 1995, **368**, 331-335.
20. J. Harder, J. Bartels, E. Christophers and J. M. Schroder, *Nature*, 1997, **387**, 861-861.
21. J. Harder, J. Bartels, E. Christophers and J. M. Schroder, *J. Biol. Chem.*, 2001, **276**, 5707-5713.
22. B. C. Schutte, J. P. Mitros, J. A. Bartlettt, J. D. Walters, H. P. Jia, M. J. Welsh, T. L. Casavant and P. B. McCray, *Proc. Natl. Acad. Sci. U.S.A.*, 2002, **99**, 2129-2133.
23. K. Taylor, P. E. Barran and J. R. Dorin, *Biopolymers*, 2008, **90**, 1-7.
24. F. Bauer, K. Schweimer, E. Kluver, J. R. Conejo-Garcia, W. G. Forssmann, P. Rosch, K. Adermann and H. Sticht, *Protein Sci.*, 2001, **10**, 2470-2479.
25. D. M. Hoover, O. Chertov and J. Lubkowski, *J. Biol. Chem.*, 2001, **276**, 39021-39026.
26. D. M. Hoover, K. R. Rajashankar, R. Blumenthal, A. Puri, J. J. Oppenheim, O. Chertov and J. Lubkowski, *J. Biol. Chem.*, 2000, **275**, 32911-32918.
27. M. V. Sawai, H. P. Jia, L. D. Liu, V. Aseyev, J. M. Wiencek, P. B. McCray, T. Ganz, W. R. Kearney and B. F. Tack, *Biochemistry*, 2001, **40**, 3810-3816.
28. D. J. Schibli, H. N. Hunter, V. Aseyev, T. D. Starner, J. M. Wiencek, P. B. McCray, B. F. Tack and H. J. Vogel, *J. Biol. Chem.*, 2002, **277**, 8279-8289.
29. G. M. Morrison, M. Rolfe, F. M. Kilanowski, S. H. Cross and J. R. Dorin, *Mamm. Genome*, 2002, **13**, 445-451.
30. D. J. Campopiano, D. J. Clarke, N. C. Polfer, P. E. Barran, R. J. Langley, J. R. W. Govan, A. Maxwell and J. R. Dorin, *J. Biol. Chem.*, 2004, **279**, 48671-48679.
31. M. J. Goldman, G. M. Anderson, E. D. Stolzenberg, U. P. Kari, M. Zasloff and J. M. Wilson, *Cell*, 1997, **88**, 553-560.
32. R. Bals, X. R. Wang, Z. R. Wu, T. Freeman, V. Bafna, M. Zasloff and J. M. Wilson, *J. Clin. Invest.*, 1998, **102**, 874-880.
33. E. de Leeuw, M. Rajabi, G. Z. Zou, M. Pazgier and W. Y. Lu, *FEBS Lett.*, 2009, **583**, 2507-2512.

34. K. Taylor, D. J. Clarke, B. McCullough, W. Chin, E. Seo, D. Yang, J. Oppenheim, D. Uhrin, J. R. W. Govan, D. J. Campopiano, D. MacMillan, P. Barran and J. R. Dorin, *J. Biol. Chem.*, 2008, **283**, 6631-6639.
35. H. G. Sahl, U. Pag, S. Bonness, S. Wagner, N. Antcheva and A. Tossi, *J. Leukocyte Biol.*, 2005, **77**, 466-475.
36. B. L. Kagan, M. E. Selsted, T. Ganz and R. I. Lehrer, *Proc. Natl. Acad. Sci. U.S.A.*, 1990, **87**, 210-214.
37. W. C. Wimley, M. E. Selsted and S. H. White, *Protein Sci.*, 1994, **3**, 1362-1373.
38. G. Fujii, M. E. Selsted and D. Eisenberg, *Protein Sci.*, 1993, **2**, 1301-1312.
39. M. Dathe and T. Wieprecht, *Biochim. Biophys. Acta*, 1999, **1462**, 71-87.
40. R. I. Lehrer, A. Barton, K. A. Daher, S. S. L. Harwig, T. Ganz and M. E. Selsted, *J. Clin. Invest.*, 1989, **84**, 553-561.
41. V. Sass, U. Pag, A. Tossi, G. Bierbaum and H. G. Sahl, *Int. J. Med. Microbiol.*, 2008, **298**, 619-633.
42. T. Schneider, T. Kruse, R. Wimmer, I. Wiedemann, V. Sass, U. Pag, A. Jansen, A. K. Nielsen, P. H. Mygind, D. S. Ravents, S. Neve, B. Ravn, A. Bonvin, L. De Maria, A. S. Andersen, L. K. Gammelgaard, H. G. Sahl and H. H. Kristensen, *Science*, 2010, **328**, 1168-1172.
43. N. Antcheva, F. Morgera, L. Creatti, L. Vaccari, U. Pag, S. Pacor, Y. Shai, H. G. Sahl and A. Tossi, *Biochem. J.*, 2009, **421**, 435-447.
44. E. Kluver, S. Schulz-Maronde, S. Scheid, B. Meyer, W. G. Forssmann and K. Adermann, *Biochemistry*, 2005, **44**, 9804-9816.
45. S. P. Liu, L. Zhou, J. Li, A. Suresh, C. Verma, Y. H. Foo, E. P. H. Yap, D. T. H. Tan and R. W. Beuerman, *Chembiochem*, 2008, **9**, 964-973.
46. H. Sahly, S. Schubert, J. Harder, P. Rautenberg, U. Ullmann, J. Schroder and R. Podschun, *Antimicrob. Agents Chemother.*, 2003, **47**, 1739-1741.
47. A. Silipo, A. Molinaro, P. Cescutti, E. Bedini, R. Rizzo, M. Parrilli and R. Lanzetta, *Glycobiology*, 2005, **15**, 561-570.
48. A. Peschel, *Trends Microbiol.*, 2002, **10**, 179-186.
49. M. Eisenbach, *Chemotaxis*, Imperial College Press, London, 2004.
50. D. Yang, A. Biragyn, L. W. Kwak and J. J. Oppenheim, *Trends Immunol.*, 2002, **23**, 291-296.
51. D. Yang, O. Chertov, N. Bykovskaia, Q. Chen, M. J. Buffo, J. Shogan, M. Anderson, J. M. Schroder, J. M. Wang, O. M. Z. Howard and J. J. Oppenheim, *Science*, 1999, **286**, 525-528.
52. A. Soruri, J. Grigat, U. Forssmann, J. Riggert and J. Zwirner, *Eur. J. Immunol.*, 2007, **37**, 2474-2486.
53. Z. B. Wu, D. M. Hoover, D. Yang, C. Boulegue, F. Santamaria, J. J. Oppenheim, J. Lubkowski and W. Y. Lu, *Proc. Natl. Acad. Sci. U.S.A.*, 2003, **100**, 8880-8885.
54. M. Pazgier, A. Prahl, D. M. Hoover and J. Lubkowski, *J. Biol. Chem.*, 2007, **282**, 1819-1829.
55. E. J. Hollox, U. Huffmeier, P. Zeeuwen, R. Palla, J. Lascorz, D. Rodijk-Olthuis, P. C. M. van de Kerkhof, H. Traupe, G. de Jongh, M. den Heijer, A. Reis, J. A. L. Armour and J. Schalkwijk, *Nat. Genet.*, 2008, **40**, 23-25.
56. I. Nomura, E. Goleva, M. D. Howell, Q. A. Hamid, P. Y. Ong, C. F. Hall, M. A. Darst, B. F. Gao, M. Boguniewicz, J. B. Travers and D. Y. M. Leung, *J. Immunol.*, 2003, **171**, 3262-3269.
57. S. I. Candille, C. B. Kaelin, B. M. Cattanach, B. Yu, D. A. Thompson, M. A. Nix, J. A. Kerns, S. M. Schmutz, G. L. Millhauser and G. S. Barsh, *Science*, 2007, **318**, 1418-1423.
58. J. R. Dorin and I. J. Jackson, *Science*, 2007, **318**, 1395.
59. I. Zelezetsky and A. Tossi, *Biochim. Biophys. Acta*, 2006, **1758**, 1436-1449.
60. G. Wei, E. de Leeuw, M. Pazgier, W. Yuan, G. Zou, J. Wang, B. Ericksen, W.-Y. Lu, R. I. Lehrer and W. Lu, *J. Biol. Chem.*, 2009, **284**, 29180-29192.
61. C. A. Michels, *Genetic Techniques for Biological Research: A Case Study Approach*, John Wiley & Sons, Ltd., Chichester, 2002.
62. C. B. Park, K. S. Yi, K. Matsuzaki, M. S. Kim and S. C. Kim, *Proc. Natl. Acad. Sci. U.S.A.*, 2000, **97**, 8245-8250.

63. B. Deslouches, S. M. Phadke, V. Lazarevic, M. Cascio, K. Islam, R. C. Montelaro and T. A. Mietzner, *Antimicrob. Agents Chemother.*, 2005, **49**, 316-322.
64. A. Tossi, C. Tarantino and D. Romeo, *Eur. J. Biochem.*, 1997, **250**, 549-558.
65. J. Drenth, *Principles of Protein X-ray Crystallography*, 2nd edn., Springer-Verlag, Heidelberg, 1999.
66. K. Wuthrich, *J. Biol. Chem.*, 1990, **265**, 22059-22062.
67. D. L. Smith and Z. Q. Zhang, *Mass Spectrom. Rev.*, 1994, **13**, 411-429.
68. P. I. Haris and D. Chapman, *Trends Biochem.Sci.*, 1992, **17**, 328-333.
69. J. M. Beechem and L. Brand, *Annu. Rev. Biochem.*, 1985, **54**, 43-71.
70. J. L. Lippert, D. Tyminski and P. J. Desmeules, *J. Am. Chem. Soc.*, 1976, **98**, 7075-7080.
71. S. M. Kelly, T. J. Jess and N. C. Price, *Biochim. Biophys. Acta*, 2005, **1751**, 119-139.
72. D. L. Smith, Y. Z. Deng and Z. Q. Zhang, *J. Mass Spectrom.*, 1997, **32**, 135-146.
73. L. Whitmore and B. A. Wallace, *Biopolymers*, 2008, **89**, 392-400.
74. F. W. McLafferty, *Science*, 1981, **214**, 280-287.
75. J. A. Loo, *Mass Spectrom. Rev.*, 1997, **16**, 1-23.
76. A. J. R. Heck and R. H. H. van den Heuvel, *Mass Spectrom. Rev.*, 2004, **23**, 368-389.
77. J. L. P. Benesch, B. T. Ruotolo, D. A. Simmons and C. V. Robinson, *Chem. Rev.*, 2007, **107**, 3544-3567.
78. E. de Hoffmann and V. Stroobant, *Mass Spectrometry: Principles and Applications*, 3rd edn., Wiley, New York, 2007.
79. G. Siuzdak, *The Expanding Role of Mass Spectrometry in Biotechnology*, 2nd edn., MCC Press, San Diego, 2006.
80. M. Dole, L. L. Mack and R. L. Hines, *J. Chem. Phys.*, 1968, **49**, 2240-&.
81. M. Yamashita and J. B. Fenn, *J. Phys. Chem.*, 1984, **88**, 4451-4459.
82. M. Karas and F. Hillenkamp, *Anal. Chem.*, 1988, **60**, 2299-2301.
83. K. Tanaka, H. Waki, Y. Ido, S. Akita, Y. Yoshida and T. Yoshida, *Rapid Commun. Mass Spectrom.*, 1988, **2**, 151-153.
84. P. Kebarle and L. Tang, *Anal. Chem.*, 1993, **65**, A972-A986.
85. C. O'Driscoll, *Chemistry in Britain*, 2003, **39**, 33-35.
86. J. V. Iribarne and B. A. Thomson, *J. Chem. Phys.*, 1976, **64**, 2287-2294.
87. J. F. de la Mora, *Anal. Chim. Acta*, 2000, **406**, 93-104.
88. M. S. Wilm and M. Mann, *Int. J. Mass Spectrom. Ion Proc.*, 1994, **136**, 167-180.
89. M. Wilm and M. Mann, *Anal. Chem.*, 1996, **68**, 1-8.
90. R. Juraschek, T. Dulcks and M. Karas, *J. Am. Soc. Mass Spectrom.*, 1999, **10**, 300-308.
91. W. Paul and H. Steinwedel, *Z. Naturforsch.*, 1953, **8**, 448-450.
92. I. A. Kaltashov and S. J. Eyles, *Mass Spectrometry in Biophysics*, John Wiley & Sons, Inc., Hoboken, 2005.
93. W. C. Wiley and I. H. McLaren, *Rev. Sci. Instrum.*, 1955, **26**, 1150-1157.
94. B. A. Mamyrin, V. I. Karataev, D. V. Shmikk and V. A. Zagulin, *Zh. Eksp. Teor. Fiz.*, 1973, **64**, 82-89.
95. P. E. Barran, N. C. Polfer, D. J. Campopiano, D. J. Clarke, P. R. R. Langridge-Smith, R. J. Langley, J. R. W. Govan, A. Maxwell, J. R. Dorin, R. P. Millar and M. T. Bowers, *Int. J. Mass Spectrom.*, 2005, **240**, 273-284.
96. B. Ganem, Y. T. Li and J. D. Henion, *J. Am. Chem. Soc.*, 1991, **113**, 7818-7819.
97. B. Ganem, Y. T. Li and J. D. Henion, *J. Am. Chem. Soc.*, 1991, **113**, 6294-6296.
98. K. G. Standing, I. V. Chernushevich and E. W. Ens, *Abstr. Pap. Am. Chem. Soc.*, 1997, **213**, 294.
99. T. Wyttenbach and M. T. Bowers, *Annu. Rev. Phys. Chem.*, 2007, **58**, 511-533.
100. M. Sharon and C. V. Robinson, *Annu. Rev. Biochem.*, 2007, **76**, 167-193.
101. N. Medalia, M. Sharon, R. Martinez-Arias, O. Mihalache, C. V. Robinson, O. Medalia and P. Zwickl, *J. Struct. Biol.*, 2006, **156**, 84-92.
102. A. Fersht, *Structure and Mechanism in Protein Science*, W. H. Freeman and Co., New York, 1999.

103. C. V. Robinson, E. W. Chung, B. B. Kragelund, J. Knudsen, R. T. Aplin, F. M. Poulsen and C. M. Dobson, *J. Am. Chem. Soc.*, 1996, **118**, 8646-8653.
104. R. Feng, Proceedings of the 43rd ASMS Conference on Mass Spectrometry and Allied Topics, Atlanta, GA, 1995.
105. T. Simonson and C. L. Brooks, *J. Am. Chem. Soc.*, 1996, **118**, 8452-8458.
106. J. N. Murrell and A. D. Jenkins, *Properties of Liquids and Solutions*, 2nd edn., Wiley, New York, 1994.
107. A. Dobo and I. A. Kaltashov, *Anal. Chem.*, 2001, **73**, 4763-4773.
108. M. C. Kuprowski and L. Konermann, *Anal. Chem.*, 2007, **79**, 2499-2506.
109. D. E. Clemmer and M. F. Jarrold, *J. Mass Spectrom.*, 1997, **32**, 577-592.
110. C. S. Creaser, J. R. Griffiths, C. J. Bramwell, S. Noreen, C. A. Hill and C. L. P. Thomas, *Analyst*, 2004, **129**, 984-994.
111. B. C. Bohrer, S. I. Mererbloom, S. L. Koeniger, A. E. Hilderbrand and D. E. Clemmer, *Annu. Rev. Anal. Chem.*, 2008, **1**, 293-327.
112. C. Uetrecht, R. J. Rose, E. van Duijn, K. Lorenzen and A. J. R. Heck, *Chem. Soc. Rev.*, 2010, **39**, 1633-1655.
113. A. B. Kanu, P. Dwivedi, M. Tam, L. Matz and H. H. Hill, *J. Mass Spectrom.*, 2008, **43**, 1-22.
114. E. A. Mason and E. W. McDaniel, *Transport Properties of Ions in Gases*, 1st edn., Wiley, New York, 1988.
115. S. J. Valentine, J. G. Anderson, A. D. Ellington and D. E. Clemmer, *J. Phys. Chem. B*, 1997, **101**, 3891-3900.
116. S. Myung, E. R. Badman, Y. J. Lee and D. E. Clemmer, *J. Phys. Chem. A*, 2002, **106**, 9976-9982.
117. C. S. Hoaglund, S. J. Valentine, C. R. Sporleder, J. P. Reilly and D. E. Clemmer, *Anal. Chem.*, 1998, **70**, 2236-2242.
118. L. M. Matz, H. M. Dion and H. H. Hill, *J. Chromatogr. A*, 2002, **946**, 59-68.
119. S. J. Valentine, M. Kulchania, C. A. S. Barnes and D. E. Clemmer, *Int. J. Mass Spectrom.*, 2001, **212**, 97-109.
120. S. D. Pringle, K. Giles, J. L. Wildgoose, J. P. Williams, S. E. Slade, K. Thalassinos, R. H. Bateman, M. T. Bowers and J. H. Scrivens, *Int. J. Mass Spectrom.*, 2007, **261**, 1-12.
121. K. Giles, S. D. Pringle, K. R. Worthington, D. Little, J. L. Wildgoose and R. H. Bateman, *Rapid Commun. Mass Spectrom.*, 2004, **18**, 2401-2414.
122. A. A. Shvartsburg and R. D. Smith, *Anal. Chem.*, 2008, **80**, 9689-9699.
123. B. T. Ruotolo, J. L. P. Benesch, A. M. Sandercock, S. J. Hyung and C. V. Robinson, *Nat. Protoc.*, 2008, **3**, 1139-1152.
124. I. A. Buryakov, E. V. Krylov, E. G. Nazarov and U. K. Rasulev, *Int. J. Mass Spectrom. Ion Proc.*, 1993, **128**, 143-148.
125. R. Guevremont, *J. Chromatogr. A*, 2004, **1058**, 3-19.
126. A. A. Shvartsburg, F. M. Li, K. Q. Tang and R. D. Smith, *Anal. Chem.*, 2007, **79**, 1523-1528.
127. K. Q. Tang, F. M. Li, A. A. Shvartsburg, E. F. Strittmatter and R. D. Smith, *Anal. Chem.*, 2005, **77**, 6381-6388.
128. Y. Xuan, A. J. Creese, J. A. Horner and H. J. Cooper, *Rapid Commun. Mass Spectrom.*, 2009, **23**, 1963-1969.
129. R. Guevremont, D. A. Barnett, R. W. Purves and J. Vandermey, *Anal. Chem.*, 2000, **72**, 4577-4584.
130. R. Mukhopadhyay, *Anal. Chem.*, 2008, **80**, 7918-7920.
131. T. L. Pukala, B. T. Ruotolo, M. Zhou, A. Politis, R. Stefanescu, J. A. Leary and C. V. Robinson, *Structure*, 2009, **17**, 1235-1243.
132. S. L. Bernstein, N. F. Dupuis, N. D. Lazo, T. Wyttenbach, M. M. Condron, G. Bitan, D. B. Teplow, J.-E. Shea, B. T. Ruotolo, C. V. Robinson and M. T. Bowers, *Nat. Chem.*, 2009, **1**, 326-331.
133. D. P. Smith, S. E. Radford and A. E. Ashcroft, *Proc. Natl. Acad. Sci. U.S.A.*, 2010, **107**, 6794-6798.

134. G. R. Hilton, K. Thalassinos, M. Grabenauer, N. Sanghera, S. E. Slade, T. Wyttenbach, P. J. Robinson, T. J. T. Pinheiro, M. T. Bowers and J. H. Scrivens, *J. Am. Soc. Mass Spectrom.*, 2010, **21**, 845-854.
135. D. P. Smith, K. Giles, R. H. Bateman, S. E. Radford and A. E. Ashcroft, *J. Am. Soc. Mass Spectrom.*, 2007, **18**, 2180-2190.
136. V. Alverdi, H. Mazon, C. Versluis, W. Hemrika, G. Esposito, R. van den Heuvel, A. Scholten and A. J. R. Heck, *J. Mol. Biol.*, 2008, **375**, 1380-1393.
137. H. M. Berman, J. Westbrook, Z. Feng, G. Gilliland, T. N. Bhat, H. Weissig, I. N. Shindyalov and P. E. Bourne, *Nucl. Acids Res.*, 2000, **28**, 235-242.
138. E. Mack, *J. Am. Chem. Soc.*, 1925, **47**, 2468-2482.
139. G. von Helden, T. Wyttenbach and M. T. Bowers, *Int. J. Mass Spectrom. Ion Proc.*, 1995, **146**, 349-364.
140. A. A. Shvartsburg and M. F. Jarrold, *Chem. Phys. Lett.*, 1996, **261**, 86-91.
141. M. F. Mesleh, J. M. Hunter, A. A. Shvartsburg, G. C. Schatz and M. F. Jarrold, *J. Phys. Chem.*, 1996, **100**, 16082-16086.

2 Experimental

2.1 Mass Spectrometry

All of the mass spectra presented in this thesis were obtained using a quadrupole time-of-flight mass spectrometer with nano-electrospray ionisation.

2.1.1 Nano-electrospray ionisation

Peptide solutions were prepared at a concentration of 20-100 μM. Various solvent conditions were used: these are discussed in more detail in the relevant chapters. Buffered solutions at 'near-native' pH 6.8 were prepared using 10-20 mM ammonium acetate (Sigma Aldrich, Gillingham, UK). Denaturing solutions were prepared using 49.5% water, 49.5% methanol, 1.0% formic acid. High purity water was obtained from an Arium 611 water purification unit (Sartorius, Göttingen, Germany) fitted with a 0.2 μm filter. Solvents were obtained from Fisher Scientific (Loughborough, UK).

Nano-electrospray tips were made in-house from thin-walled glass capillaries (i.d. 0.5 mm, Precision Instruments, Stevenage, UK) using a Flaming/Brown micropipette puller (Sutter Instrument Company, Novato, CA, USA). These were then filled with sample using gel micro-loading tips (Eppendorf, Hamburg, Germany). A positive voltage (1.4-2.2 kV) was applied to the solution via a platinum wire inserted into the capillary. The spray voltage used depended largely on the solvent composition: typically ~1.8 kV was required.

2.1.2 Ion transfer, mass analysis and detection

In addition to the ion mobility-mass spectrometer described in section 2.2, mass spectra were recorded on the Q-ToF II (Waters, Manchester, UK) (Figure 2.1).

Ions generated by nESI enter the mass spectrometer via a 'Z-spray' source. In this arrangement, the axis of the sample capillary is orthogonal to the sampling orifice (the cone), which is in turn perpendicular to the following lens element (the extractor). This geometry improves sensitivity by allowing the transmission of ions

whilst limiting the transfer of neutral species. For each experiment in this work, the temperature of the source region was set to 80 °C to aid desolvation.

Figure 2.1 Waters Quadrupole Time of Flight (Q-ToF) mass spectrometer

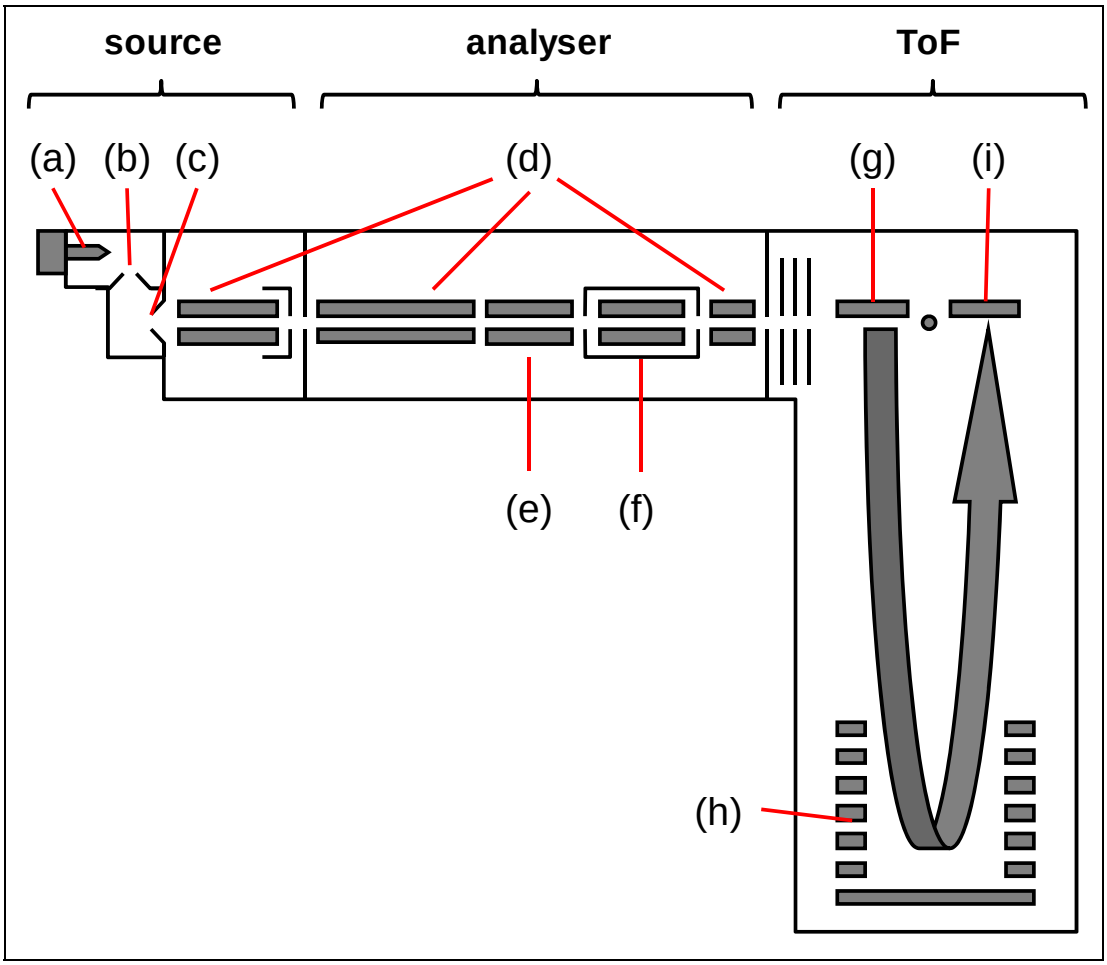

Shown are: (a) nESI capillary; (b) cone; (c) extractor; (d) transfer hexapoles; (e) quadrupole analyser; (f) collision cell; (g) pusher; (h) reflectron; (i) multichannel plate detector. The three differential pumping regions are indicated as source, analyser and ToF.

After passing through the extractor, the ions are guided through a transfer hexapole to the quadrupole analyser. Collision-induced dissociation can be performed by using the quadrupole to select ions of a particular *m/z* and then increasing the kinetic energy of these ions as they enter the collision cell. However, for all experiments in this thesis, the quadrupole was used simply as a mass filter and the ions were not subjected to fragmentation inside the collision cell.

The ions are analysed subsequently by time-of-flight mass spectrometry, where the velocity of each ion is inversely proportional to its *m/z*. The ions are pulsed down the flight tube by the pusher until they reach the reflectron. Here, the ions are

focused and reflected towards the microchannel plate detector. The signals from the ions arriving at the detector pass through a 4 GHz time-to-digital converter and are processed into mass spectra by MassLynx software (version 4.1, Waters, Manchester, UK).

The mass spectrometer contains three differential pumping regions: the source, quadrupole analyser and ToF chambers. Each chamber is pumped by a turbomolecular pump, backed by a rotary pump. On the Q-ToF II, typical pressures in each region are as follows: source ~ 1.7 mbar; analyser ~ 2.4 x 10^{-5} mbar; ToF ~ 4.4 x 10^{-7} mbar.

External mass calibration was performed prior to sample analysis. Sodium iodide clusters were used as a reference, using a 2 mg/ml solution of NaI in 50% water, 50% isopropanol.

2.2 Ion mobility-mass spectrometry

Samples for IM-MS were prepared and ionised by nano-electrospray as described in section 2.1.1.

2.2.1 Instrument description: the MoQToF

Ion mobility measurements were made on the 'MoQToF' (mobility quadrupole time-of-flight) instrument. This is a Q-ToF mass spectrometer, similar to that described above, that has been customised to include a 5.1 cm copper drift cell for ion mobility spectrometry.[1] The drift cell is filled with helium as a buffer gas and is situated between the first transfer hexapole and the quadrupole analyser, as shown in Figure 2.2. The instrument can be used for both mass spectrometry and ion mobility-mass spectrometry. In MS mode, a continuous beam of ions is allowed to pass through the drift cell. In IM-MS operation, ions are pulsed through the drift cell to allow for separation based on their mobility.

In addition to the differential pumping regions present in the QToF II mass spectrometer, the MoQToF contains an additional vacuum chamber that houses the drift cell. This is pumped by a turbomolecular pump, backed by a dual stage rotary

pump. On the MoQToF, typical pressures in each region are: source ~ 0.5 mbar; drift chamber ~ 1.3 x 10^{-3} mbar; analyser ~ 3.0 x 10^{-6} mbar; ToF ~ 1.0 x 10^{-7} mbar.

Figure 2.2 The MoQToF ion mobility-mass spectrometer

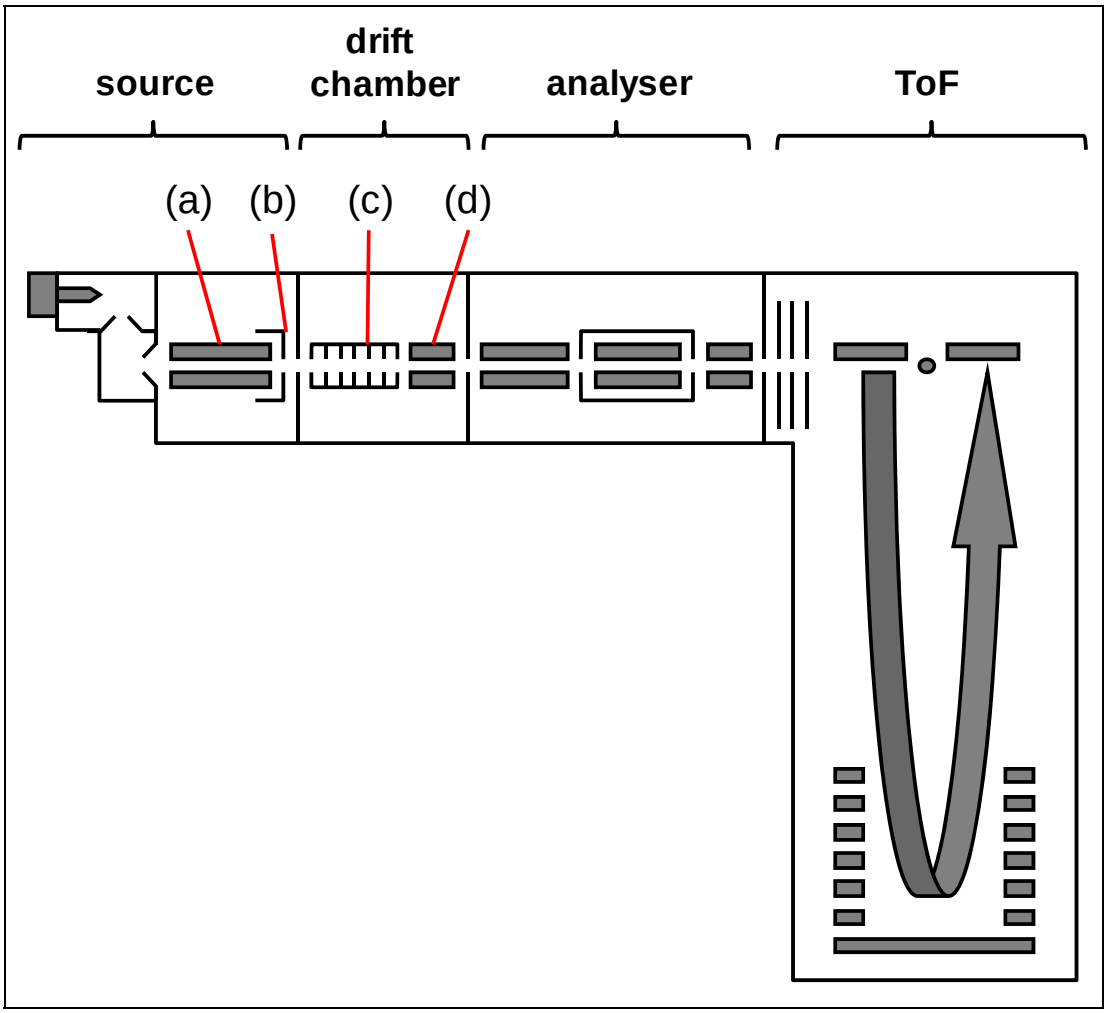

Highlighted are: (a) pre-cell hexapole; (b) top hat lens; (c) drift cell; (d) post-cell hexapole. Note the presence of an additional differential pumping region – the drift chamber.

During each IM-MS experiment, ions are accumulated in the pre-cell region as a result of a raised potential on the 'top hat', the lens element immediately prior to the entrance lenses of the drift cell. At regular intervals, this trapping voltage is lowered for 40 μs to inject a pulse of ions into the drift cell. The frequency of this pulse is set using a signal generator (Stanford Research Systems, Sunnyvale, CA, USA) and is dependent on the ToF pusher period. Typically, a pusher period of 90 μs is used to cover a *m/z* range of 2500: this corresponds to a pulse frequency of 55.6 Hz. Upon

exiting the drift cell, the ions pass via a short re-focusing lens through a second hexapole and from that into a Q-ToF mass spectrometer.

Ion arrival time distributions (mobility spectra) are recorded by synchronisation of the release of ions into the drift cell with mass spectral acquisition. The cell contains helium (99.999%, BOC Speciality Gases) at a pressure of 3.0-3.8 Torr and a temperature of 37 ± 5 °C. For all experiments, the injection energy (the potential difference between the first transfer hexapole and the drift cell) was between 34 and 39 V. Within an acquisition, the pressure in the cell does not drift by more than 0.01 Torr and for each experiment the temperature of the drift cell does not vary by more than 3 °C. Ion mobility measurements of 'standard' proteins on this instrument compare favourably with literature values.[1]

2.2.2 Data acquisition and analysis: an example

The following experiment is provided as an example of the procedure for acquiring IM-MS data and as a proof of concept. Two linear peptides and two cyclic peptides, shown in Figure 2.3, were analysed by ion mobility-mass spectrometry. Each peptide was prepared at 50 μM in 0.01% formic acid and ionised by nESI as described in section 2.1.1.

Figure 2.3 Linear and cyclic peptide sequences

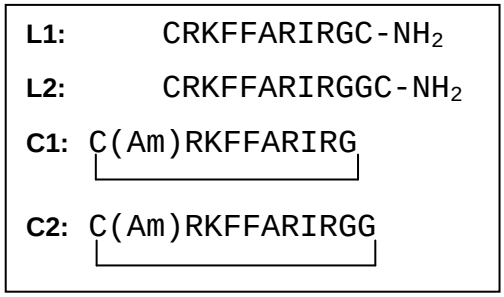

The linear peptides (L1 and L2) have an amide group at the C-terminus. In the cyclic peptides (C1 and C2), the 'termini' are connected via *an intramolecular amide bond. 'C(Am)' denotes a cysteine in which the thiol group is protected by an acetamide group.*

Data acquisition

In IM-MS mode, a total arrival time distribution (ATD), corresponding to one mobility separation, is generated once every 200 MS scans. Spectra were acquired for a minimum of ten pulses (*i.e.* 2000 MS scans) per drift voltage (Figure 2.4) and summed. Initially the drift voltage (*i.e.* the electric potential difference across the

cell) was set to 60 V. The process was repeated at eight further drift voltages: 50, 40, 35, 30, 25, 20, 15 and 10 V. Pressure and temperature were recorded for every measurement taken.

Figure 2.4 Total arrival time distributions for peptide L2 at drift voltage = 20 V

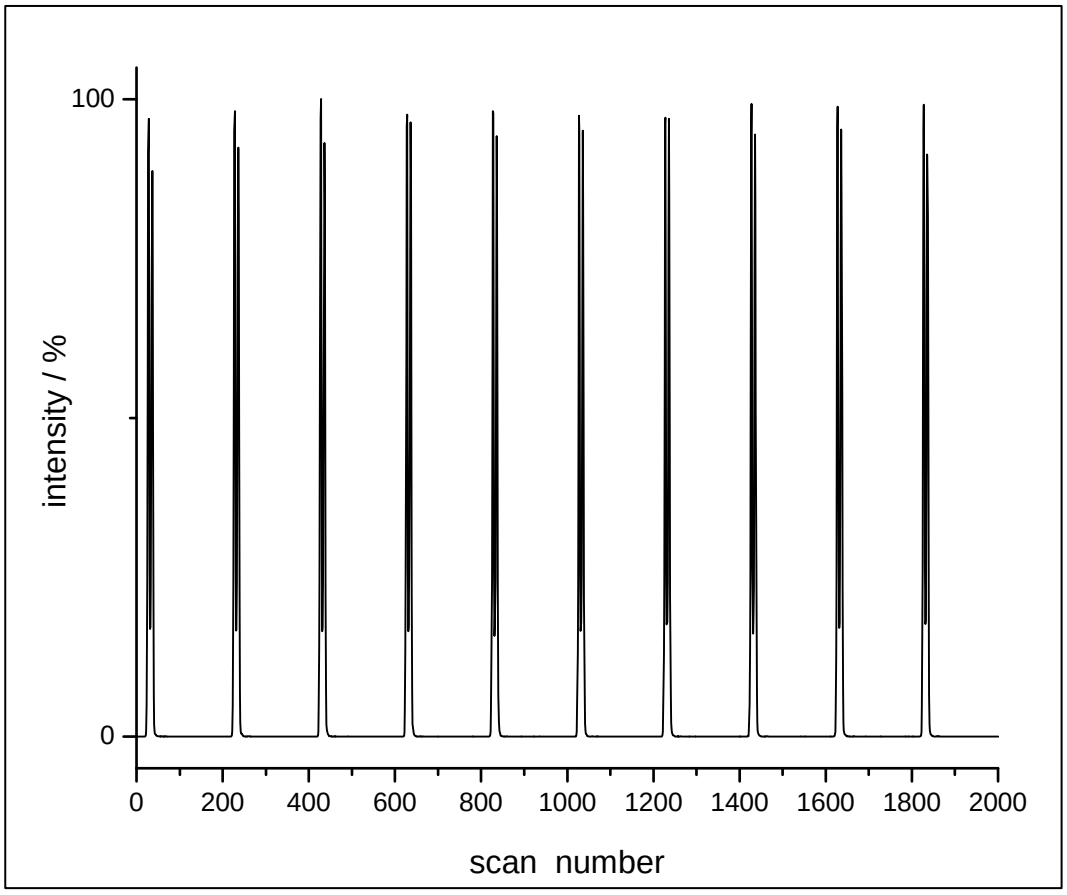

Each pulse corresponds to 200 MS scans.

Data analysis

A mass spectrum (Figure 2.5) was generated from the total ATD using the MassLynx software. This shows the *m/z* of each species arriving at the detector across the entire range of arrival time. For each peptide, three charge states $[M+zH]^{z+}$ were observed, with z = 2-4. The software allows the arrival time distribution of each separate ion to be reconstructed (Figure 2.6). The average scan number was calculated in Origin 8.0 (OriginLab, Northampton, MA, USA) by fitting a Gaussian distribution and determining the midpoint (Figure 2.7). Multiplication of the average scan number by the MS pusher period gives the average arrival time. This was performed for the ATD of every ion at each drift voltage.

Figure 2.5 Mass spectrum of peptide L1 at 100 μM in 0.01% formic acid

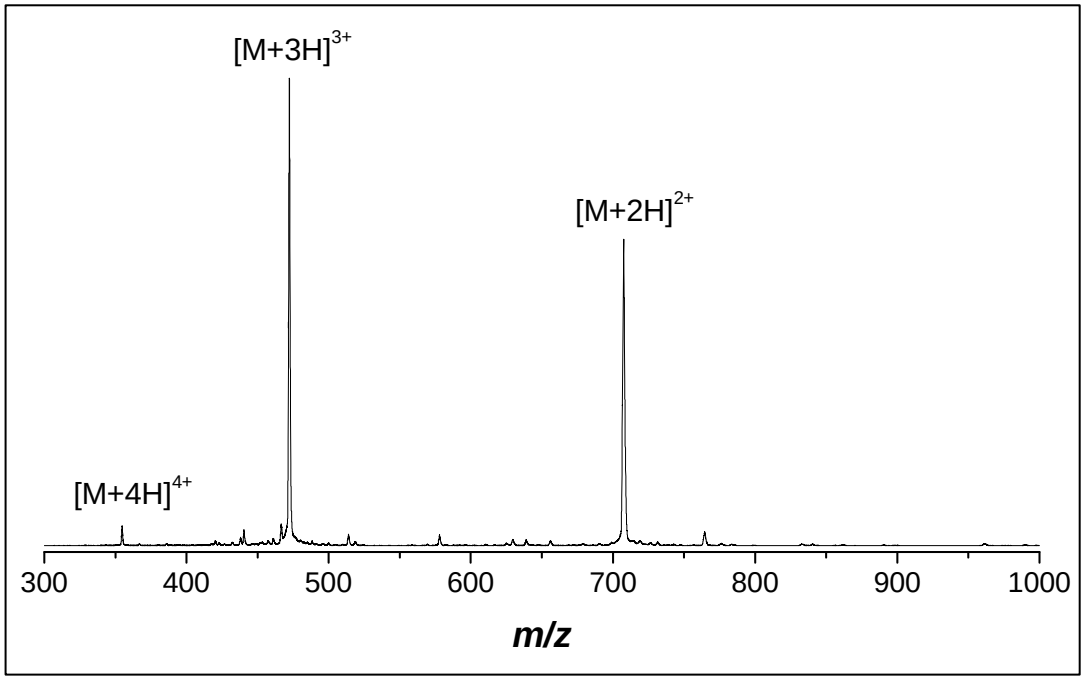

Figure 2.6 Arrival time distributions of peptide L2 at drift voltage = 20 V

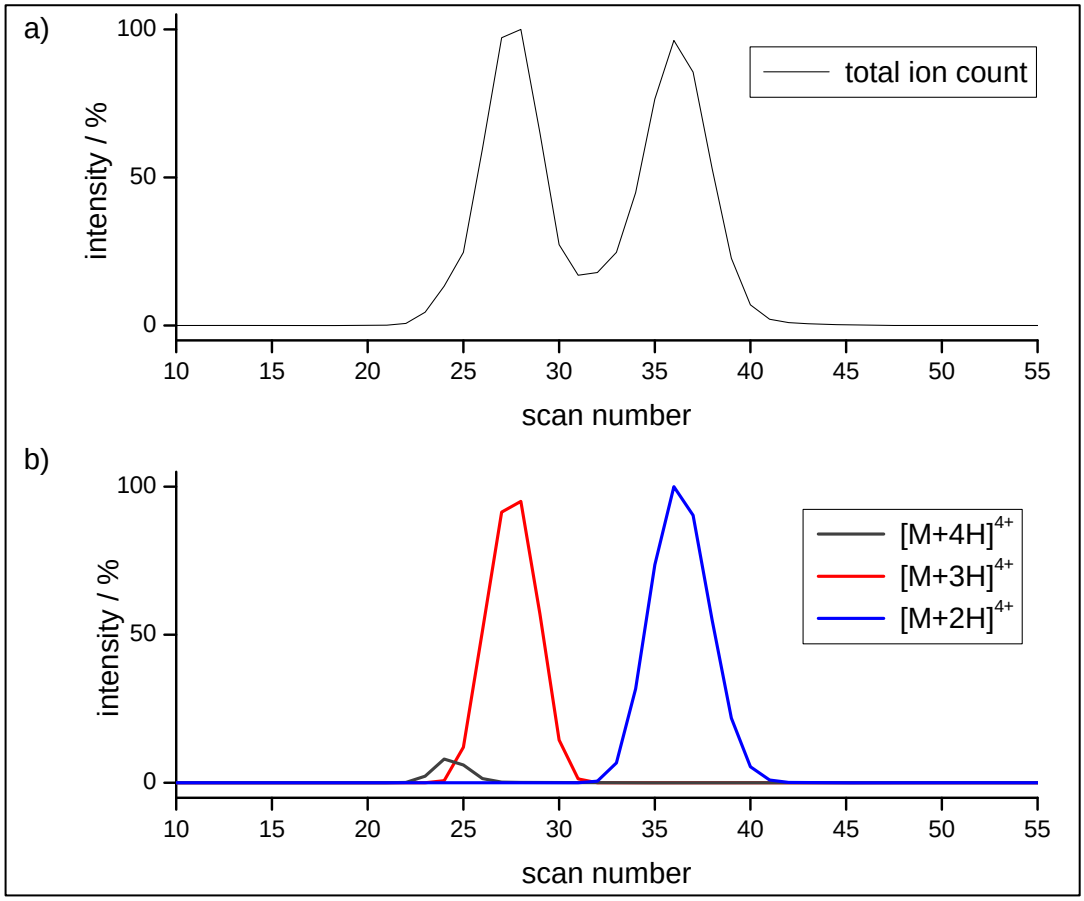

Shown are: (a) total ATD; (b) reconstructed ATDs for the 2+, 3+ and 4+ charge states.

Figure 2.7 Gaussian fit of peptide L2 $[M+2H]^{2+}$ ion at drift voltage = 20 V

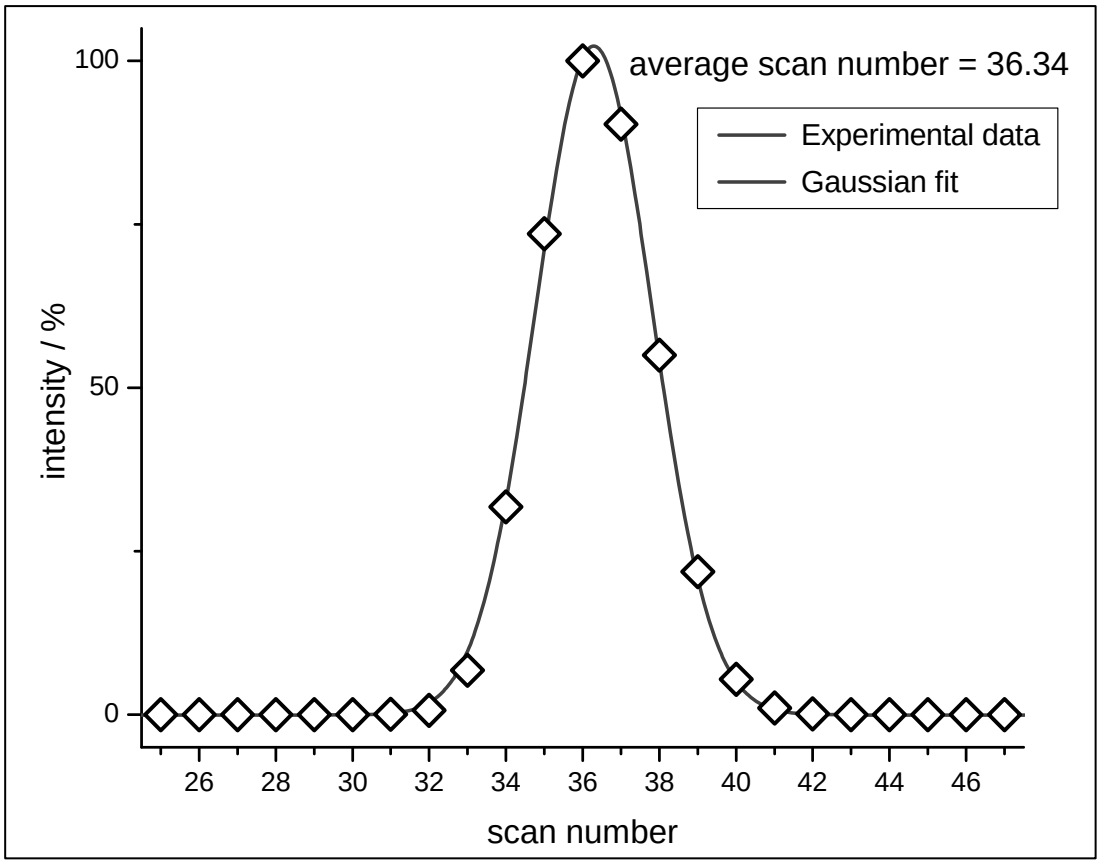

For each ion, the arrival time (t_a) comprises the time taken to traverse the drift cell (the drift time, t_d) plus the time taken to reach the detector upon exiting the drift cell (the dead time, t_0). The dead time can be obtained from a plot of the arrival time versus the ratio of pressure to drift voltage (Figure 2.8, y = t_0 at x = 0). As expected, the arrival time increases with increasing *P/V*. The good linear fit of these data indicates that, as required, the experiment was conducted within the low-field limit, that is to say that there was no alignment of the ions in the electric field and the drift time is directly proportional to the rotationally-averaged collision cross-section.

The gradient of this line is inversely proportional to the reduced mobility (K_o) of the ion (equation {2.1}). The rotationally-averaged collision cross-section (Ω) can then be calculated from K_o (equation {2.2}). Each complete IM-MS experiment was performed in triplicate and the mean collision cross-section calculated for each charge state.

{2.1} $$t_d = t_a - t_0 = \frac{L^2 T_0 P}{K_0 T P_0 V}$$

Where L is the length of the drift tube, K_o is reduced mobility, V is the drift voltage, P is pressure, P_0 is 760 Torr, T is temperature and T_0 is 273.15 K.

{2.2} $$\Omega = \frac{3ze}{16N}\left(\frac{2\pi}{\mu k_B T}\right)^{1/2}\frac{1}{K_0}$$

Where Ω is the rotationally-averaged collision cross-section (strictly, the momentum transfer integral), N is the number density of the buffer gas, μ is the reduced mass of the analyte and the buffer gas, k_B is the Boltzmann constant.

Figure 2.8 Plot of arrival time versus *P/V* for peptide L2 $[M+2H]^{2+}$ ion

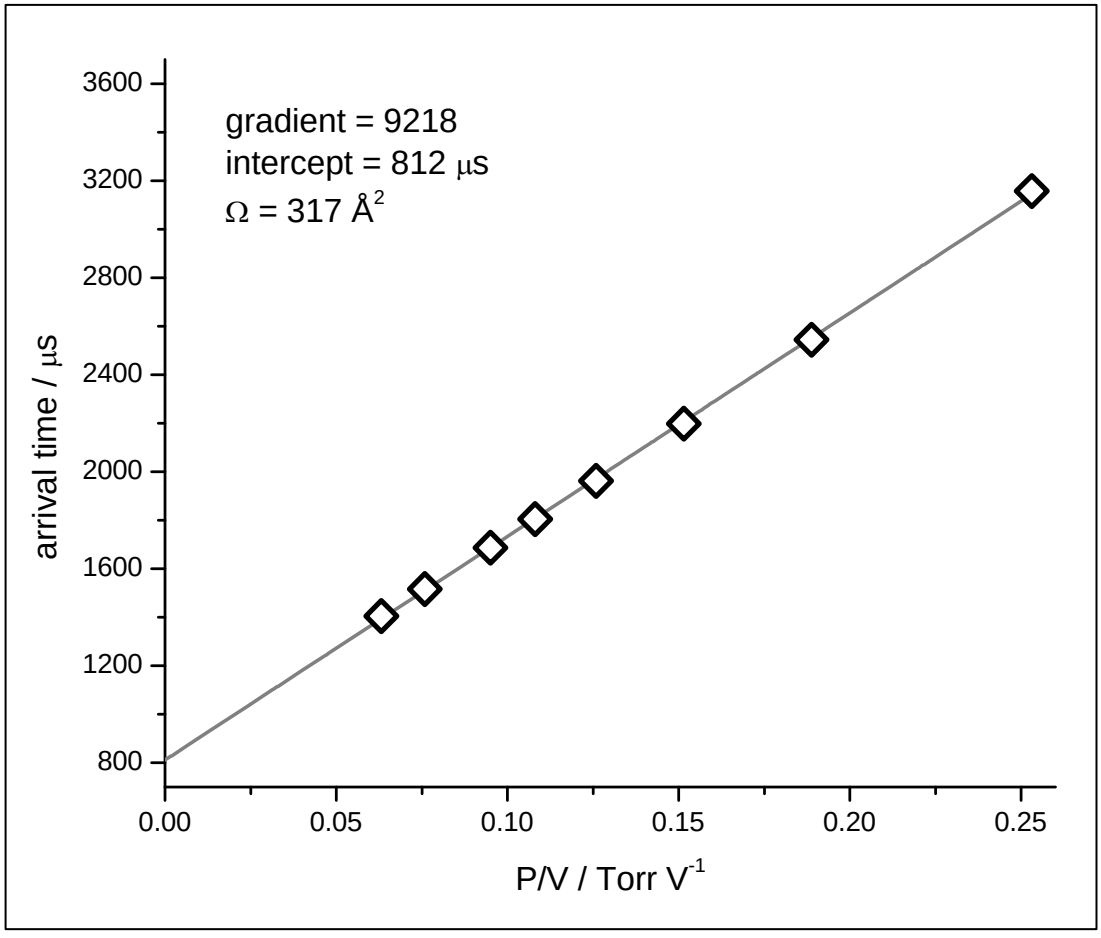

Results and discussion

The rotationally-averaged collision cross-sections for each of the linear and cyclic peptides are shown (Table 2.1).

Table 2.1 Mean collision cross-sections of the linear and cyclic peptides

	Collision cross-section ($Å^2$) [a]			
Peptide	L1	L2	C1	C2
$[M+2H]^{2+}$	316 ± 4	319 ± 2	288 ± 6	295 ± 7
$[M+3H]^{3+}$	324 ± 7	320 ± 6	282 ± 5	296 ± 5
$[M+4H]^{4+}$	349 [b]	365 [b]	298 [b]	306 [b]

[a] *Uncertainties are quoted as the standard deviation.*
[b] *The $[M+4H]^{4+}$ charge state was observed with significant intensity in one run only.*

It might be expected that the cyclic peptides would present more compact conformations than the linear peptides.[2] From the IM-MS data, it can be seen that this is indeed the case. For each charge state, the cyclic peptide has a smaller cross-section than its linear precursor. Comparison of L1 and C2, which each have 11 amino acids, shows that this is not solely attributable to a difference in chain length. Instead the difference in cross-section results from the more extended structure of linear peptide, relative to the cyclic peptide.

Further evidence of the difference in conformation can be obtained by considering the change in collision cross-section with increasing charge state of a given peptide. For the linear peptides, Ω increases with increasing positive charge. At higher charge states, the L1 and L2 are able to adopt more extended conformations to minimise Coulombic repulsion. For example, the $[M+4H]^{4+}$ ion of L2 has a collision cross-section 14% greater than the $[M+2H]^{2+}$ ion. In contrast, the 'termini' of the cyclic peptides are joined by a covalent bond, which constrains their three-dimensional structure. As a result, they cannot unfold to the same extent: the difference between the 4+ and 2+ charge states of C2 is 4%, which is within two standard deviations.

Thus in this example it has been demonstrated that IM-MS can be used to separate peptide ions of differing conformations.

2.2.3 Estimation of collision cross-sections from PDB structures

The program Mobcal[3, 4] provides algorithms for calculating the momentum transfer integral, Ω (*i.e.* collision cross-section). This was used to estimate the collision cross-sections of NMR and X-ray crystal structures of proteins/peptides provided in the protein databank, as well as theoretical models. Three methods are available in Mobcal: the projection approximation (PA), the exact hard-sphere scattering model (EHSS) and the trajectory method (TM). As discussed in Chapter 1, the PA approach underestimates Ω and so only the EHSS or TM values are reported in this thesis.

2.3 Homology modelling

In cases where a suitable template structure exists, homology modelling can be a useful tool to generate a three-dimensional model of a protein whose structure has yet to be characterised experimentally.[5] Homology modelling, where employed, was performed by utilising the alignment mode of the SWISS-MODEL homology modelling server.[6] Explicit hydrogens were then added to the model using the Leap application, which is contained in the Amber 9 suite of programs.[7] Finally, a limited energy minimisation was performed by relaxing strained bonds, angles, and torsions: no additional optimisation of geometry was carried out.

2.4 Liquid chromatography-mass spectrometry

Reversed-phase high performance liquid chromatography-mass spectrometry (HPLC-MS) was employed to evaluate the relative molecular hydrophobicity of peptides. An Ultimate 3000 LC system (Dionex, Camberley, UK), coupled to a VG Platform II mass spectrometer, was used. The HPLC system was equipped with a Famos autosampler (Dionex).

30 μl of each sample, containing 50 μM peptide and 50 μM melittin (Sigma-Aldrich, Gillingham, UK) as an internal standard, was injected onto a Waters Symmetry C18 column (3.9 x 150 mm). Samples were prepared both in water and in 10 mM dithiothreitol (DTT). DTT was used to prevent dimerisation of the peptides via

cysteine oxidation and this was confirmed by mass analysis following the HPLC separation.

High purity water was obtained from an Arium 611 water purification unit (Satorius, Göttingen, Germany) fitted with a 0.2 μm filter. Solvents were obtained from Fisher Scientific (Loughborough, UK). Initial buffer conditions were as follows: 100% eluent A (96% water, 3% acetonitrile, 1% formic acid); 0% eluent B (4% water, 95% acetonitrile, 1% formic acid); flow rate 1 ml min^{-1}. These conditions were held for 3 minutes before commencing a linear gradient of 0 – 40% eluent B over 40 minutes to elute the samples from the column. The flow was split 1/50 prior to introduction to the electrospray ionisation source of the mass spectrometer.

2.5 Circular dichroism spectroscopy

The secondary structure content of peptides was probed by circular dichroism spectroscopy. Peptide solutions were prepared at an approximate concentration of 200 μg/ml in: (i) 10 mM ammonium acetate, pH 6.8, and (ii) 50% water, 50% 2,2,2-trifluoroethanol (TFE). Samples were placed in quartz cuvette (Hellma, Essex, UK) of pathlength 1 mm. CD spectra were recorded over the range 190 – 260 nm at 20 °C using a J-810 spectropolarimeter (Jasco, Essex, UK). Five scans were acquired for each sample at a rate of 10 nm min^{-1} and averaged to give a final sample spectrum. A blank spectrum, acquired in the absence of peptide in precisely the same way, was subtracted from each final sample spectrum. The concentration of each peptide solution was determined subsequently by assaying with bicinchoninic acid[8] (Pierce) and the mean residue ellipticity was calculated at each wavelength. The CDSSTR algorithm[9] on the DICROWEB server[10] was used to help assign secondary structure.

2.6 References

1. B. J. McCullough, J. Kalapothakis, H. Eastwood, P. Kemper, D. MacMillan, K. Taylor, J. Dorin and P. E. Barran, *Anal. Chem.*, 2008, **80**, 6336-6344.
2. B. T. Ruotolo, C. C. Tate and D. H. Russell, *J. Am. Soc. Mass Spectrom.*, 2004, **15**, 870-878.
3. A. A. Shvartsburg and M. F. Jarrold, *Chem. Phys. Lett.*, 1996, **261**, 86-91.
4. M. F. Mesleh, J. M. Hunter, A. A. Shvartsburg, G. C. Schatz and M. F. Jarrold, *J. Phys. Chem.*, 1996, **100**, 16082-16086.
5. A. Tramontano and V. Morea, *Proteins: Struct., Funct., Genet.*, 2003, **53**, 352-368.

6. B. Rost, *Protein Eng.*, 1999, **12**, 85-94.
7. D. A. Case, T. A. Darden, T. E. Cheatham III, C. L. Simmerling, J. Wang, R. E. Duke, R. Luo, K. M. Merz, D. A. Pearlman, M. Crowley, R. C. Walker, W. Zhang, B. Wang, S. Hayik, A. Roitberg, G. Seabra, K. F. Wong, F. Paesani, X. Wu, S. Brozell, V. Tsui, H. Gohlke, L. Yang, C. Tan, J. Mongan, V. Hornak, G. Cui, P. Beroza, D. H. Mathews, C. Schafmeister, W. S. Ross and P. A. Kollman, *AMBER 9*, University of California, San Francisco, 2006.
8. P. K. Smith, R. I. Krohn, G. T. Hermanson, A. K. Mallia, F. H. Gartner, M. D. Provenzano, E. K. Fujimoto, N. M. Goeke, B. J. Olson and D. C. Klenk, *Anal. Biochem.*, 1985, **150**, 76-85.
9. W. C. Johnson, *Proteins: Struct., Funct., Genet.*, 1999, **35**, 307-312.
10. L. Whitmore and B. A. Wallace, *Biopolymers*, 2008, **89**, 392-400.

3 Chemically modified single-cysteine derivatives of Defb14

The understanding of how β-defensin structures are related to their functions was complicated by the discovery of a peptide that was fully active despite its lack of disulfide bridges. The peptide – an analogue of the murine β-defensin Defb14 – contains a single cysteine residue that is crucial to its chemotactic activity. This chapter studies the importance of this amino acid with regard to the peptide's overall structure.

3.1 Introduction

As described previously, the three-dimensional structure of β-defensins is defined by a characteristic pattern of intramolecular disulfide bonds between six highly-conserved cysteine residues.[1-3] In a key study in 2003, Lu and co-workers showed that the ability of human β-defensin 3 to chemoattract immune cells is highly dependent on how the cysteines are connected.[4] Six topological analogues of HBD3, differing only in the connectivities of the disulfide bonds, were synthesised and their ability to attract monocytes and cells expressing CCR6 was assayed. The analogues displayed a range of chemotactic activities, spanning three to four orders of magnitude. A further variant, in which all cysteines were replaced with α-aminobutyric acid, was found to be inactive.

Subsequently, Taylor *et al.* described synthetic analogues of HBD3 and its mouse orthologue Defb14 (Figure 3.1) that each have only one cysteine but possess chemotactic activities equivalent to their parent peptide *in vitro*.[5] The location of this cysteine residue is important: the peptide is active with cysteine in the fifth position (Cys^V) but inactive with cysteine in the first position (Cys^I). In agreement with the work of Lu and colleagues, Taylor *et al.* also observed that cysteine-free derivatives of HBD3 and Defb14, in which each cysteine was replaced by alanine, do not chemoattract. In all cases, the absence of disulfide bonds did not impede the antimicrobial activity of the peptide.

Figure 3.1 Sequences of HBD3, Defb14 and its analogues Defb14-1Cys^V and Defb14-0Cys

HBD3:	GIINTLQKYY**C**RVRGGR**C**AVLS**C**LPKEEQIGK**C**STRGRK**CC**RRKK
Defb14:	FLPKTLRKFF**C**RIRGGR**C**AVLN**C**LGKEEQIGR**C**SNSGRK**CC**RKKK
Defb14-1Cys^V:	FLPKTLRKFF**A**RIRGGR**A**AVLN**A**LGKEEQIGR**A**SNSGRK**CA**RKKK
Defb14-0Cys:	FLPKTLRKFF**A**RIRGGR**A**AVLN**A**LGKEEQIGR**A**SNSGRK**AA**RKKK

Cysteine to alanine mutations highlighted in bold. Disulfide bonds of HBD3 and Defb14 are omitted for clarity.

The discovery of active β-defensin analogues that lack intramolecular disulfide bonds has important consequences. One of the greatest obstacles to the development of β-defensins as drugs is the expense of manufacturing peptides of sufficient purity.[6] It is therefore important to identify the minimum structural requirements for biological activity. The synthesis of native β-defensins is particularly challenging because of the intricacy required to obtain the 'correct' fold: a mixture of isomers is often obtained during oxidation of the cysteines.[4, 7] Removing the need for intramolecular disulfide bond formation would eliminate this step and help decrease the cost of manufacture.

Taylor *et al.* showed that replacing Cys^V with alanine results in a loss of chemotactic activity. Whilst this demonstrates that Cys^V is essential to the chemoattractant properties of Defb14, it raises the question: does the side-chain of this cysteine interact directly with the chemokine receptor, or is this residue important to the conformation of the rest of the molecule?

In this chapter, the role of Cys^V within Defb14 is investigated. The single-cysteine containing peptide Defb14-1Cys^V was chemically modified to obtain three derivatives as shown in Figure 3.2. Thus, the reactivity of the thiol group in cysteine was exploited to obtain a series of single-point mutants without the need for further peptide synthesis. These derivatives were chosen so that this group of peptides contained a variety of different functional groups in the place of Cys^V. The chemotactic activity of each peptide was then assayed and the structures of these derivatives were probed by ion mobility-mass spectrometry to establish possible links between structure and activity.

Figure 3.2 Structure of the single-cysteine derivatives, Defb14-1X^V

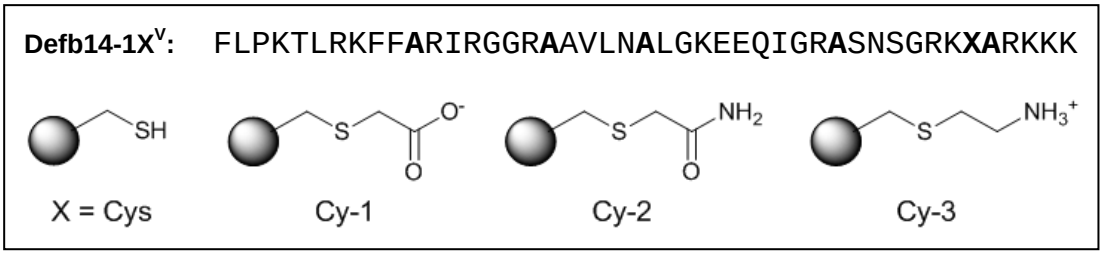

X = Cys represents the unmodified single-cysteine peptide. Cy-1 denotes the carboxymethylated derivative, Cy-2 the carboxamidomethylated derivative and Cy-3 the ethylamine derivative.

3.2 Experimental

3.2.1 Peptide synthesis

All peptides were chemically synthesised by standard solid-phase methodology as described previously.[5] Defb14-1Cys^V was obtained from Albachem Ltd. (Gladsmuir, UK) and subsequently derivatised by Emily Seo and David Clarke. Further detail is available elsewhere[8] but, in brief, Defb14-1Cys^V was reduced with tris(2-carboxyethyl)phosphine and then reacted with either iodoacetate, iodoacetamide or bromoethylamine hydrobromide. This yielded the carboxymethylated derivative, Defb14-1(Cy-1)^V, the carboxyamidomethylated derivative, Defb14-1(Cy-2)^V, and the ethylamine derivative, Defb14-1(Cy-3)^V, respectively (Figure 3.2). Defb14-0Cys was synthesised by Derek Macmillan.

3.2.2 Chemotaxis assays

The chemotactic activity of Defb14-1Cys^V and its derivatives was assessed by Karen Taylor as reported previously.[5] In this assay, the migration of human embryonic kidney (HEK293) cells expressing CCR6 in response to peptides at different concentrations was measured.

3.2.3 Mass spectrometry

Samples were prepared at a peptide concentration of 50 μM in either buffered (10 mM ammonium acetate) or denaturing (49.5% water, 49.5% methanol, 1.0% formic acid) solutions. Mass spectra were recorded on a Q-ToF II mass spectrometer

(Waters, Manchester, UK), with ions produced by positive nano-electrospray ionization. Tuning conditions were identical for each sample.

3.2.4 Ion mobility-mass spectrometry

Samples were prepared and ionised by nESI as described above (section 3.2.3). Ion mobility measurements were made using the MoQToF instrument as detailed previously.[9] For each of the experiments in this chapter, the drift cell was filled with helium at a pressure of 3.0-3.5 Torr and a temperature of 37 ± 5 °C. The electric potential difference across the cell was varied from 60 to 15 V, with measurements taken at eight different voltages.

3.2.5 Theoretical collision cross-section of Defb14

At present there is no NMR or X-ray crystal structure available in the protein databank for Defb14. Given the well-conserved tertiary structure of β-defensins and the high sequence homology of the peptides (Figure 3.1), HBD3 is considered to be a good template for Defb14.[10] Homology modelling of Defb14 was performed on the SWISS-MODEL homology modelling server,[11] using the NMR structure of HBD3 as a template.[12] The rotationally-averaged collision cross-section of this structure was then calculated according to both the exact hard-spheres scattering model (EHSS) and the trajectory method, using the program Mobcal.[13, 14]

In addition, to represent a theoretical structure of a fully-extended peptide, a model of Defb14-1Cys^{V} was built as a linear chain of amino acids in Leap.[15] A limited energy minimisation of this structure was performed without further geometry optimisation and the collision cross-section of this structure calculated using Mobcal.

3.3 Results and discussion

3.3.1 Chemotaxis assays

The unmodified peptide, the carboxymethylated (Defb14-1(Cy-1)^{V}) and the carboxamidomethylated (Defb14-1(Cy-2)^{V}) derivatives were found to induce migration of significantly ($p < 0.05$) more cells than control medium alone.[8] In contrast, modification of Defb14-1Cys^{V} to form the ethylamine derivative (Defb14-

1(Cy-3)^{V}) rendered the peptide unable to induce cell migration, as observed for the cysteine-free peptide Defb14-0Cys.[8]

Clearly small chemical changes at a single residue of Defb14-1Cys^{V} – a forty-five amino acid peptide – greatly influence its ability to act as a chemoattractant. Given that Defb14-1(Cy-1)^{V} and Defb14-1(Cy-2)^{V} have similar activities to Defb14 and Defb14-1Cys^{V} despite the different functional groups of the side-chain at position V, it would appear unlikely that Cys^{V} interacts directly with CCR6.

3.3.2 Mass spectrometry

The mass spectrum of each peptide displays several charge states corresponding to protonated species $[M+zH]^{z+}$ generated by nano-electrospray ionisation. In both ammonium acetate and acidified water/methanol, charge states z = 3-9 are observed for each derivative of Defb14-1Cys^{V} (Figures 3.3 and 3.4). In comparison, $[M+7H]^{7+}$ was the most highly-charged species observed by McCullough *et al.* for the wild-type Defb14 on the same instrument.[9] This difference in charge state distribution can be attributed to the presence of three disulfide bridges in the wild-type Defb14, which constrict the conformation of the peptide in solution and thus limit the availability of sites available for protonation in the nESI process.

Under buffered conditions the charge state distribution of each derivative is centred around $[M+5H]^{5+}$, whereas under denaturing conditions there is an increase in the population of higher charge states, with the most intense peak being $[M+6H]^{6+}$. In solution, the peptide structure is expected to change to maximise favourable solute-solvent interactions, which are dependent on the pH and hydrophobicity of the solution.[16] Such changes in the solution-phase conformation of a peptide are often reflected in a change in the charge state distribution in the mass spectrum.[17] In this case, it appears that the presence of acid and organic solvent induces slightly more open conformations of the peptides in solution prior to ionisation.

Despite the different functional groups introduced at Cys^{V}, the mass spectra of the derivatives are remarkably similar to each other. Thus by mass spectrometry alone it is not possible to discern any structural differences between the active and inactive peptides.

Figure 3.3 Mass spectra of the derivatives Defb14-1X^{V} in 10 mM ammonium acetate

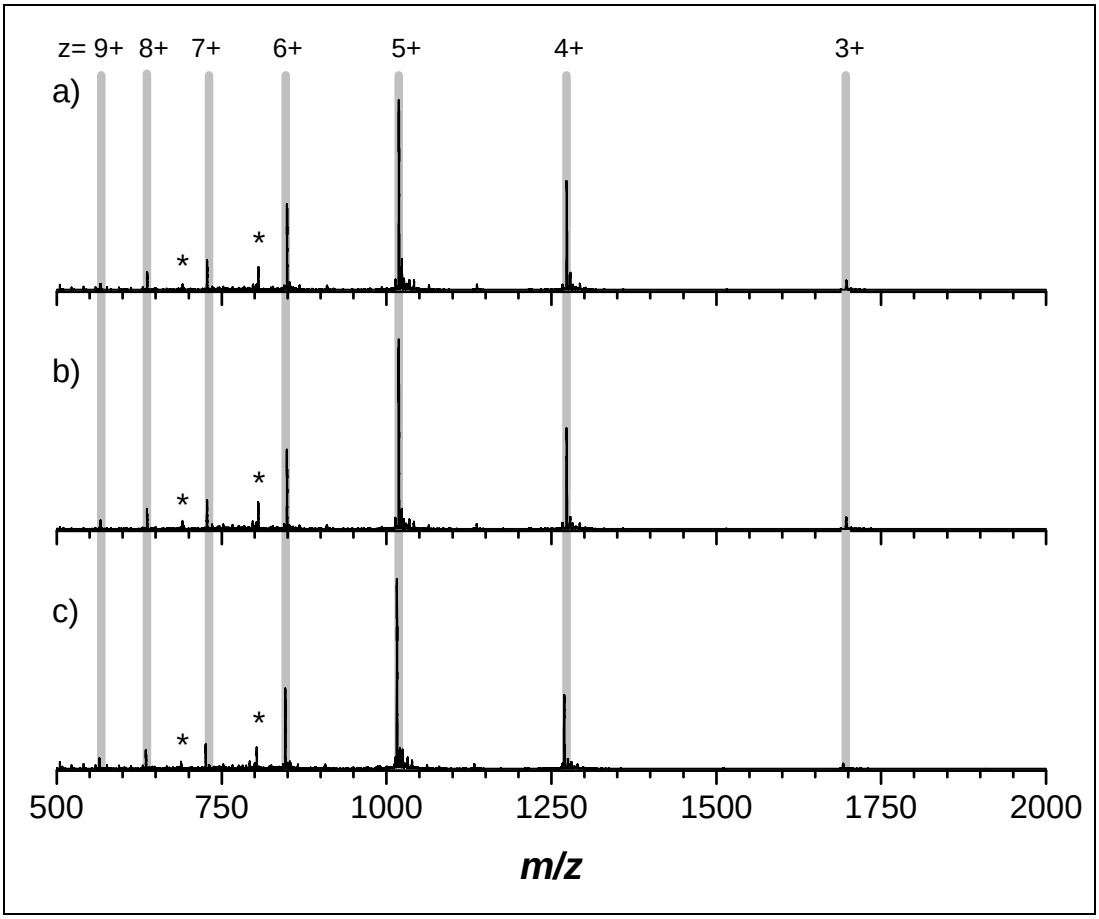

Peptides: (a) Defb14-1(Cy-1)^{V}; (b) Defb14-1(Cy-2)^{V}; (c) Defb14-1(Cy-3)^{V}. Charge states [M+3H]$^{3+}$ to [M+9H]$^{9+}$ are highlighted in grey. Peaks marked with an asterisk (*) correspond to peptide fragments formed in-source.

Figure 3.4 Mass spectra of the derivatives Defb14-1XV in 49.5% water, 49.5% methanol, 1% formic acid

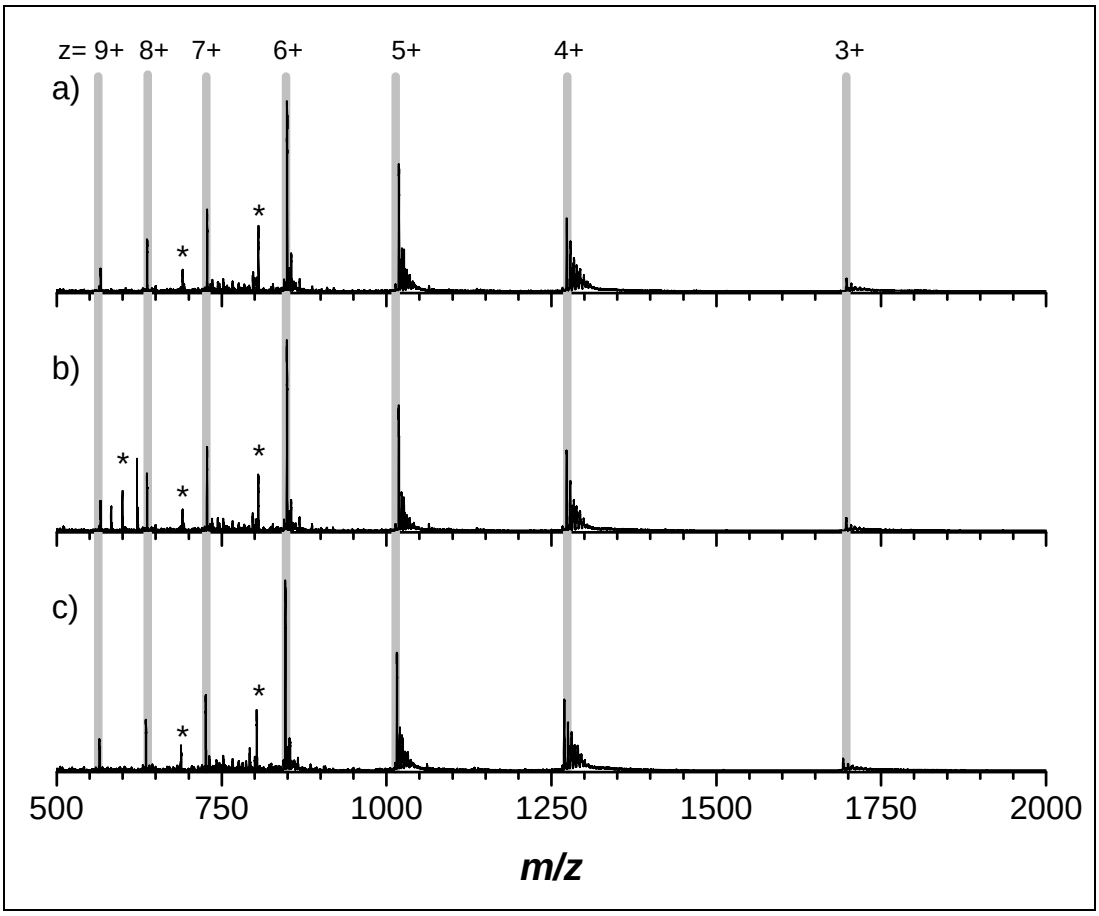

Peptides: (a) Defb14-1(Cy-1)^{V}; (b) Defb14-1(Cy-2)^{V}; (c) Defb14-1(Cy-3)^{V}. Charge states [M+3H]$^{3+}$ to [M+9H]$^{9+}$ are highlighted in grey. Peaks marked with an asterisk (*) correspond to peptide fragments formed in-source.

3.3.3 Ion mobility-mass spectrometry

Collision cross-sections under buffered conditions

A single, relatively narrow arrival time distribution is observed for all species studied by IM-MS under buffered conditions (as illustrated in Figure 3.5 for the [M+9H]$^{9+}$ ions). This implies that the gas-phase conformations adopted by each peptide ion are closely-related in size. In addition, the widths of the arrival time distributions are comparable for each peptide at a given charge state, indicating that each of the peptides populate a similar range of conformational space.

Figure 3.5 Drift time distributions of the $[M+9H]^{9+}$ ion under buffered conditions

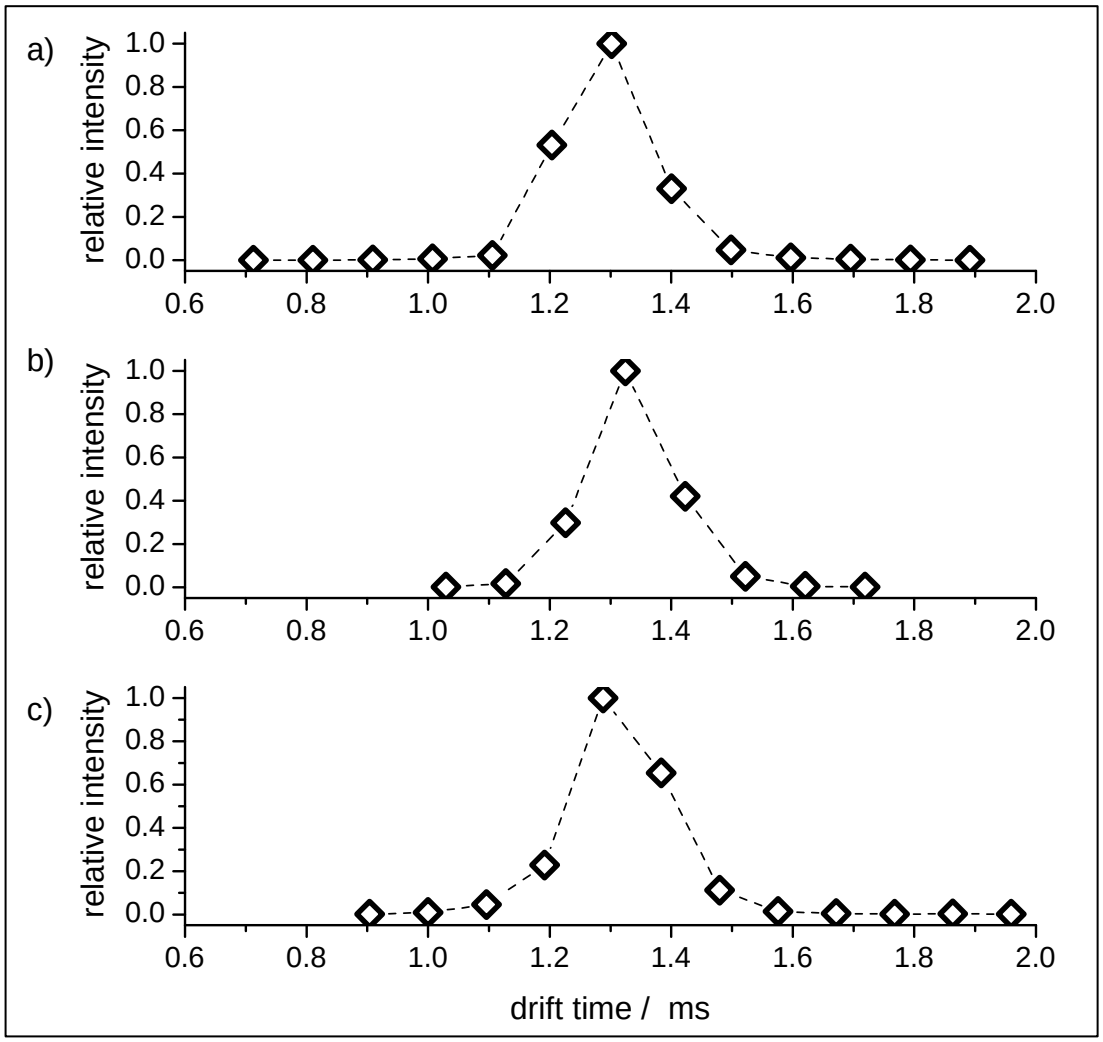

Drift times for the $[M+9H]^{9+}$ charge state of each peptide at a drift voltage of 20 V: (a) Defb14-1(Cy-1)^{V}; (b) Defb14-1(Cy-2)^{V}; (c) Defb14-1(Cy-3)^{V}. Drift times are scaled to 3.5 Torr and 37 ^{o}C to account for fluctuations in pressure and temperature between experiments

The mean collision cross-section of each ion increases with increasing charge (Table 3.1), which can be attributed to expansion of the peptide structure to minimise Coulomb repulsion as an increasing number of protons are accepted.[18, 19] When ionised from 10 mM ammonium acetate, similar collision cross-sections are measured for each of the derivatives at a given charge state.

An exception is that the $[M+3]^{3+}$ ion of Defb14-1(Cy-2)^{V} is larger than the same charge state of Defb14-1(Cy-1)^{V} and Defb14-1(Cy-3)^{V}. In this case, it is possible that the 'fixed' charges on the side-chains of Cy-1 and Cy-3 are involved in electrostatic interactions that constrict the structure of these ions at low charge states;

at higher charge states, these proposed interactions may be less important as the peptide unfolds with increasing charge. In the main, however, it appears that the peptide derivatives in this study adopt similar gas-phase conformations to each other upon ionisation from aqueous buffer.

Table 3.1 Mean collision cross-sections (Å^2) under buffered conditions

	Defb14-1(Cy-1)^V	Defb14-1(Cy-2)^V	Defb14-1(Cy-3)^V
$[M+3H]^{3+}$	586 ± 3	666 ± 28	586 ± 7
$[M+4H]^{4+}$	761 ± 5	768 ± 10	777 ± 10
$[M+5H]^{5+}$	987 ± 8	973 ± 17	969 ± 9
$[M+6H]^{6+}$	1033 ± 4	1040 ± 11	1056 ± 12
$[M+7H]^{7+}$	1060 ± 18	1087 ± 18	1071 ± 8
$[M+8H]^{8+}$	1110 ± 17	1126 ± 23	1136 ± 11
$[M+9H]^{9+}$	1176 ± 19	1218 ± 18	1200 ± 12

Errors are quoted as the standard error of the mean.

To survey a wider range of possible conformations, and to examine the ease with which the peptides unfold, the peptides were also ionised from an acidified solution of water/methanol.

Collision cross-sections under denaturing conditions

As with the buffered conditions, a single arrival time distribution is observed for the ions generated from an acidified solution of water/methanol (Figure 3.6). However, the peaks are wider in the mobility spectra recorded under denaturing conditions: this shown in Figure 3.7 for the $[M+9H]^{9+}$ ion of Defb14-1(Cy-1)^V and is observed for all of the other species also.

Figure 3.6 Drift time distributions of the $[M+9H]^{9+}$ ion under denatured conditions

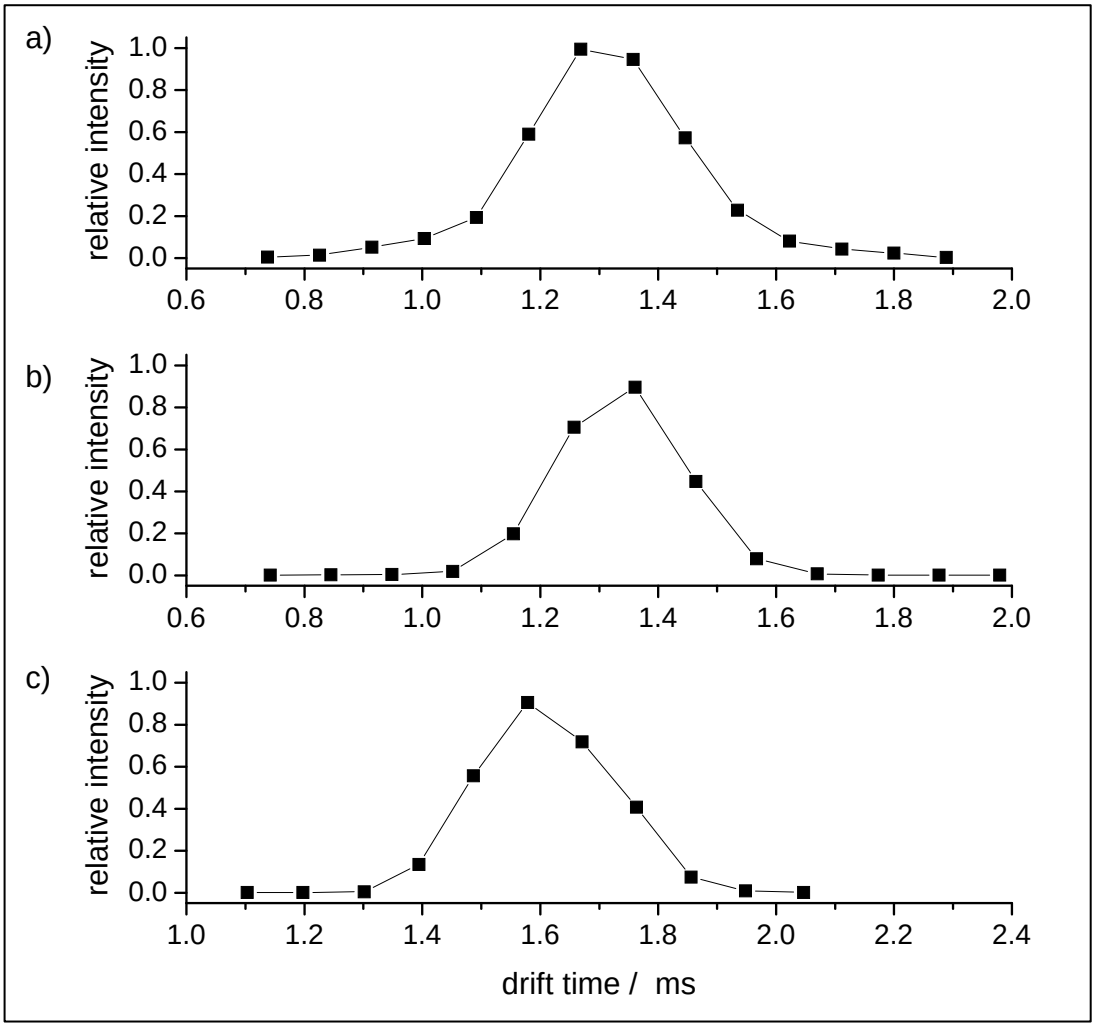

Drift times for the $[M+9H]^{9+}$ charge state of each peptide at a drift voltage of 20 V: (a) Defb14-1(Cy-1)^{V}; (b) Defb14-1(Cy-2)^{V}; (c) Defb14-1(Cy-3)^{V}. Drift times are scaled to 3.5 Torr and 37 ^{o}C to account for fluctuations in pressure and temperature between experiments

This observation implies that the peptides produced from acidified solution possess a greater range of peptide conformations in the gas-phase, though these different structures within a single charge state cannot be resolved on this IM-MS instrument. Separation of these various peptide conformations may be possible on higher-resolution instruments, in which the drift time is extended by the use of longer drift tubes[20] or larger, more polarisable buffer gases.[21] Increasing the pressure of the buffer gas would also provide better resolution.

Figure 3.7 Drift time distributions under buffered and denaturing conditions

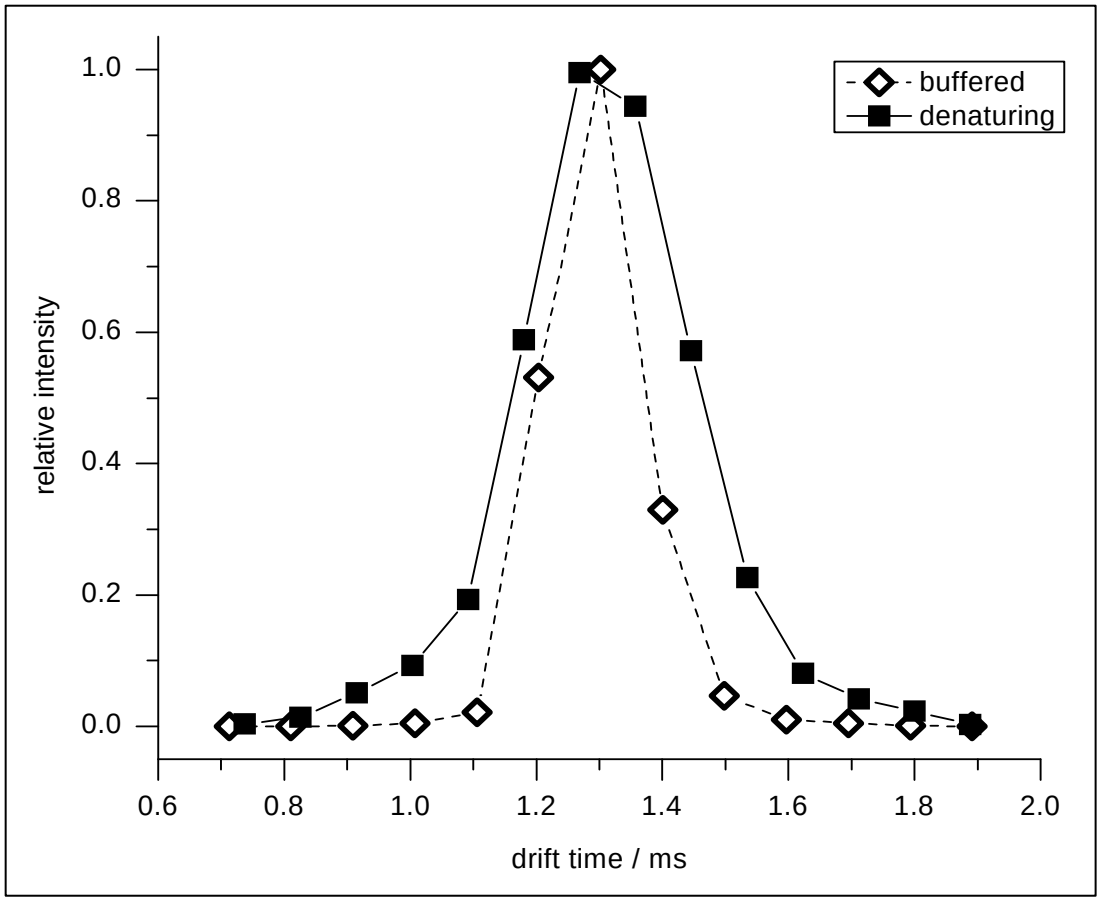

Drift times are for the $[M+9H]^{9+}$ ion of Defb14-1(Cy-1)^{V} at a drift voltage of 20 V and are scaled to 3.5 Torr and 37 ^{o}C to account for fluctuations in pressure and temperature between experiments.

Again an increase in collision cross-section with increasing charge is observed for the peptides (Table 3.2). When these cross-sections are compared with those obtained from aqueous buffer (Table 3.1), it is evident that there is a steeper increase in size between $[M+5H]^{5+}$ and $[M+9H]^{9+}$ for the species under denaturing conditions. Together with the increased peak width, this indicates the derivatives have greater conformational flexibility under these denaturing conditions.

Although all peptide ions exhibit a greater range of sizes under denaturing conditions, the average cross-sections of some peptide ions are smaller under denaturing conditions than under buffered conditions, especially at lower charge states. It is possible that this reflects the solution-phase change from unstructured peptide to helical peptide upon the addition of methanol.[22]

Table 3.2 Mean collision cross-sections (Å^2) under denaturing conditions

	Defb14-1(Cy-1)^V	Defb14-1(Cy-2)^V	Defb14-1(Cy-3)^V
$[M+3H]^{3+}$	n.o.	n.o.	n.o.
$[M+4H]^{4+}$	673 ± 13	676 ± 20	n.o.
$[M+5H]^{5+}$	753 ± 13	758 ± 3	924 ± 32
$[M+6H]^{6+}$	906 ± 22	909 ± 8	1021 ± 3
$[M+7H]^{7+}$	1029 ± 15	1037 ± 3	1127 ± 12
$[M+8H]^{8+}$	1089 ± 16	1123 ± 5	1235 ± 20
$[M+9H]^{9+}$	1162 ± 7	1212 ± 4	1328 ± 31

Errors are quoted as the standard error of the mean. Species marked n.o. were not observed in sufficient intensity to accurately determine collision cross-sections by IM-MS.

It is clear that the different solution conditions have resulted in different geometries post-ionisation. For example, the $[M+4H]^{4+}$ to $[M+6H]^{6+}$ ions of Defb14-1(Cy-1)^V and Defb14-1(Cy-2)^V are more compact under denaturing conditions than the equivalent ions produced from ammonium acetate. Meanwhile Defb14-1(Cy-3)^V is more extended at z = 7-9 under denaturing conditions.

The ability to distinguish between protein ions obtained from different solutions has been reported previously: for example Jarrold and co-workers measured different cross-sections for ions of cytochrome *c* produced from buffered, acidified and methanol-denatured solutions.[23] Here, a similar approach shows how a single chemical change in the sequence of a given polypeptide can significantly alter the ease by which it can unfold, and by inference its structural stability, as seen in the relative changes of collision cross-section versus charge state.

Comparison of chemotactic and non-chemotactic peptide conformations

For comparison, a panel of peptides has been constructed that, in addition to the three derivatives of Defb14-1Cys^V investigated as part of this thesis, consists of Defb14, Defb14-1Cys^V and Defb14-0Cys, whose cross-sections have been reported previously (reference 9 and Appendix 1).

Under denaturing conditions, the carboxymethylated and carboxamidomethylated derivatives have cross-sections that are indistinguishable from unmodified Defb14-

1Cys^{V} as $[M+7H]^{7+}$ and $[M+8H]^{8+}$ ions and similar to wild-type Defb14 for the charges states z = 4-7. The ethylamine derivative and Defb14-0Cys have significantly larger collision cross-sections than Defb14-1Cys^{V} as $[M+7H]^{7+}$ and $[M+8H]^{8+}$ ions and greater than Defb14-1(Cy-1)^{V}, Defb14-1(Cy-2)^{V} and wild-type Defb14 across all of the observed charge states.

From these observations it appears that the small changes to the functionality at Cys^{V} have altered the conformational preferences of the peptides. It is not surprising that the modification a single amino acid can induce changes in the fold of a protein or peptide: it is well-documented that mutations can shift the equilibrium between native and unfolded states.[24] Indeed, in some cases a small number of changes can give rise to completely distinct tertiary structures.[25] A dramatic example of this is the synthetic system designed by Alexander *et al.*, in which a single amino acid substitution changes the protein fold completely from α-helix to β-sheet (and *vice versa*).[26]

The peptides with chemotactic activity are significantly more compact at higher charge states than those that do not chemoattract, suggesting that the active peptides experience less Coulomb-driven unfolding in the gas-phase. This is illustrated by considering the percentage change in the observed collision cross-section for the modified peptides versus unmodified Defb14-1Cys^{V} (Figure 3.8).

The change in collision cross-section due to the size of the substituent does not appear to be a factor here, since the smallest substituent (X = Ala) gives the second largest collision cross section for z = 6, 7 and 8. The Cy-3 and Cy-1 side-chains are of comparable size but the collision cross section for the z = 8 ion of Defb14-1(Cy-3)^{V} is 12% larger than that observed for the Defb14-1(Cy-1)^{V}. This may be due to electrostatic effects: if the amino group of Cy-3 is protonated, given its proximity to the basic residues in the C-terminus of the peptide, it is likely that it will induce local unfolding due to electrostatic repulsion. The Cy-1 acidic group if deprotonated will interact favourably with the protonated basic groups thus tightening the conformation for this peptide.

Figure 3.8 Comparison of collision cross-sections of Defb14 and Defb14-1X^{V} derivatives versus unmodified Defb14-1Cys^{V}

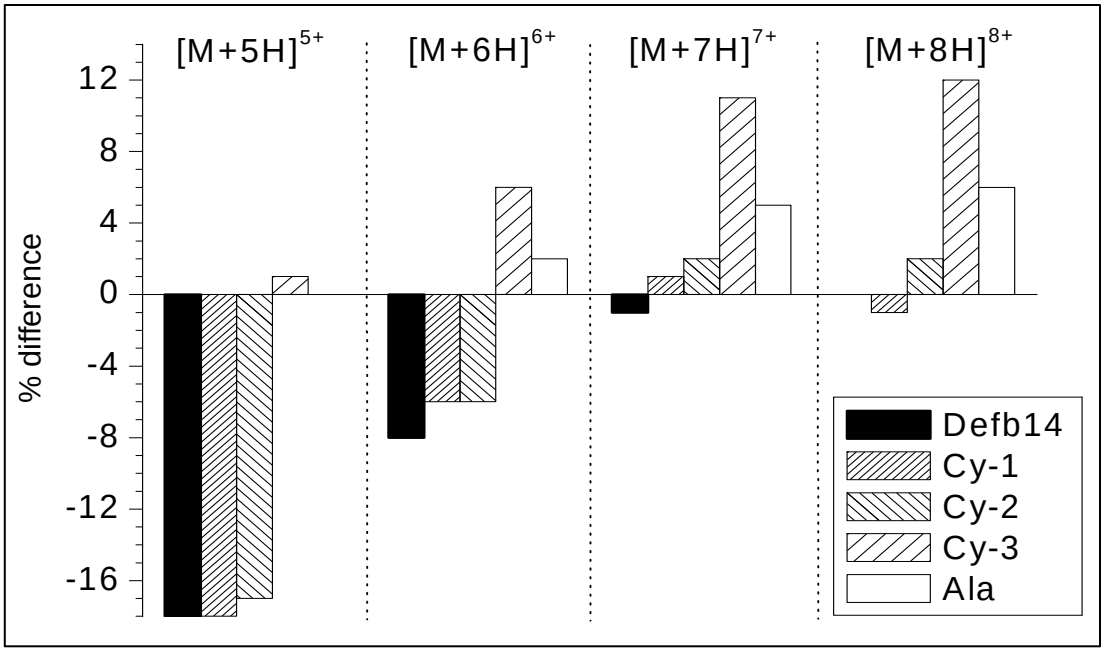

In considering the protonation state of the carboxymethyl and ethylamine derivatives, one can approximate the functional groups of Cy-1 and Cy-3 to the side-chains of aspartic acid ($pK_a \sim 3.9$) and lysine ($pK_a \sim 10.5$) respectively.[27] This implies that Cy-1 is mostly charge-neutral in 1% formic acid (pH ~ 2.5), whilst Cy-3 is highly likely to be protonated. If these protonation states were preserved post-ionisation, it would explain the greater collision cross-sections observed for Cy-3 compared to Cy-1 and Cy-2 under denaturing conditions. However, aspartic acid (and by inference Cy-1) is readily deprotonated in the gas-phase.[28] In addition, there was no evidence of this solvent memory effect upon ionisation from ammonium acetate (pH 6.8), from which the collision cross-sections were indistinguishable despite the likely differences in protonation state.

The difference between the conformations of the unmodified peptide and the non-chemotactic derivatives is most pronounced at elevated charge states. Other researchers have also reported greater resolution of related structures at higher charge states by IM-MS: for example Hill and colleagues could resolve the sequence-reversed oligopeptides SNGRG and GRGNS as $[M+2H]^{2+}$ ions but not $[M+H]^{+}$ ions.[29] This may reflect a divergence of three-dimensional structure as the peptides undergo Coulombic unfolding *via* different pathways.

In general, the active derivatives have similar cross-sections to those of the wild-type Defb14, although Defb14-1Cys^{V} has a larger cross-section than the other active peptides at low charge states (z = 5-6). The reason for this is unclear but suggests that the unmodified cysteine peptide has a looser configuration than the other peptides with a smaller net number of charges.

Interestingly, although the non-chemotactic peptides are generally larger than the chemotactic peptides at increased charge states, the width of the arrival time distributions is approximately the same (Figure 3.6). This indicates that, although the sizes of the peptides vary, each exhibits a similar number of different conformations.

The ability to discriminate between chemotactic and non-chemotactic peptides is dependent on the solution conditions prior to ionisation. Under buffered conditions (Table 3.1 and Appendix 2), the peptides generally adopt similar geometries and it is not possible make any distinction between the peptides of different activities. From a solution of acidified water/methanol, the peptides have a greater degree of conformational flexibility and can adopt different three-dimensional structures, as observed both by the widening of the arrival time distributions (Figure 3.7) and the relative change in the collision cross-sections for the substituted peptides. It is possible that the greater structural freedom afforded by these solutions conditions allows the peptides to explore conformations that also exist upon interaction with CCR6. Although this choice of solvent is clearly not representative of the environment of the chemokine receptor *in vivo*, it does allow an *in vacuo* method to distinguish between ions from chemotactic and non-chemotactic peptides for this set of β-defensin derivatives.

3.3.4 Theoretical collision cross-section of Defb14

For comparison with the ion mobility data, a three-dimensional model of Defb14 was obtained by homology modelling (Figure 3.9) and was used as an estimate of the solution-phase structure of Defb14. The collision cross-section of this structure was calculated and compared with the cross-section of a theoretical, fully extended structure of Defb14-1Cys^{V} (Table 3.3).

Figure 3.9 Model structure of Defb14 based on homology to HBD3

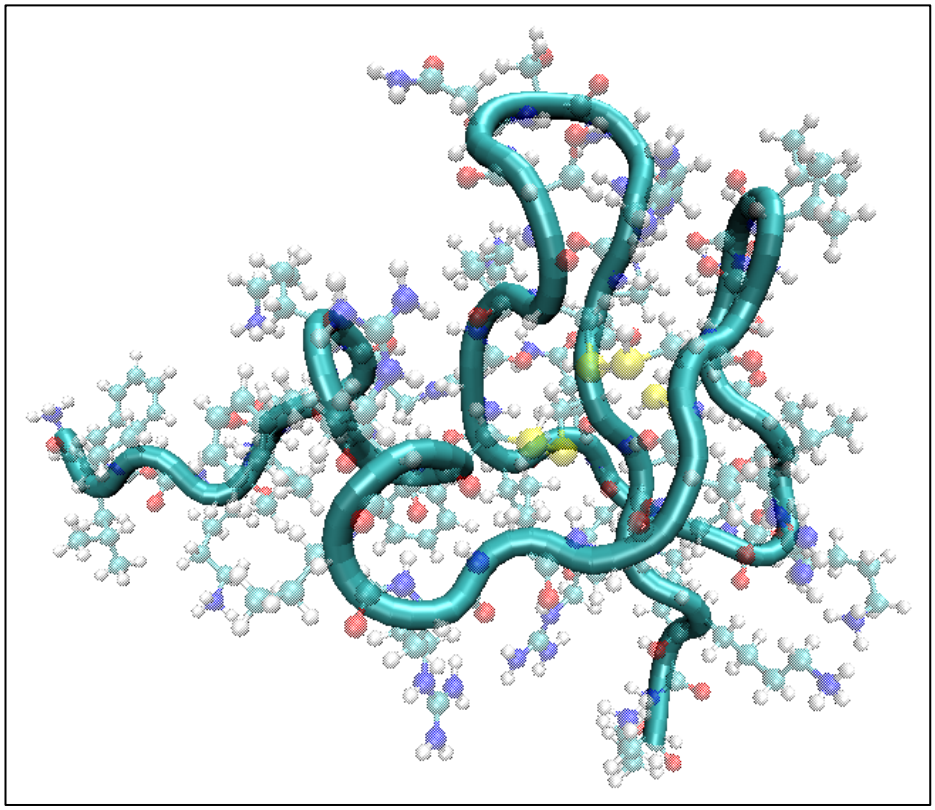

In the above model, the amide backbone is shown in cyan. All other atoms are shown in the CPK style.

Table 3.3 Collision cross-sections (Å^2) calculated for model structures

	EHSS	TM
Defb14 (homology)	900	872
Defb14-1Cys^V (extended)	1624	[a]

[a] *The TM calculation for the extended structure failed, presumably because of its unrealistic geometry.*

Comparison of the collision cross-sections calculated for the theoretical models and those determined experimentally for the derivatives (Tables 3.1 and 3.2) reveals a couple of interesting points. First, the lowest charge states of the derivative ions are more compact than the homology model. This effect is commonly observed in the study of proteins in the gas-phase and is known as a 'hydrophobic collapse'.[30] In solution, the side-chains of polar amino acids will be orientated outwards to interact with the surrounding water molecules. Upon transfer to the more hydrophobic

environment of the gas-phase, these residues will tend to turn inwards to maximise favourable interactions, resulting in a more compact conformation.

For higher charge states, Coulomb repulsion results in expansion of the peptide structure and mitigates this effect. Therefore, as the derivatives unfold in the gas-phase their collision cross-sections become larger than those obtained for the homology model of Defb14 in solution. However the peptides never become as large as the fully extended model of Defb14-1Cys^{V}. Thus it can be concluded that the derivatives do not unfold completely and retain some degree of structure, even under denaturing conditions and at the highest observable charge states.

3.4 Conclusions

Taylor *et al.* illustrated the importance of Cys^{V} to the chemotactic activity of HBD3 and Defb14.[5] In this thesis it has been shown that modification of Cys^{V} alters the unfolding behaviour of linear Defb14 analogues (as evidenced by the differences in collision cross-sections under denaturing conditions). Further investigation is required to fully understand how these subtle chemical changes alter the ability of the peptide to interact favourably with CCR6.

Ion mobility-mass spectrometry has been used to probe the tertiary structures of single-cysteine Defb14 derivatives. The conformations of these peptides in the gas-phase are dependent on the solvent environment prior to ionisation. Under denaturing conditions, the peptide ions exhibit greater conformational freedom and the chemotactic peptides can be distinguished from non-chemotactic derivatives on the basis of their collision cross-section. Ion mobility-mass spectrometry has been used to great effect in several previous studies to probe the unfolding of proteins[18] and, taking a similar approach, here it has been shown how small chemical changes to the structure of a peptide can significantly affect its gas-phase unfolding behaviour.

Traditionally, the energy of protein folding is determined by differential scanning calorimetry, in which the heat absorption upon thermal denaturation of the protein is measured.[31, 32] Additionally, protein stability can be assessed by quantifying the extent of hydrogen/deuterium exchange following chemical denaturation.[33] Either of

these methods could be used in future work to establish if the differences in the gas-phase unfolding of the Defb14-1Cys^{V} derivatives are observed also in solution.

3.5 References

1. R. I. Lehrer, *Nat. Rev. Microbiol.*, 2004, **2**, 727-738.
2. M. E. Selsted and A. J. Ouellette, *Nat. Immunol.*, 2005, **6**, 551-557.
3. K. Taylor, P. E. Barran and J. R. Dorin, *Biopolymers*, 2008, **90**, 1-7.
4. Z. B. Wu, D. M. Hoover, D. Yang, C. Boulegue, F. Santamaria, J. J. Oppenheim, J. Lubkowski and W. Y. Lu, *Proc. Natl. Acad. Sci. U.S.A.*, 2003, **100**, 8880-8885.
5. K. Taylor, D. J. Clarke, B. McCullough, W. Chin, E. Seo, D. Yang, J. Oppenheim, D. Uhrin, J. R. W. Govan, D. J. Campopiano, D. MacMillan, P. Barran and J. R. Dorin, *J. Biol. Chem.*, 2008, **283**, 6631-6639.
6. R. E. W. Hancock and H. G. Sahl, *Nat. Biotechnol.*, 2006, **24**, 1551-1557.
7. E. Kluver, K. Adermann and A. Schulz, *J. Peptide Sci.*, 2006, **12**, 243-257.
8. M. De Cecco, E. S. Seo, D. J. Clarke, B. J. McCullough, K. Taylor, D. Macmillan, J. R. Dorin, D. J. Campopiano and P. E. Barran, *J. Phys. Chem. B*, 2010, **114**, 2312-2318.
9. B. J. McCullough, J. Kalapothakis, H. Eastwood, P. Kemper, D. MacMillan, K. Taylor, J. Dorin and P. E. Barran, *Anal. Chem.*, 2008, **80**, 6336-6344.
10. B. Rost, *Protein Eng.*, 1999, **12**, 85-94.
11. K. Arnold, L. Bordoli, J. Kopp and T. Schwede, *Bioinformatics*, 2006, **22**, 195-201.
12. D. J. Schibli, H. N. Hunter, V. Aseyev, T. D. Starner, J. M. Wiencek, P. B. McCray, B. F. Tack and H. J. Vogel, *J. Biol. Chem.*, 2002, **277**, 8279-8289.
13. A. A. Shvartsburg and M. F. Jarrold, *Chem. Phys. Lett.*, 1996, **261**, 86-91.
14. M. F. Mesleh, J. M. Hunter, A. A. Shvartsburg, G. C. Schatz and M. F. Jarrold, *J. Phys. Chem.*, 1996, **100**, 16082-16086.
15. D. A. Case, T. A. Darden, T. E. Cheatham III, C. L. Simmerling, J. Wang, R. E. Duke, R. Luo, K. M. Merz, D. A. Pearlman, M. Crowley, R. C. Walker, W. Zhang, B. Wang, S. Hayik, A. Roitberg, G. Seabra, K. F. Wong, F. Paesani, X. Wu, S. Brozell, V. Tsui, H. Gohlke, L. Yang, C. Tan, J. Mongan, V. Hornak, G. Cui, P. Beroza, D. H. Mathews, C. Schafmeister, W. S. Ross and P. A. Kollman, *AMBER 9*, University of California, San Francisco, 2006.
16. G. Nemethy, W. J. Peer and H. A. Scheraga, *Annu. Rev. Biophys. Bioeng.*, 1981, **10**, 459-497.
17. S. K. Chowdhury, V. Katta and B. T. Chait, *J. Am. Chem. Soc.*, 1990, **112**, 9012-9013.
18. D. E. Clemmer and M. F. Jarrold, *J. Mass Spectrom.*, 1997, **32**, 577-592.
19. S. J. Valentine, A. E. Counterman and D. E. Clemmer, *J. Am. Soc. Mass Spectrom.*, 1997, **8**, 954-961.
20. P. R. Kemper, N. F. Dupuis and M. T. Bowers, *Int. J. Mass Spectrom.*, 2009, **287**, 46-57.
21. S. D. Pringle, K. Giles, J. L. Wildgoose, J. P. Williams, S. E. Slade, K. Thalassinos, R. H. Bateman, M. T. Bowers and J. H. Scrivens, *Int. J. Mass Spectrom.*, 2007, **261**, 1-12.
22. C. Tyrrell, M. De Cecco, N. L. Reynolds, F. Kilanowski, D. Campopiano, P. Barran, D. Macmillan and J. R. Dorin, *Mol. Immunol.*, 2010, **47**, 1378-1382.
23. R. R. Hudgins, J. Woenckhaus and M. F. Jarrold, *Int. J. Mass Spectrom.*, 1997, **165**, 497-507.
24. A. R. Davidson, *Proc. Natl. Acad. Sci. U.S.A.*, 2008, **105**, 2759-2760.
25. X. I. Ambroggio and B. Kuhlman, *Curr. Opin. Struct. Biol.*, 2006, **16**, 525-530.
26. P. A. Alexander, Y. He, Y. Chen, J. Orban and P. N. Bryan, *Proc. Natl. Acad. Sci. U.S.A.*, 2009, **106**, 21149-21154.
27. D. D. Perrin, B. Dempsey and E. P. Serjeant, *pKa Prediction for Organic Acids and Bases*, Chapman & Hall, London, 1981.

28. Z. Li, M. H. Matus, H. A. Velazquez, D. A. Dixon and C. J. Cassady, *Int. J. Mass Spectrom.*, 2007, **265**, 213-223.
29. C. Wu, W. F. Siems, J. Klasmeier and H. H. Hill, *Anal. Chem.*, 2000, **72**, 391-395.
30. E. Jurneczko and P. E. Barran, *Analyst*, 2011, **136**, 20-28.
31. J. A. Schellman, *Annu. Rev. Biophys. Biophys. Chem.*, 1987, **16**, 115-137.
32. P. L. Privalov and N. Khechina, *J. Mol. Biol.*, 1974, **86**, 665-684.
33. S. Ghaemmaghami, M. C. Fitzgerald and T. G. Oas, *Proc. Natl. Acad. Sci. U.S.A.*, 2000, **97**, 8296-8301.

4 N-terminal modifications of Defb14-1Cys^V

In the previous chapter, the role of a residue near the C-terminus of Defb14-1Cys^V was investigated. In this chapter, the importance of the other end of the molecule, the N-terminus, is considered in terms of the chemotactic and antimicrobial activity of the peptide.

4.1 Introduction

In the preceding chapter it was concluded that the single cysteine residue in Defb14-1Cys^V is not likely to interact directly with the chemokine receptor CCR6. In another study, Rohrl *et al.* produced a fusion protein that comprised an immunoglobulin attached to the C-terminus of Defb14, which chemoattracted cells expressing CCR6.[1] This suggests that the C-terminal region of Defb14 can tolerate some degree of structural adjustment without losing its chemotactic activity. Taken together, these results imply that it is likely to be the N-terminal region of Defb14 that interacts with CCR6.

This hypothesis is supported by a study of human β-defensin 1, conducted by Lubkowski and colleagues, in which a large number of HBD1 analogues were produced with single-point mutations at various positions of the peptide sequence.[2] With regard to chemotactic activity, the most deleterious substitutions were found to occur in the N-terminal α-helical section. Analysis by X-ray crystallography revealed that the mutations did not significantly alter the peptide's tertiary structure, implying that the change in biological function results from changes in the chemical functionalities of the amino acid side-chains.

In addition to its potential significance for chemotaxis, the N-terminal region of Defb14 is also important to the antimicrobial activity of the peptide. In 2008, Taylor *et al.* synthesised two analogues of Defb14-1Cys^V: one corresponding to the N-terminal half of the peptide, the other to the C-terminal side, each being of similar length and net charge.[3] Whilst the C-terminal fragment was found to be inactive against *P. aeruginosa* and *S. aureus*, the N-terminal fragment was as potent as the

full-length peptide *in vitro*. This difference in activity was attributed to the greater number of hydrophobic residues that are present in the N-terminal half. In contrast, Lubkowski and co-workers found that the activity of HBD1 against *E. coli* could be ascribed to four basic residues at C-terminus.

In this chapter, two series of Defb14 analogues are described: one comprising successive N-terminal truncations of Defb14-1Cys^{V} (Figure 4.1); and one containing single-point mutations of Defb14-1Cys^{V} (Figure 4.2). The chemotactic and antimicrobial activity of these derivatives was assayed. The biological activity of the peptides is discussed with reference to their structures, which were examined by circular dichroism spectroscopy, high performance liquid chromatography and ion mobility-mass spectrometry.

Figure 4.1 N-terminal truncated analogues of Defb14-1Cys^{V}

Defb14-1Cys^{V}:	FLPKTLRKFFARIRGGRAAVLNALGKEEQIGRASNSGRKCARKKK
Δ(1-2):	PKTLRKFFARIRGGRAAVLNALGKEEQIGRASNSGRKCARKKK
Δ(1-5):	LRKFFARIRGGRAAVLNALGKEEQIGRASNSGRKCARKKK
Δ(1-8):	FFARIRGGRAAVLNALGKEEQIGRASNSGRKCARKKK
Δ(1-11):	RIRGGRAAVLNALGKEEQIGRASNSGRKCARKKK
Δ(1-14):	GGRAAVLNALGKEEQIGRASNSGRKCARKKK
Δ(1-17):	AAVLNALGKEEQIGRASNSGRKCARKKK

The amino acids deleted in the truncated peptides are shown in brackets after the Δ sign. Each truncated peptide was synthesised with an acetyl group at the N-terminus rather than the free amino group as in Defb14-1Cys^{V}.

Figure 4.2 Single-point mutated analogues of Defb14-1Cys^{V}

Defb14-1Cys^{V}:	F**L**PKTLRKFFARIRGGRAAVLNALGKEEQIGRASNSGRKCARKKK
L2I:	F**I**PKTLRKFFARIRGGRAAVLNALGKEEQIGRASNSGRKCARKKK
L2G:	F**G**PKTLRKFFARIRGGRAAVLNALGKEEQIGRASNSGRKCARKKK
L2K:	F**K**PKTLRKFFARIRGGRAAVLNALGKEEQIGRASNSGRKCARKKK

The amino acid substitutions at position 2 are shown in bold.

4.2 Experimental

4.2.1 Peptide synthesis

All peptides (Figures 4.1 and 4.2) were chemically synthesised by standard solid-phase methodology as described.[4, 5] Each truncated peptide was synthesised with an acetyl group at the N-terminus (thus giving an amide bond rather than the free amino group) to best represent the conformation of the terminal amino acid as it exists in the full-length peptide.

4.2.2 Chemotaxis assays

The migration of human embryonic kidney (HEK293) cells expressing CCR6 in response to peptides at different concentrations was measured using a microchemotaxis chamber. These assays were performed by Kirsty Tyrrell as described.[4]

4.2.3 Bactericidal assays

The minimum bactericidal concentration (MBC) of each peptide was determined for *Pseudomonas aeruginosa* and *Staphylococcus aureus*.[4, 5] These assays were performed by Natalie Reynolds. The MBC is defined as the concentration of peptide required for >99.99% killing of the initial inoculum. Reduction of the peptides, where performed, was performed by the addition of 10 mM dithiothreitol (DTT) to the peptide solution. DTT was used to prevent dimerisation of the peptides *via* cysteine oxidation and the oxidation state of each peptide was confirmed by mass spectrometry.

4.2.4 High performance liquid chromatography

Reversed-phase high performance liquid chromatography (HPLC) was employed to evaluate the relative molecular hydrophobicity of the N-terminal truncation peptides. Samples were prepared both in water and in 10 mM DTT. Each sample contained 50 μM peptide plus 50 μM melittin (Sigma) as an internal standard.

Using an Ultimate 3000 LC system (Dionex), 30 μl of each sample was injected onto a Waters Symmetry C18 column (3.9 x 150 mm). Initial buffer conditions were as follows: 100% eluent A (96% water, 3% acetonitrile, 1% formic acid); 0% eluent B

(4% water, 95% acetonitrile, 1% formic acid); flow rate 1 ml min^{-1}. These conditions were held for 3 minutes before commencing a linear gradient of 0 – 40% eluent B over 40 minutes. Detection by mass spectrometry was performed by splitting the flow 1/50 prior to introduction to the ESI source of a VG Platform II mass spectrometer.

The hydrophobicity of each peptide is proportional to the time it is retained on the column. This is quoted relative to the peptide melittin, as described below:

$$r = \frac{t_{R(peptide)}'}{t_{R(melittin)}'} \qquad \{4.1\}$$

where r is the relative retention time and t_R' is the adjusted retention time (*i.e.* the retention time minus the column dead time).

4.2.5 Circular dichroism spectroscopy

CD spectroscopy was used to probe the secondary structures of peptides in: (i) 10 mM ammonium acetate, pH 6.8, and (ii) 50% water, 50% 2,2,2-trifluoroethanol (TFE). CD spectra were recorded over the wavelength range 190 – 260 nm at 20 °C using a Jasco J-810 spectropolarimeter. A total of five scans were acquired for each sample and averaged to give a final sample spectrum. Buffer in the absence of peptide was used as a reference. Peptide concentration was determined by assaying with bicinchoninic acid (Pierce)[6] and the mean residue ellipticity was calculated at each wavelength.

The CDSSTR algorithm[7] on the DICROWEB server[8] was used to help the assign secondary structure. As this algorithm is only applicable to peptides in aqueous solution, the percentage helicity in 50% TFE was estimated from the ellipticity at 208 and 222 nm, using the empirical relationships given in equations {4.2} and {4.3}.[9, 10]

{ 4.2 } $$\%helix_{208nm} = 100\left(\frac{-[\theta_{208nm}] - (-4000)}{-33000 - (-4000)}\right)$$

{ 4.3 } $$\%helix_{222nm} = 100\left(\frac{-[\theta_{222nm}] - 3000}{-36000 - 3000}\right)$$

4.2.6 Ion mobility-mass spectrometry

Both the truncated and point mutation series of peptides were analysed by IM-MS on the MoQToF as described previously.[11] Peptides were prepared at a concentration of 50 μM. The truncated peptides were dissolved in 10 mM ammonium acetate plus 10 mM dithiothreitol; the mutatation peptides were ionised from 49.5% water, 49.5% methanol, 1.0% formic acid. For these experiments, the temperature and pressure of helium in the drift cell was ~ 28 °C and ~ 3.4 Torr respectively. Measurements were made at eight different drift voltages from 60 to 15 V.

4.3 Results and discussion

4.3.1 Chemotaxis activity

N-terminal truncations

The assays reveal that none of the truncated peptides are chemotactic; only the full-length Defb14-1Cys^{V} peptide chemoattracts cells expressing CCR6.[4] Loss of the first two amino acids (phenylalanine and leucine) renders the peptide inactive, thus one or both of these residues are crucial to the chemotactic activity of the peptide. Comparison of homologous peptides across several mammalian species reveals that the second amino acid is often either leucine or its isomer isoleucine.[4] In contrast, the first residue is much less well conserved, suggesting that it is the second amino acid (leucine) that is more important.

N-terminal modifications

To test the hypothesis that the chemotactic activity of Defb14-1Cys^{V} is dependent on the nature of the second amino acid, a series of mutant peptides was synthesised in which leucine (L) was substituted for either isoleucine (I), glycine (G), or lysine (K).

The L2G and L2K mutants were found to be inactive, whilst the chemotactic activity of the L2I peptide was reduced.[4]

These data confirm that the second amino acid is vital to peptide's ability to act as a chemoattractant. The modest activity of the L2I peptide can be explained by the fact that leucine to isoleucine is a conservative substitution since both amino acids are hydrophobic and of similar size. More drastic changes in the chemical functionality, such as to glycine or positively-charged lysine, are not tolerated.

4.3.2 Bactericidal activity

N-terminal truncations

For this series of peptides, the general trend is that the MBC increases (*i.e.* activity decreases) as more amino acids are removed from the N-terminus.[5] However, significant antimicrobial activity is retained even upon deletion of the first eleven residues. Thereafter, the monomeric peptides become much less potent upon deletion of further amino acids.

Interestingly, truncation of the dimeric peptides does not diminish the activity against *P. aeruginosa* as much as it affects the monomeric peptides. As dimers, even the Δ(1-14) and Δ(1-17) peptides are potent antimicrobials.[5] Similarly, other defensin-related peptides possess greater antimicrobial activity as covalent dimers than as monomers or non-covalent dimers.[12, 13] The greater activity of the dimers may stem from a number of factors, including better protection against bacterial proteases or differences in their hydrophobicity and charge.

N-terminal modifications

The antimicrobial activities of the Defb14-1Cys^{V} mutants did not differ significantly from the parent peptide and therefore the nature of the second amino acid is relevant only to the chemotactic properties of Defb14 and not to its antimicrobial activity.[4]

4.3.3 Hydrophobicity and charge

Hydrophobicity

The relative hydrophobicity of the N-terminal truncation peptides was evaluated by reversed-phase HPLC. Samples were prepared in the presence and absence of DTT

for the analysis of the monomer and dimer respectively. HPLC was not performed for the N-terminal modification peptides since no variation in antimicrobial activity was observed for the single point mutants.

For every peptide analysed, the dimer was retained on the column longer than the monomer: an example of this is shown for the Δ(1-17) peptide (Figure 4.3), with the relative retention times of all the peptides shown in Figure 4.4. This indicates that in each case the dimer is more hydrophobic than the monomer.

This is not intuitive from inspection of the primary structure of the peptides alone. Several scales that have been established to estimate the hydrophobicity of peptides based on their sequence.[14-17] A hydrophobicity 'score' is obtained for every amino acid by measuring the partitioning of individual residues between hydrophobic and hydrophilic solvent phases. The hydrophobicity of a peptide can then be approximated by simple addition of the scores for each amino acid that comprises the primary structure. Figure 4.5 shows the hydrophobicities of the N-terminal truncation peptides estimated using the scale of Wimley and White.[17] It can be seen that, contrary to what is observed experimentally, this scale predicts the dimers to be *less* hydrophobic than the monomers.

Figure 4.3 Selected ion chromatograms for the Δ(1-17) monomer and dimer

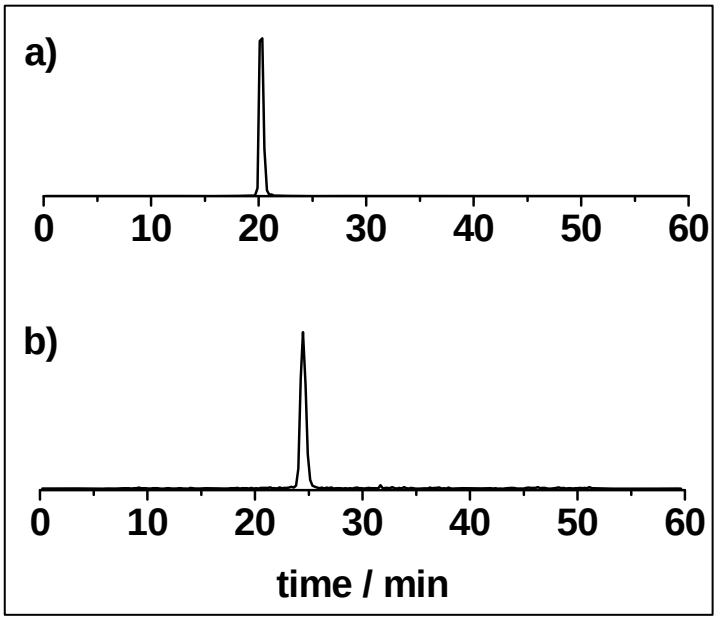

Selected ion chromatograms for Δ(1-17) (a) monomer and (b) dimer ions at m/z 606, corresponding to the $[M+5H]^{5+}$ and $[M+10H]^{10+}$ charge states respectively. The hydrophobicity of each peptide is proportional to the time it is retained on the column.

Figure 4.4 Relative HPLC retention times of the N-terminal truncation peptides

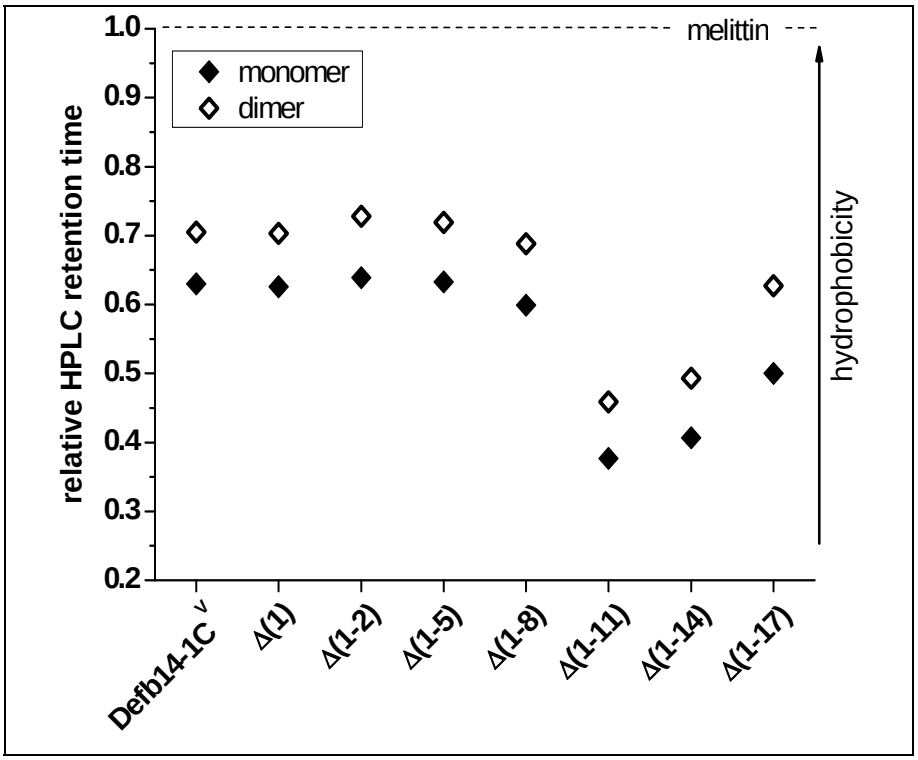

Increasing hydrophobicity is denoted by an increased retention time. All values are quoted relative to the retention time of the peptide melittin.

Figure 4.5 Relative hydrophobicity scores of the N-terminal truncation peptides as estimated by the Wimley and White scale

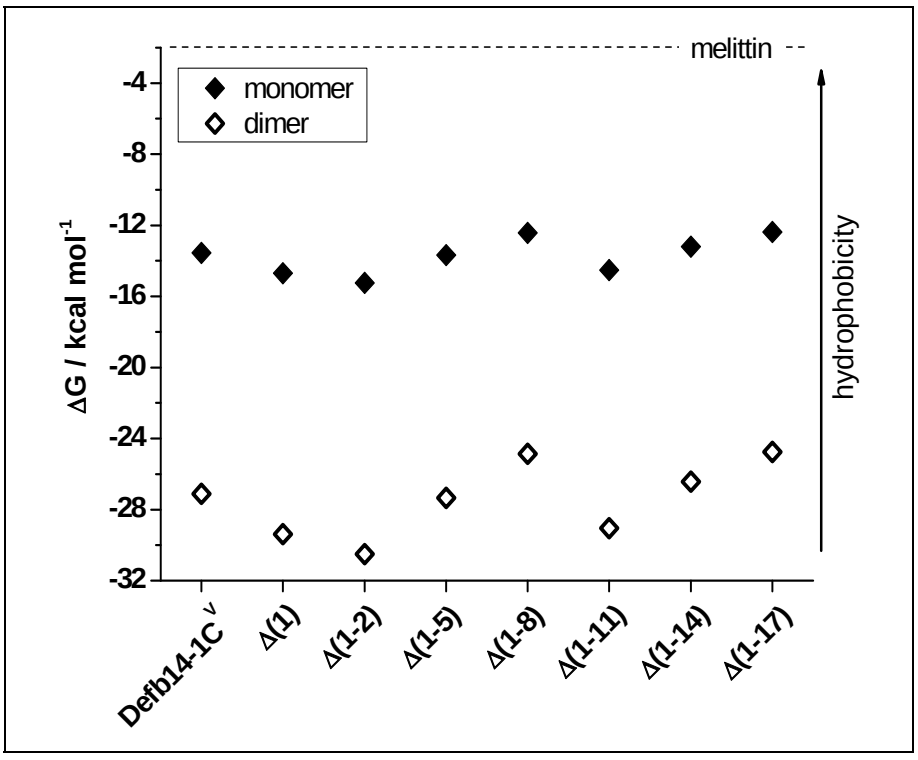

Increasing hydrophobicity is denoted by a less negative value of ΔG.

Thus the dimer hydrophobicity is not well represented by treating the amino acids in an additive fashion. This discrepancy arises because this theoretical approach does not consider the tertiary structures of the peptides. It follows that these dimers are more hydrophobic because of their three-dimensional structure: presumably a number of charged residues are involved in electrostatic interactions between the monomer subunits and are therefore orientated inwards, whilst a greater proportion of hydrophobic residues reside at the outer surface of the peptide.

Comparison of the relative retention times of the different peptides reveals little change in hydrophobicity from the full length Defb14-1Cys^{V} to Δ(1-8). Thereafter, deletion of the amino acids FFA causes an appreciable decrease in hydrophobicity, however this does not result in a significant decrease in activity towards *P. aeruginosa*. Loss of the next three amino acids RIR, *i.e.* truncation Δ(1-14), gives rise to an increase in hydrophobicity, yet this corresponds to the point at which bactericidal activity of the monomeric peptide is lost. Thus, it would appear that the variation in antimicrobial activity within this series of peptides cannot be ascribed solely to differences in their hydrophobicity.

Charge

Each of the peptides in this study with activity towards *P. aeruginosa* has a net charge greater than +7 (Table 4.1). It is possible that, whilst the Δ(1-14) and Δ(1-17) monomers are inactive, the corresponding dimers are potent on account of their increased charge. However the peptide Δ(1-23), which has the same charge as Δ(1-17) but which lacks the hydrophobic residues AAVLNA, is reported by Taylor *et al.* to be inactive as both a monomer and a dimer.[3] Therefore it may be that a balance of both charge *and* hydrophobicity is necessary.

In addition, particular amino acid sequences may be important. A recent study that showed that arginine-to-lysine mutations (which do not alter the charge of the peptide) were deleterious to the activity of an α-defensin.[18] The authors postulate that the arginine side-chains offer stronger interactions with the bacterial membrane. It is notable that two arginines are lost in the truncation from Δ(1-11) to Δ(1-14) in this work.

Table 4.1 Net charge of N-terminal truncation peptides

Peptide	Net charge	
	Monomer	Dimer
Defb14-1Cys^{V}	**12+**	**24+**
Δ(1-2)	**11+**	**22+**
Δ(1-5)	**10+**	**20+**
Δ(1-8)	**8+**	**16+**
Δ(1-11)	**8+**	**16+**
Δ(1-14)	6+	**12+**
Δ(1-17)	5+	**10+**
Δ(1-23)*	5+	10+

*The net charge is based on the protonation state of each amino acid side-chain and the termini at neutral pH. The charges of peptides active towards P. aeruginosa are highlighted in bold. *Data for peptide Δ(1-23) is taken from reference (3) and is included for comparison.*

4.3.4 Circular dichroism spectroscopy

N-terminal truncations

A helical wheel projection of Defb14-1Cys^{V} (Figure 4.6a) predicts that the N-terminal region of the full-length peptide has the potential to form an α-helix, with charged residues concentrated on one face of the helix and hydrophobic residues on the other. The distinction between hydrophilic and hydrophobic faces is less clear in helical wheel projections of the shorter peptides, for example truncation Δ(1-14) (Figure 4.6b). This suggests a lesser propensity to form an α-helix, which may contribute to the diminished activity of the truncated peptides. To verify this experimentally, CD spectroscopy was performed for each of the N-terminal truncation peptides.

Figure 4.6 Helical wheel projections for Defb14-1Cys^{V} and Δ(1-14)

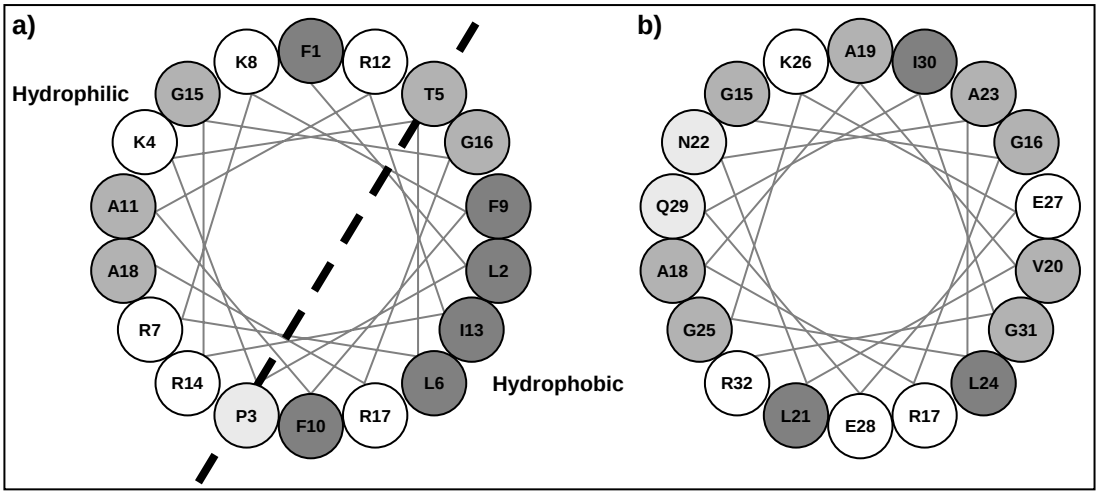

Schematic representation of Defb14-1Cys^{V}: (a) residues 1-18 and (b) residues 15-32, which correspond to the N-terminal regions of the full-length peptide and Δ(1-14) respectively. Residues are plotted so that the angle of rotation between consecutive amino acids is 100°, giving a final representation that looks down the axis of helical rotation. Charged residues are denoted by white circles; increasing hydrophobicity is denoted by increasing shading.

The CD spectrum of each of the N-terminal truncations in aqueous solution exhibits a minimum at ~201 nm (Figure 4.7) that is typical of a peptide whose secondary structure is a mixture of β-sheet or β-turn and random coil. This is in good qualitative agreement with published CD spectra of other β-defensins.[19, 20]

Figure 4.7 CD spectra of N-terminal truncation peptides in aqueous buffer

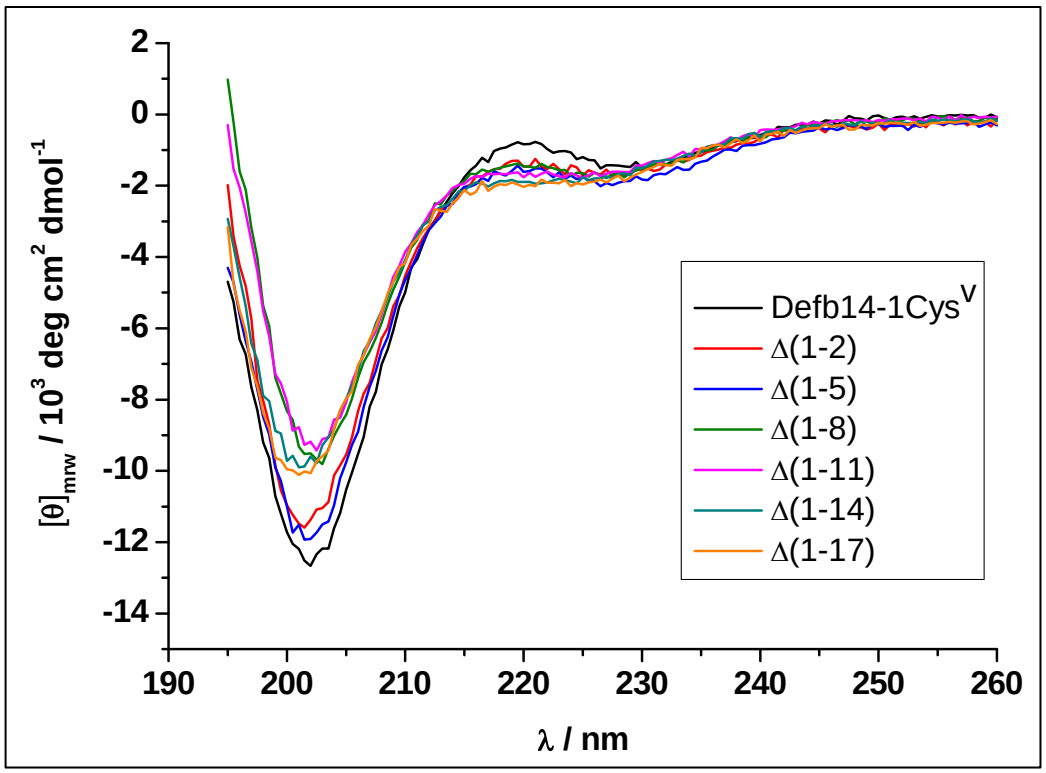

The addition of trifluoroethanol to an aqueous peptide solution can induce helix formation and is commonly used to evaluate the propensity of a given peptide to form an α-helix.[21] The minima observed at 208 and 222 nm in the spectra of each peptide in 50% TFE are characteristic of α-helical structure (Figure 4.8). The intensity of these minima decreases with decreasing chain length, corresponding to a reduction in the percentage helical content of the peptide as an increasing number of amino acids are deleted from the N-terminus (Figure 4.9). This reflects a decreasing propensity to form an α-helix, as suggested by the helical wheel projections.

This may be pertinent to the varying antimicrobial activities of these peptides since the formation of helical oligomers is implicated in the pore model of antimicrobial action.[22] It is notable, therefore, that the shortest peptides with the least helix-forming potential also have the lowest potencies. However, the modes of action of these peptides are not known and the killing mechanism of the truncated peptides may differ from that of the full-length peptide.

Figure 4.8 CD spectra of N-terminal truncation peptides in 50% TFE

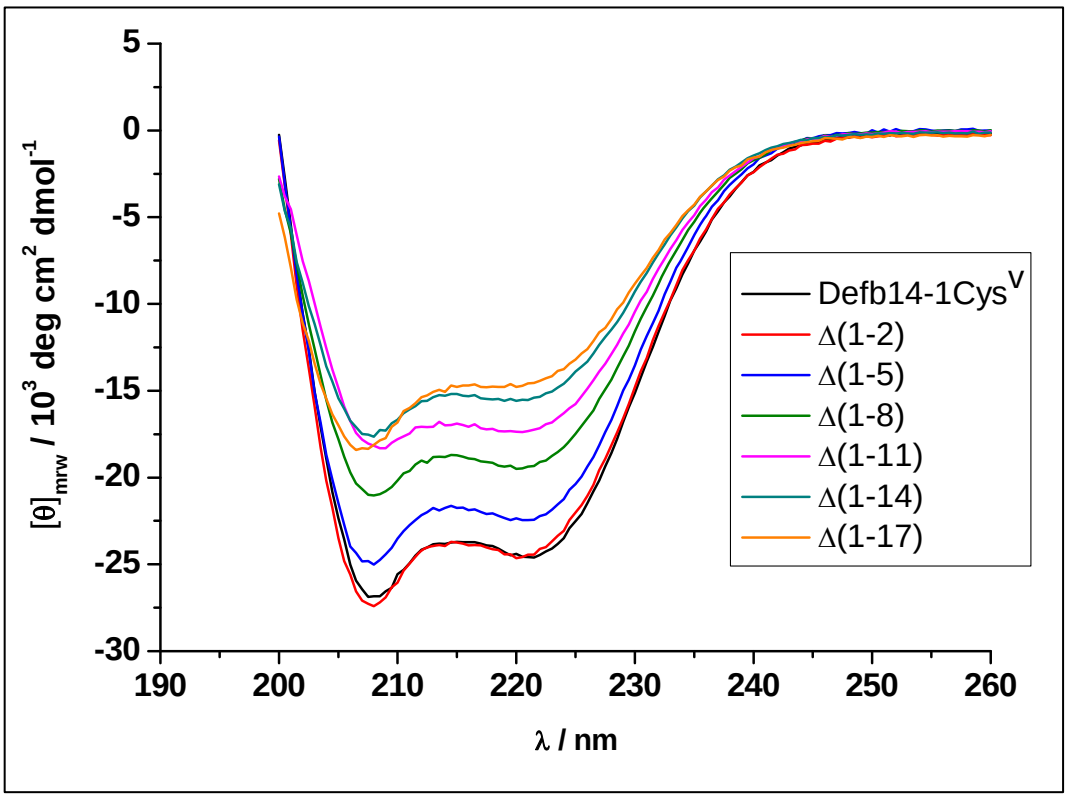

Figure 4.9 Estimated helical content of N-terminal truncation peptides in 50% TFE

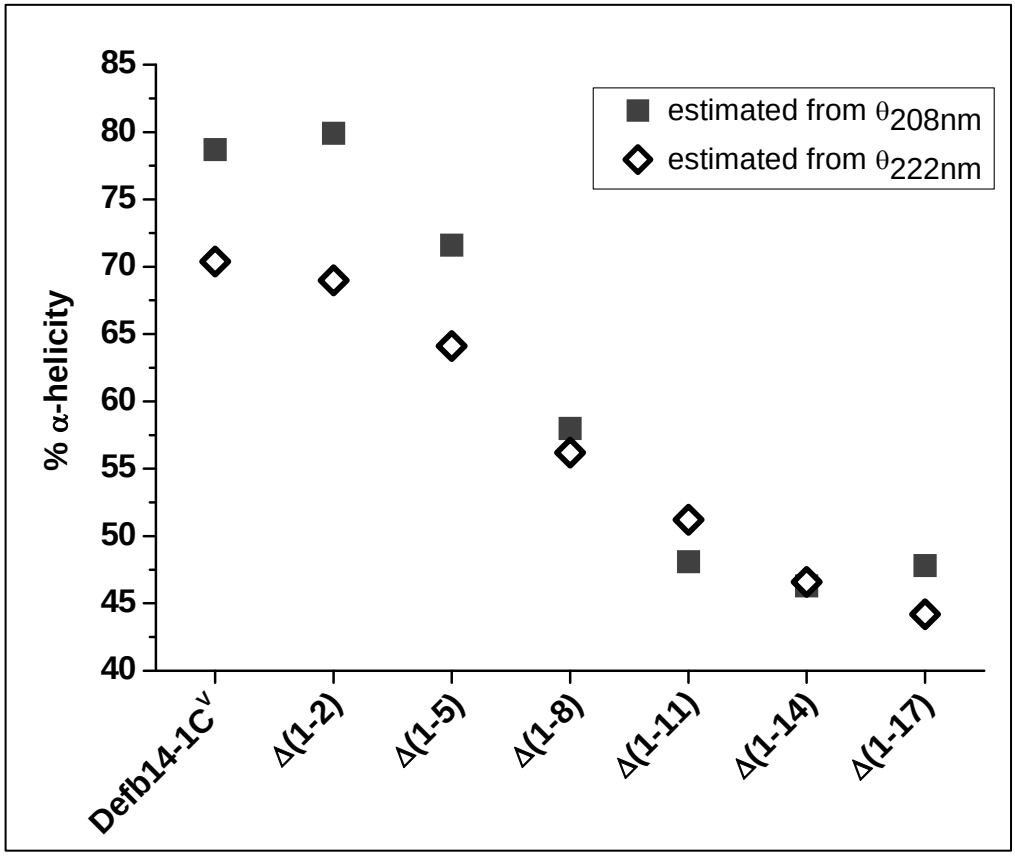

N-terminal modifications

To evaluate if the variation in chemotactic activity upon substitution of leucine-2 is the result of a change in secondary structure, CD spectroscopy was performed. As observed with the other series of peptides, the CD spectrum of each peptide in aqueous solution (Figure 4.10) shows an absorption minimum at ~201 nm that is consistent with a mix of unstructured peptide and β-sheet/turn. In buffer, Defb14-1Cys^{V} exhibits a slightly more intense absorption minimum than that of the other peptides but was found to contain the same proportions of secondary structure as all of the other peptides according to analysis by the CDSSTR algorithm (Appendix 5).[7]

If interaction with the chemokine receptor CCR6 occurs at the N-terminal region of Defb14, this corresponds to an α-helical region of the peptide. Upon the addition of TFE (Figure 4.11), all of these peptides form an α-helix, as evident by the minima at 208 and 222 nm, which strongly suggests that all of these peptides can readily form α-helices under increased hydrophobic conditions, as might exist in the proximity of the receptor on the cell surface.

Figure 4.10 CD spectra of N-terminal modification peptides in aqueous buffer

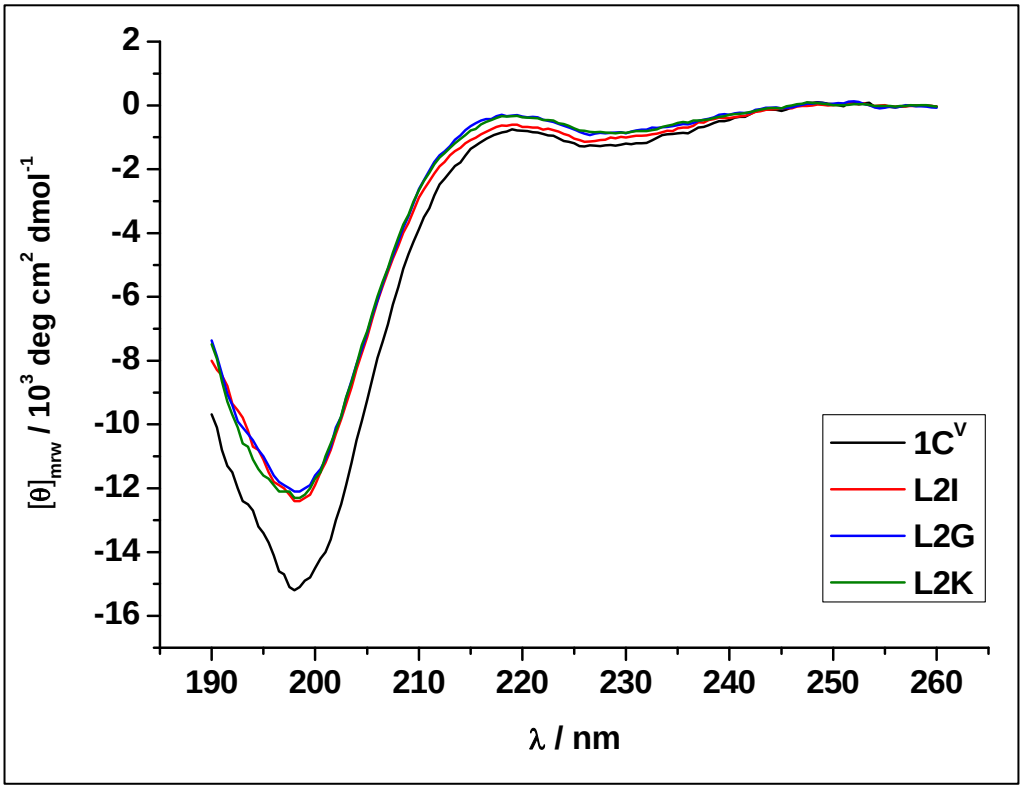

Figure 4.11 CD spectra of N-terminal modification peptides in 50% TFE

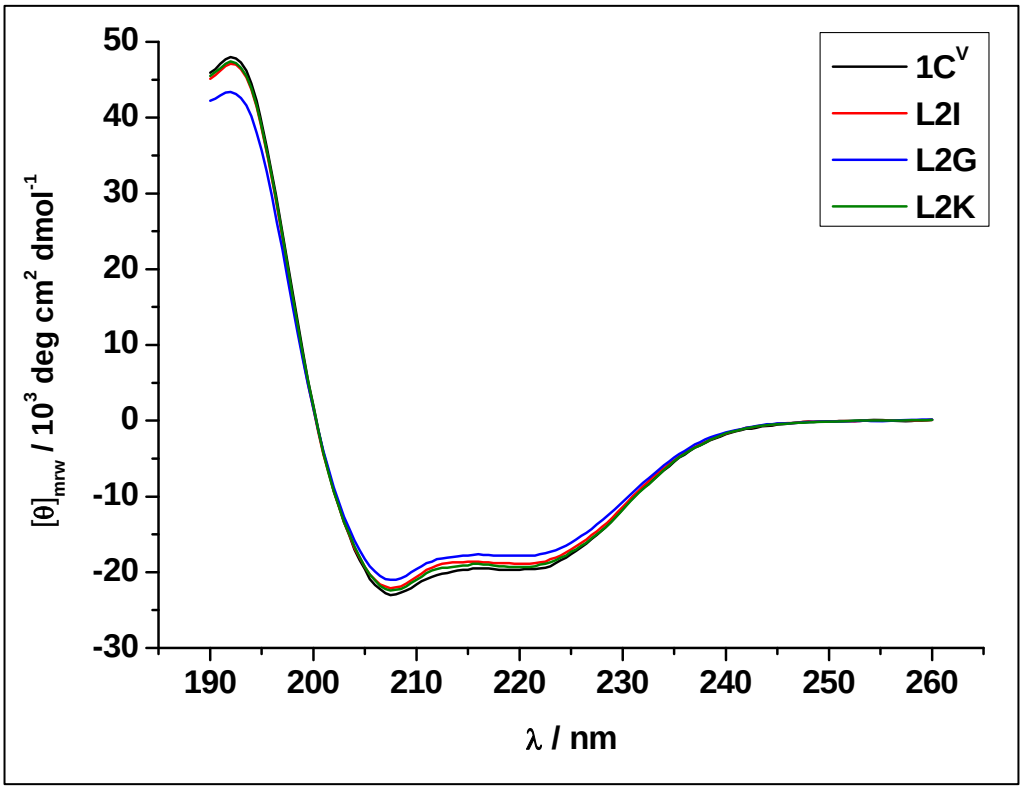

The CD spectrum of Defb14-1 Cys^{V} in 50% TFE is indistinguishable from those of the substitution mutants (Figure 4.11). This demonstrates that substitution of the leucine at position 2 has not diminished the helix-forming potential of the peptide and so the reduced chemotactic activity of the mutants is not due to impairment of the N-terminal helix. In the absence of any evidence of structural change, it suggests that leucine-2 in Defb14 interacts directly with the chemokine receptor CCR6.

4.3.5 Ion mobility-mass spectrometry

N-terminal truncations

As an increasing number of residues are deleted from the peptide, there is a shift towards narrower charge state distributions and a decrease in the highest charge state observed (Figure 4.12).

Figure 4.12 Example mass spectra of N-terminal truncation peptides

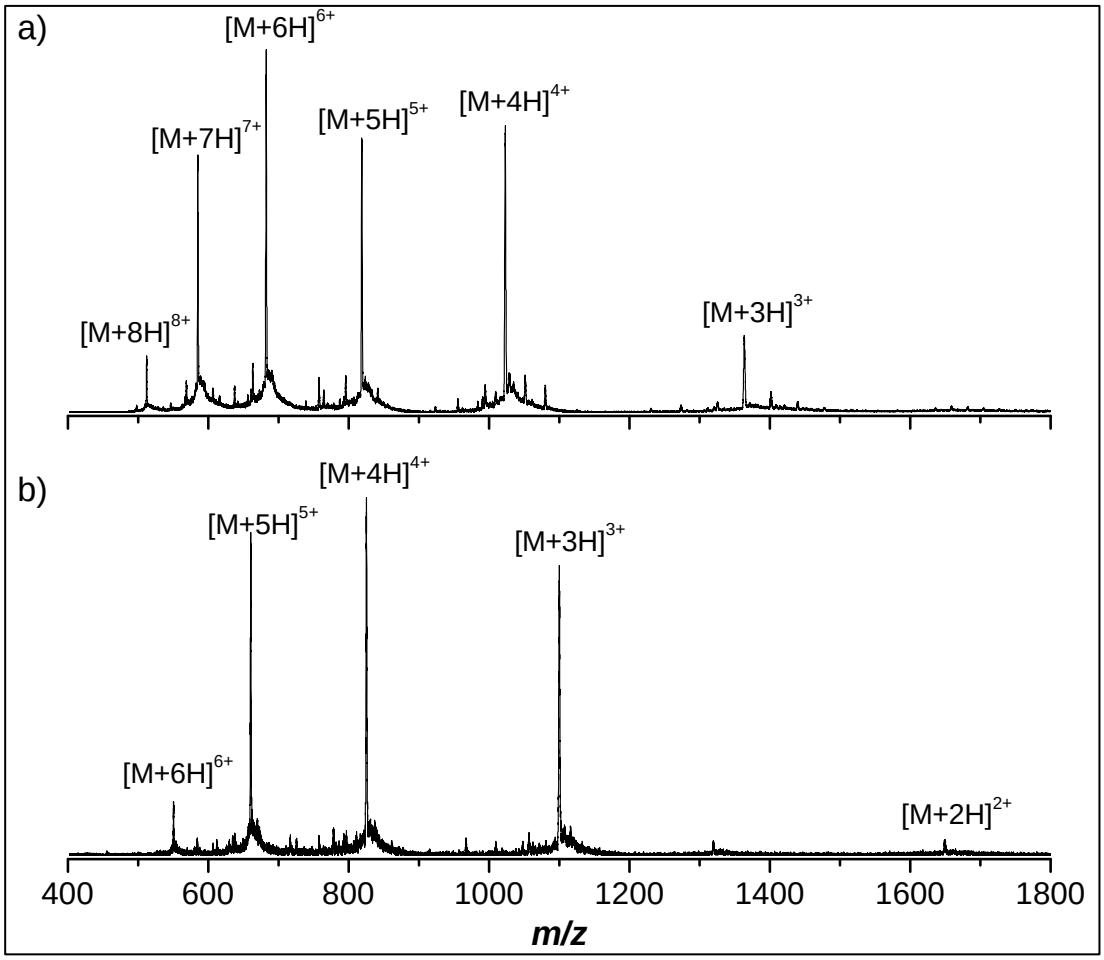

Mass spectra of monomeric truncated peptides: (a) Δ(1-8); (b) Δ(1-14).

For example, charge states $[M+3H]^{3+}$ to $[M+8H]^{8+}$ are observed in the mass spectrum of the Δ(1-8) peptide, compared to $[M+2H]^{2+}$ to $[M+6H]^{6+}$ for Δ(1-14). This is due to the fact that as more amino acids are removed, fewer sites are available for protonation.

Two general trends are apparent in the series of collision cross-sections measured for the N-terminal truncation peptides (Table 4.2). First, the collision cross-section of each peptide increases with increasing charge state as a result of stronger Coulomb repulsion. Second, as might be expected, the overall size of a peptide ion at a given charge state generally decreases with progressive N-terminal truncations.

Table 4.2 Collision cross-sections (Å^2) of N-terminal truncation peptides

	Δ(1-2)	Δ(1-5)	Δ(1-8)
$[M+2H]^{2+}$	n.o.	-	n.o.
$[M+3H]^{3+}$	580 ± 22	-	638 ± 4
$[M+4H]^{4+}$	688 ± 1	-	746 ± 7
$[M+5H]^{5+}$	844 ± 18	-	883 ± 7
$[M+6H]^{6+}$	925 ± 9	-	914 ± 17
$[M+7H]^{7+}$	1008 ± 6	-	967 ± 24
$[M+8H]^{8+}$	1106 ± 5	-	1021 ± 29
$[M+9H]^{9+}$	1182 ± 9	-	n.o.

	Δ(1-11)	Δ(1-14)	Δ(1-17)
$[M+2H]^{2+}$	439 ± 14	397 ± 10	405 ± 16
$[M+3H]^{3+}$	613 ± 3	515 ± 1	567 ± 9
$[M+4H]^{4+}$	749 ± 4	628 ± 3	637 ± 12
$[M+5H]^{5+}$	812 ± 13	689 ± 3	663 ± 12
$[M+6H]^{6+}$	835 ± 21	780 ± 6	670 ± 3
$[M+7H]^{7+}$	881 ± 21	n.o.	n.o.
$[M+8H]^{8+}$	n.o.	n.o.	n.o.
$[M+9H]^{9+}$	n.o.	n.o.	n.o.

Cross-sections of Δ(1-5) were not determined. Species marked n.o. were not observed.

An exception to this is the truncated peptide Δ(1-2), which is actually smaller than the shorter peptide Δ(1-8) at charge states $[M+3H]^{3+}$ to $[M+5H]^{5+}$. As discussed above in section 4.3.4, the N-terminal region of Defb14-1Cys^{V} has the potential to form an α-helix. It is possible that the N-terminal amino acids of truncation Δ(1-2) are part of an α-helix (or other region of localised structure) that is preserved in the gas-phase at low charge states, leading to a more compact conformation.

N-terminal modifications

Ion mobility-mass spectrometry was used to probe the conformation of the N-terminal modification peptides to establish if the range in chemotactic activities observed for this series of peptides is a result of differences in tertiary structure. In the previous chapter, chemotactic peptides could be distinguished from non-chemotactic peptides by IM-MS under denaturing conditions. Based on this observation, the same solution conditions were used in this experiment. As acknowledged previously, the solvent is not representative of the environment *in vivo* but is chosen to allow a wider range of conformations to be surveyed *in vacuo*.

The mass spectra of the N-terminal modification peptides under denaturing conditions are shown in Figure 4.12. Each peptide is observed in charge states $[M+3H]^{3+}$ to $[M+8H]^{8+}$, with no difference in the charge distribution of each peptide. The collision cross-sections of these ions are listed in Table 4.3. The collision cross-sections measured for the unmodified peptide, Defb14-1Cys^{V}, are available in reference (11) and in Appendix 1.

Once again the collision cross-section of each peptide increases with increasing charge state. At most charge states, the mean collision cross-section of each of the N-terminal modification peptides is the same within experimental error. Moreover, similar arrival time distributions are observed (Figure 4.13), demonstrating that each peptide exhibits the same range of conformations. An exception to this is the $[M+5H]^{5+}$ ion of the L2K peptide, which is larger than both the L2G and L2I analogues. In general, however, the mutants all adopt similar conformations *in vacuo*, implying that the tertiary structures of these peptides are similar in solution.

Figure 4.12 Mass spectra of N-terminal modification peptides

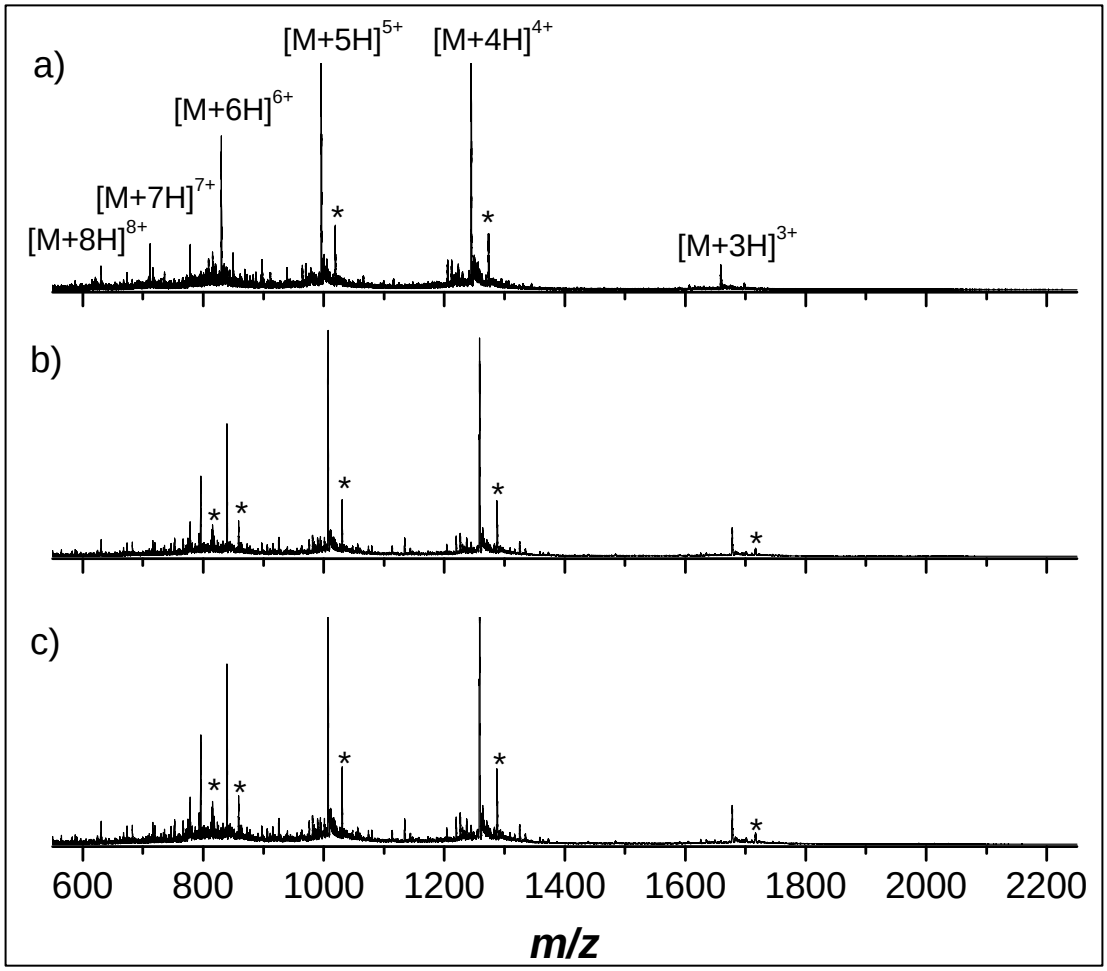

Mass spectra of (a) L2G; (b) L2I; (c) L2K modification peptides. Charge states $[M+3H]^{3+}$ to $[M+8H]^{8+}$ are indicated for L2G; a similar distribution is observed for the other peptides. Peaks marked with an asterisk (*) correspond to an adduct of mass +116 Da.

Table 4.3 Mean collision cross-sections (Å^2) of N-terminal modification peptides

Peptide	L2G	L2I	L2K
$[M+3H]^{3+}$	n.o.	n.o.	n.o.
$[M+4H]^{4+}$	772 ± 6	777 ± 22	797 ± 4
$[M+5H]^{5+}$	937 ± 6	925 ± 37	997 ± 2
$[M+6H]^{6+}$	1029 ± 4	1030 ± 2	1045 ± 27
$[M+7H]^{7+}$	1070 ± 13	1089 ± 18	1098 ± 3
$[M+8H]^{8+}$	1128 ± 26	1101 ± 36	1126 ± 33

Errors are quoted as the standard error of the mean. Species marked n.o. were not observed at sufficient intensity to obtain accurate collision cross-sections by IM-MS.

Figure 1.13 Drift time distributions of the $[M+8H]^{8+}$ ion

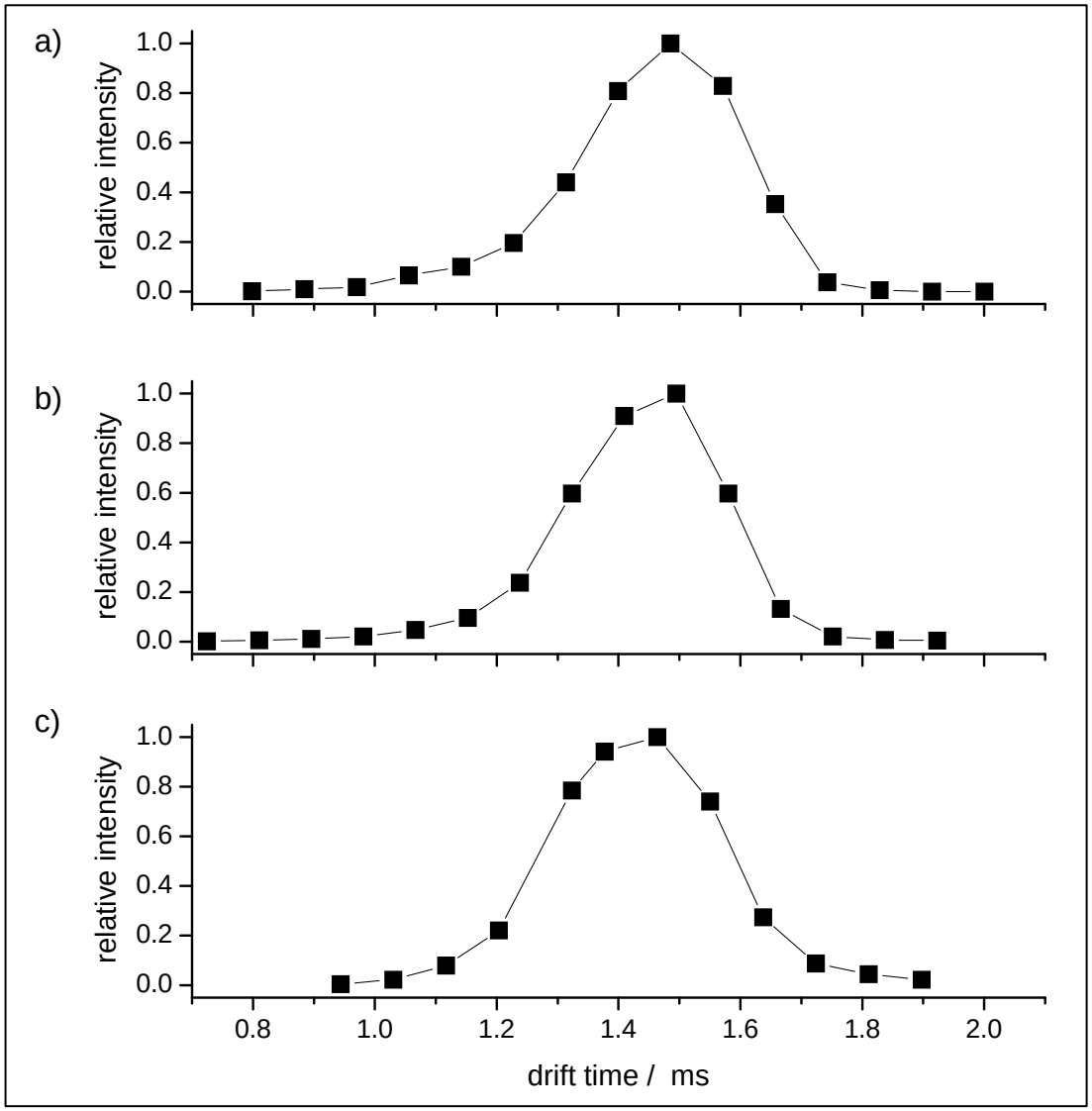

Drift times for the $[M+8H]^{8+}$ charge state of each N-terminal modification peptide at a drift voltage of 20 V: (a) L2I; (b) L2G; (c) L2K. Drift times are scaled to 3.5 Torr and 300 K to account for fluctuations in pressure and temperature between experiments

The collision cross-sections of the mutants are generally larger than those reported for the unmodified peptide Defb14-1Cys^{V}.[11] This may reflect a partial destabilisation of the three-dimensional fold upon substitution of leucine. However, no distinction can be made between the tertiary structures of the peptides L2G, L2I and L2K despite their varying chemotactic activities. Only the side-chain of the second residue was modified: the absence of any other observable structural change supports the hypothesis that the second amino acid of Defb14 interacts directly with the chemokine receptor CCR6.

4.4 Conclusions

In this chapter, the N-terminal region of Defb14 was investigated using two series of peptides based on the single-cysteine peptide Defb14-1Cys^{V}. Single-point mutations revealed that the second amino acid – leucine – is important to the chemotactic activity of this molecule. Analysis by CD spectroscopy and IM-MS indicated that these modifications did not induce significant changes in the three-dimensional structure of the peptide. These data, coupled with the observation that a conservative leucine-to-isoleucine substitution retains some chemotactic activity, suggest that the second residue interacts directly with the receptor CCR6.

A succession of N-terminal truncations showed that deletion of up to eleven of the initial amino acids did not severely impair antimicrobial potency. This has important implications for the design of peptide therapeutics, where there is a drive to identify active, shorter analogues since they are cheaper to manufacture. Loss of further amino acids did result in a decrease in antimicrobial activity. Using reverse-phase HPLC, it was established that this was not due to a reduction in hydrophobicity and therefore likely to be a result of decreased net positive charge. In addition, the inactive peptides were shown by CD spectroscopy to have a lesser ability to form an α-helix under more hydrophobic conditions, as would exist in the proximity of a bacterial membrane. Whilst the mechanism by which these peptides kill bacteria remains unclear, this finding may be relevant if the peptides act by forming pores in the bacterial membrane since helix formation is required by this mechanism.

4.5 References

1. J. Rohrl, D. Yang, J. J. Oppenheim and T. Hehlgans, *J. Biol. Chem.*, 2008, **283**, 5414-5419.
2. M. Pazgier, A. Prahl, D. M. Hoover and J. Lubkowski, *J. Biol. Chem.*, 2007, **282**, 1819-1829.
3. K. Taylor, D. J. Clarke, B. McCullough, W. Chin, E. Seo, D. Yang, J. Oppenheim, D. Uhrin, J. R. W. Govan, D. J. Campopiano, D. MacMillan, P. Barran and J. R. Dorin, *J. Biol. Chem.*, 2008, **283**, 6631-6639.
4. C. Tyrrell, M. De Cecco, N. L. Reynolds, F. Kilanowski, D. Campopiano, P. Barran, D. Macmillan and J. R. Dorin, *Mol. Immunol.*, 2010, **47**, 1378-1382.
5. N. L. Reynolds, M. De Cecco, K. Taylor, C. Stanton, F. Kilanowski, J. Kalapothakis, E. Seo, D. Uhrin, D. Campopiano, J. Govan, D. Macmillan, P. Barran and J. R. Dorin, *Antimicrob. Agents Chemother.*, 2010, **54**, 1922-1929.
6. P. K. Smith, R. I. Krohn, G. T. Hermanson, A. K. Mallia, F. H. Gartner, M. D. Provenzano, E. K. Fujimoto, N. M. Goeke, B. J. Olson and D. C. Klenk, *Anal. Biochem.*, 1985, **150**, 76-85.

7. W. C. Johnson, *Proteins: Struct., Funct., Genet.*, 1999, **35**, 307-312.
8. L. Whitmore and B. A. Wallace, *Biopolymers*, 2008, **89**, 392-400.
9. N. Greenfield and G. D. Fasman, *Biochemistry*, 1969, **8**, 4108-4116.
10. J. D. Morriset, J. S. K. David, H. J. Pownall and A. M. Gotto, *Biochemistry*, 1973, **12**, 1290-1299.
11. B. J. McCullough, J. Kalapothakis, H. Eastwood, P. Kemper, D. MacMillan, K. Taylor, J. Dorin and P. E. Barran, *Anal. Chem.*, 2008, **80**, 6336-6344.
12. D. J. Campopiano, D. J. Clarke, N. C. Polfer, P. E. Barran, R. J. Langley, J. R. W. Govan, A. Maxwell and J. R. Dorin, *J. Biol. Chem.*, 2004, **279**, 48671-48679.
13. N. Antcheva, F. Morgera, L. Creatti, L. Vaccari, U. Pag, S. Pacor, Y. Shai, H. G. Sahl and A. Tossi, *Biochem. J.*, 2009, **421**, 435-447.
14. T. P. Hopp and K. R. Woods, *Proc. Natl. Acad. Sci. U.S.A.*, 1981, **78**, 3824-3828.
15. G. D. Rose, A. R. Geselowitz, G. J. Lesser, R. H. Lee and M. H. Zehfus, *Science*, 1985, **229**, 834-838.
16. D. Eisenberg, R. M. Weiss and T. C. Terwilliger, *Proc. Natl. Acad. Sci. U.S.A.*, 1984, **81**, 140-144.
17. W. C. Wimley and S. H. White, *Nat. Struct. Biol.*, 1996, **3**, 842-848.
18. R. A. Llenado, C. S. Weeks, M. J. Cocco and A. J. Ouellette, *Infect. Immun.*, 2009, **77**, 5035-5043.
19. E. Kluver, S. Schulz-Maronde, S. Scheid, B. Meyer, W. G. Forssmann and K. Adermann, *Biochemistry*, 2005, **44**, 9804-9816.
20. S. P. Liu, L. Zhou, J. Li, A. Suresh, C. Verma, Y. H. Foo, E. P. H. Yap, D. T. H. Tan and R. W. Beuerman, *Chembiochem*, 2008, **9**, 964-973.
21. S. M. Kelly, T. J. Jess and N. C. Price, *Biochim. Biophys. Acta*, 2005, **1751**, 119-139.
22. K. A. Brogden, *Nat. Rev. Microbiol.*, 2005, **3**, 238-250.

5 Interaction of human β-defensins 2 and 3 with glycosaminoglycans

In this chapter the ability of human β-defensins 2 and 3 to behave like chemokines, particularly in terms of their oligomerisation properties and their interactions with glycosaminoglycans, is examined.

5.1 Introduction

β-defensins share several structural and functional similarities to another family of immunomodulatory proteins known as chemokines.[1, 2] Chemokines contain four highly conserved cysteine residues (compared with six in β-defensins) that stabilise a well-defined three-dimensional structure. The tertiary structure of chemokines contains three anti-parallel β-strands and a C-terminal α-helix, which is somewhat reminiscent of the characteristic fold of β-defensins (Figure 5.1). Chemokines are classified according to the spacing of the first two cysteines: for example these residues are adjacent in CC chemokines, whereas in CXC chemokines they are separated by one amino acid.

Figure 5.1 Tertiary structures of the chemokine CCL20 (ref 3) and human β-defensin 3 (ref 4)

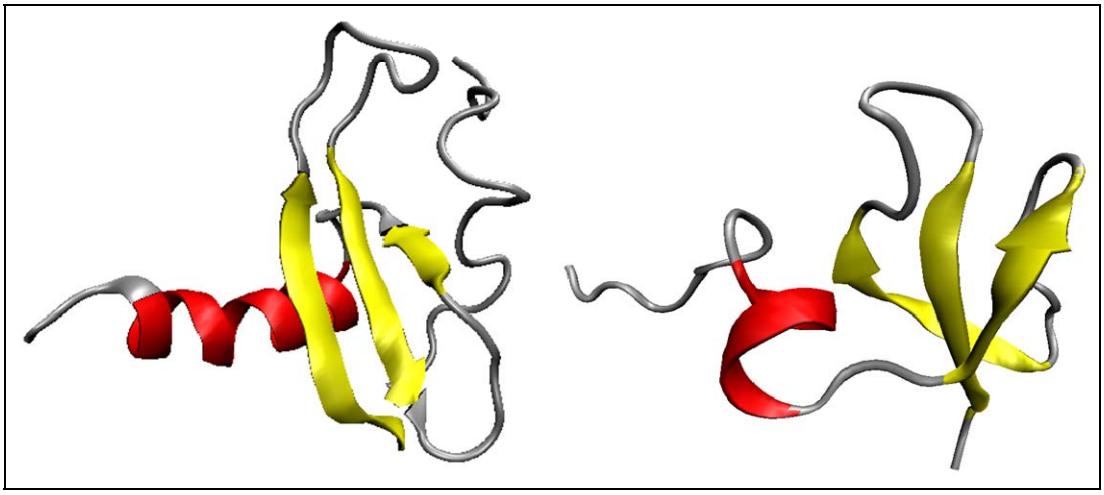

NMR structures of the chemokine CCL20 (left) and HBD3 (right). Both peptides contain three anti-parallel β-strands and an α-helix.

β-defensins and chemokines have a notable function in common: the ability to induce the migration of immune cells.[5, 6] Indeed, this is the primary role of chemokines; their name deriving from the fact that they are *chemo*tactic cyto*kines*. The process of chemotaxis begins by the chemokine binding to and activating a G protein-coupled receptor (GPCR). Interestingly, several chemokines bind more than one receptor and most receptors interact with numerous chemokines. However, whilst it appears that there is a large degree of redundancy in this system, in general receptors are only activated by chemokines belonging to the same structural sub-family (CC, CXC, *etc.*). The chemokine CCL20 induces chemotaxis *via* the receptor CCR6.[7] This receptor is also activated by some β-defensins, including HBD2 and HBD3.[5, 8] Similar to the CC chemokines, β-defensins possess two adjacent cysteine residues, although these are located near the C- rather than N-terminus.

An important attribute of chemokines that relates to their chemotactic activity is their ability to bind glycosaminoglycans (GAGs).[1, 9] In an influential study, Proudfoot *et al.* mutated the GAG binding sites of three chemokines and assessed their chemotactic activity.[10] All were active *in vitro* but could not recruit cells *in vivo*. GAGs are polysaccharides located on the surface of mammalian cells. By binding to GAGs on the surfaces of cells, chemokines can overcome vascular flow *in vivo* to form a concentration gradient that is necessary for directional cell migration. In addition to helping chemokines adhere to cells, it is speculated that GAGs may play a more active role in cell signalling. It is believed that chemokines could be directed to different locations on the basis of their varying affinity for different types of GAG.[11]

Another feature of the chemokine-GAG interaction is its effect on oligomerisation.[1, 12] Several chemokines are known to form oligomers in solution: most exist as dimers, though tetramers (effectively 'dimers of dimers') have also been observed. By binding to GAGs, the population of chemokine dimers is increased, whilst oligomerisation is promoted also for those chemokines that are observed only as monomers alone in solution. McCornack *et al.* studied this quantitatively and found that GAG binding lowered the dissociation co-efficient (K_d) of chemokine dimers by approximately one order of magnitude.[13]

Leary and collaborators have applied mass spectrometry to the study of chemokine oligomerisation and GAG binding. For example, they observed that certain chemokines were capable of forming heterodimers in the presence of GAG.[14] In another study, the pentasaccharide fondaparinux was found to preferentially bind dimers of the chemokine CCL2.[15] This GAG-bound complex was more resistant towards collision-induced dissociation than the dimer alone.

Despite the fact that the monomeric proteins of different chemokine sub-families have a common three-dimensional structure, the CC and CXC chemokine dimers have distinct arrangements of the subunits. In CC chemokines the dimer interface generally occurs between residues near the N-terminus, whereas CXC chemokines tend to dimerise at the first β-strand. This difference in quaternary structure had previously been used to justify the selectivity of the receptors for a particular chemokine sub-family, however, it is now believed that it is the monomeric protein that interacts with the GPCR.[16] Clark-Lewis and co-workers synthesised a mutated form of the chemokine CXCL8 that was unable to form a dimer and demonstrated that the monomeric analogue possessed the same ability to chemoattract cells *in vitro* as the wild-type protein.[16] This is supported by a similar study in which the prevention of CCL2 dimer formation did not lead to loss in activity *in vitro*.[10] In contrast, it has been demonstrated that the dimerisation of CCL2 and other chemokines is necessary to induce cell migration *in vivo*.[10] This implies that although it is the monomer that binds and activates the receptor, oligomerisation is necessary for some other facet of the chemotaxis process *in vivo*. One possibility is that the increased aggregation of chemokines decreases their susceptibility to proteolysis.

Several studies have investigated the multimeric state of β-defensins. Most β-defensins have been observed to exist predominantly as monomers in solution.[4, 17, 18] By X-ray crystallography, HBD2 was found to exist mainly as a dimer in the solid-state, with an octameric species also present.[19] The dimer is formed *via* interactions between the first β-strands of each monomer, creating a six-stranded β-sheet. In solution HBD2 is a monomer at sub-millimolar levels[4, 18] but a dimer at elevated concentrations.[19] HBD3 has also been observed as a dimer in solution by various

methods, although the dimer interface could not be identified by homonuclear NMR.[4]

In contrast, very few studies have considered the interaction of β-defensins with glycosaminoglycans. McCullough *et al.* examined the conformational changes of a series of defensin-related peptides upon binding a heparin-derived disaccharide.[20] Schmidtchen and co-workers reported that an α-defensin binds dermatan sulfate.[21] Both of these studies found that GAG binding diminished the antimicrobial activity of canonically-folded defensins. Neither study reported GAG-induced oligomerisation of defensins nor considered GAG binding in the context of chemotaxis.

In a very recent study, conducted in parallel with the research contained in this thesis, Seo *et al.* used a gel mobility shift assay (GMSA) and NMR spectroscopy to probe the binding of GAGs to HBD2.[22] Using a range of heparin oligosaccharides, the GMSA indicated that tetrasaccharide was the minimum size of oligosaccharide required for binding to HBD2. Two GAGs, a pentasaccharide (fondaparinux) and a hexasaccharide (dermatan sulfate), were studied by NMR. The findings are discussed in more detail later in this chapter but, in brief, both GAGs bound HBD2.

Given the apparent similarity of β-defensins and chemokines, this chapter investigates the interaction of β-defensins and glycosaminoglycans by mass spectrometry and ion mobility-mass spectrometry. The potential implications for chemotactic activity are discussed.

5.2 Experimental

5.2.1 Peptide synthesis and glycosaminoglycans

The peptides HBD2 and HBD3 were chosen as examples of natively-folded, chemotactic β-defensins. HBD2 was produced by recombinant expression in *E. coli* and purified by Emily Seo as described previously.[23] HBD3, produced by solid-phase synthesis, was purchased from the Peptide Institute (Osaka, Japan).

Three glycosaminoglycans were used in this study: heparin dp4, fondaparinux and dermatan sulfate dp6 (Figure 5.2), where ‘dp’ refers to the degree of polymerisation.

Figure 5.2 Structures of glycosaminoglycans used in this study

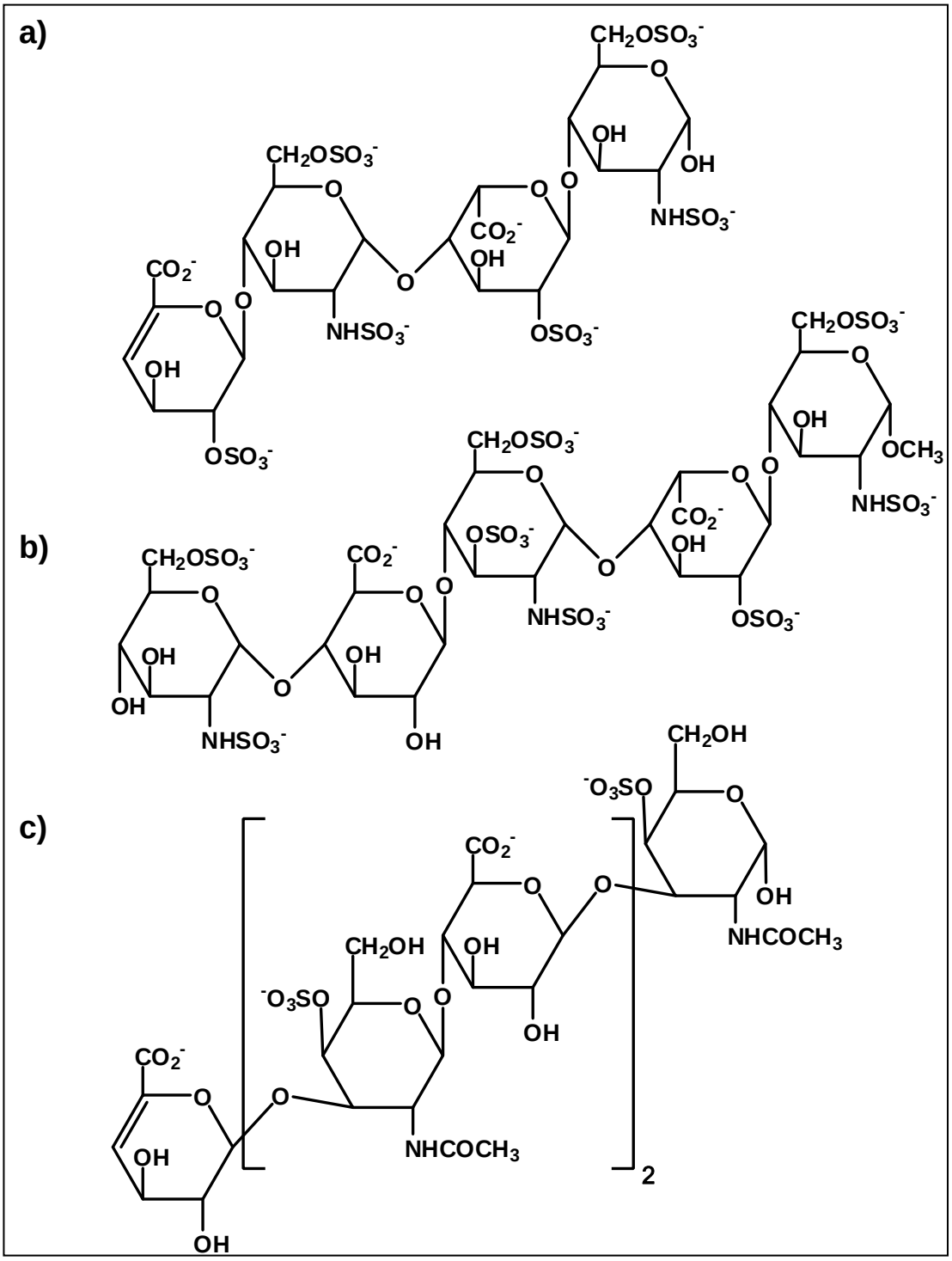

Structures of: (a) heparin dp4; (b) fondaparinux; (c) dermatan sulfate dp6.

Heparin and fondaparinux are oligosaccharides used to mimic heparin sulfate. Heparin sulfate occurs in all animal tissues and binds a variety of proteins in its proteoglycan form.[24] Dermatan sulfate is found mostly in skin[25] and was chosen

because of its possible interaction with human β-defensins 2 and 3, which are both expressed in epithelial cells.[26]

Fondaparinux sodium was a gift from GlaxoSmithKline. Heparin dp4 and dermatan sulfate dp6 were prepared by Conny Johansson and Haris Panagos using an enzymatic digestion protocol as described.[27]

5.2.2 Mass spectrometry

Stock solutions of the glycosaminoglycans were prepared at 1 mg/ml in water and dialysed overnight versus water using a 1,000 molecular weight cut-off Micro DispoDialyzer (Harvard Apparatus, MA, USA). Samples were prepared in 20 mM ammonium acetate (pH 6.8) at 1:1 molar ratios of GAG to HBD2 or HBD3. The final peptide concentration was 135 μM. Mass spectra were recorded on a Q-ToF II mass spectrometer (Waters, Manchester, UK), with ions produced by positive nano-electrospray ionization. Identical tuning conditions were employed for each sample. Photographs of the nano-electrospray tips were obtained using an LCD digital microscope (Aigo, Beijing, China) at 100x magnification.

5.2.3 Ion mobility-mass spectrometry

Samples of HBD2, HBD2 plus fondaparinux and HBD3 were prepared as described above and analysed by IM-MS on the MoQToF as detailed previously.[28] For these experiments, the temperature and pressure of helium in the drift cell was approximately 28 °C and 3.2 Torr respectively. Measurements were made at eight different drift voltages from 60 to 15V.

5.2.4 Estimation of collision cross-sections from PDB structures

The following protein databank entries were downloaded: 1FD3 (X-ray crystal structure of HBD2 dimer)[19], 1FQQ (NMR structure of HBD2 monomer)[18] and 1KJ6 (NMR structure of HBD3 monomer)[4]. Using the Leap program in Amber 9, hydrogen atoms were added to the crystal structure of HBD2 and a limited energy minimisation was performed on the resulting structure.[29] This procedure was not carried out for the NMR structures of HBD2 and HBD3, which contain explicit hydrogens. The rotationally-averaged collision cross-section of each structure was then calculated according to the trajectory method, using the program Mobcal.[30] For

the NMR data, collision cross-sections were calculated for each of the twenty lowest energy structures available. For the crystal structure, the collision cross-section was calculated for the dimer and its monomer subunit.

5.2.5 Chemotaxis

The *in vitro* chemotactic activity of HBD2 towards cells expressing CCR6 was assessed in the presence and absence of GAG. These experiments were performed by Kirsty Tyrrell as reported previously.[31] For the assays with GAG, an equimolar amount of fondaparinux to HBD2 was used.

5.3 Results and discussion

5.3.1 Mass spectrometry

Human β-defensin 2

The mass spectrum of HBD2 alone in 20 mM ammonium acetate buffer is shown overleaf (Figure 5.3a). Charge states $[M+3H]^{3+}$ to $[M+5H]^{5+}$ are observed for the HBD2 monomer, in addition to a small peak corresponding to the $[M+5H]^{5+}$ charge state of a HBD2 dimer (shown enlarged in Figure 5.4a). From studying the peak intensities it can be concluded that the peptide exists predominantly as a monomer in solution at 135 μM, in agreement with the observations of others by NMR spectroscopy.[4, 17] The narrow charge state distribution of the monomer indicates that the peptide adopts a compact tertiary structure in solution. This is clearly attributable to the three disulfide bonds in HBD2, which help to maintain a tight three-dimensional fold.

The HBD2 dimer was only seen clearly as a $[M+5H]^{5+}$ ion; other charge states may be present also but the signal intensities are too weak to be detected. The identification of a HBD2 dimer by mass spectrometry is interesting. As discussed previously, the crystal structure of HBD2 is that of a dimer (or multiple thereof).[19] This is supported by a dynamic light scattering experiment that indicated that HBD2 exists as a dimer in solution, but only at concentrations greater than 3 mM. The concentration of peptide in those experiments was considerably higher than in the solutions used in this experiment prior to ionisation.

Figure 5.3 Mass spectra of HBD2 in the absence and presence of glysoaminoglycan

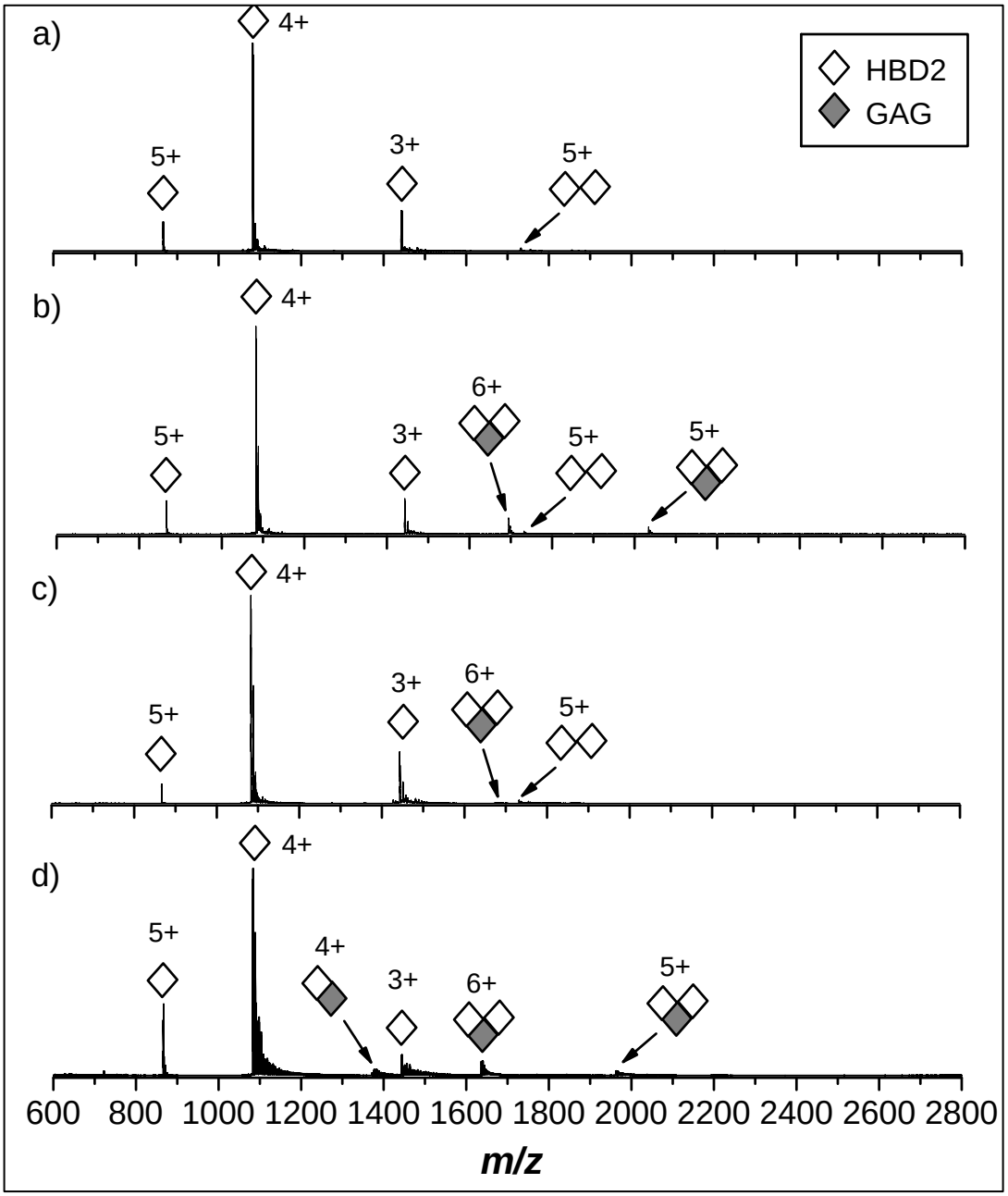

Mass spectra of: (a) HBD2 only; (b) HBD2 plus fondaparinux; (c) HBD2 plus dermatan sulfate dp6; (d) HBD2 plus heparin dp4. GAGs present at 1:1 ratio in spectra (b)-(d). List of expected/observed masses given in Appendix 6.

Figure 5.4 Mass spectra of HBD2 in the absence and presence of glysoaminoglycan, *m/z* region 1620 – 1750 enlarged

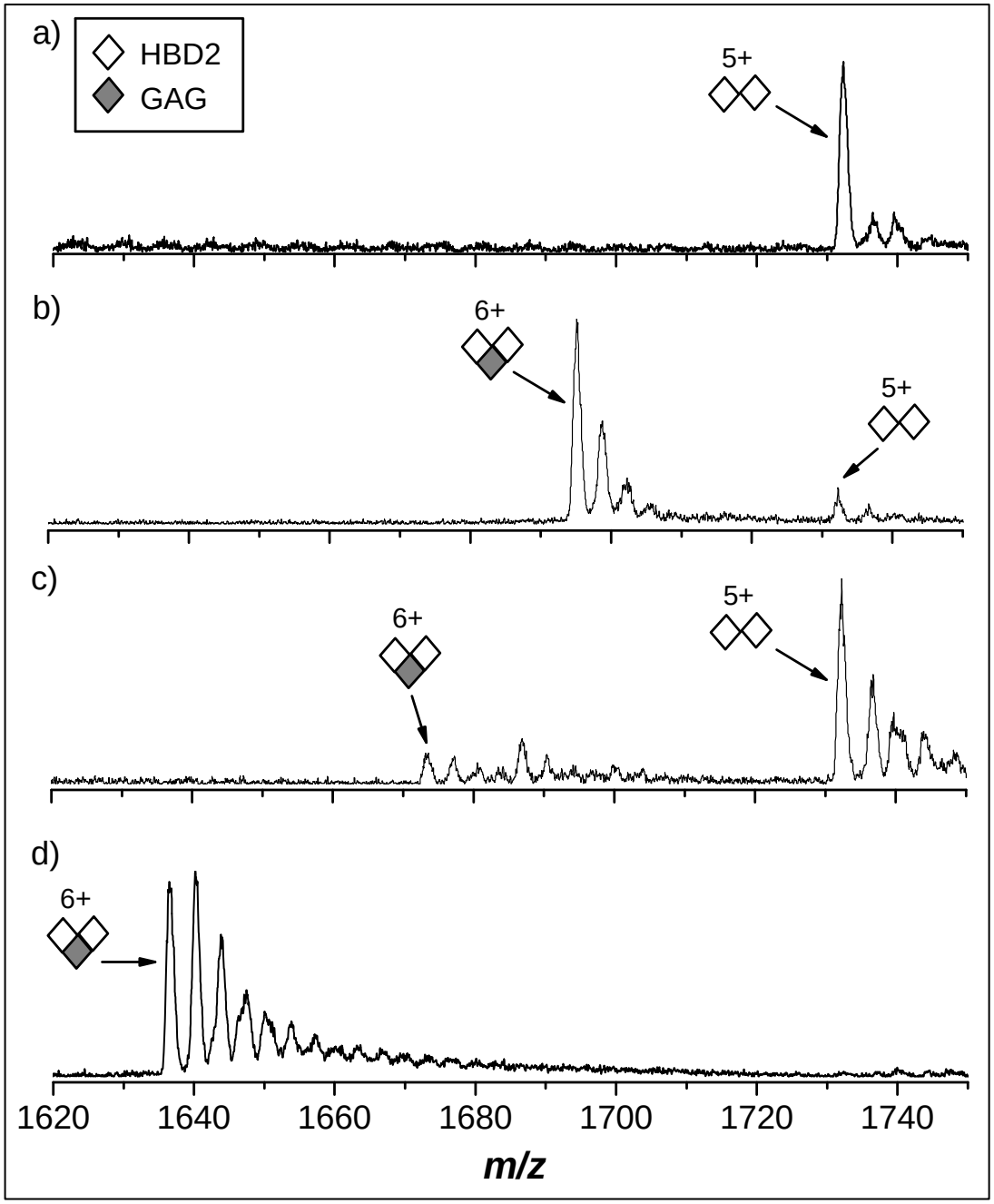

m/z 1620-1750 enlarged for mass spectra of: (a) HBD2 only; (b) HBD2 plus fondaparinux; (c) HBD2 plus dermatan sulfate dp6; (d) HBD2 plus heparin dp4. Unlabelled peaks correspond to sodium adducts of the preceding labeled species.

The electrospray ionisation of proteins is believed to proceed mainly according to the 'charged residue' model,[32] where the evaporation and fission of solvent droplets produces a desolvated analyte ion.[33] In droplets containing more than one molecule of interest, the analyte concentration is enriched.[34] Thus the electrospray process

may provide the elevated levels of peptide required to observe the HBD2 dimer. It is worth noting that dimeric species are not observed for several similar peptides studied by nESI-MS (see previous chapters).

Human β-defensin 2 plus glycosaminoglycan

Upon the addition of an equimolar amount of fondaparinux to HBD2, a complex composed of a peptide dimer plus one GAG molecule is observed (Figure 5.3b). On the Q-ToF II instrument, charge states $[M+5H]^{5+}$ to $[M+6H]^{6+}$ are observed for this species. The stoichiometry of the binding is very specific: only a dimer-GAG complex is observed, with no monomer-GAG complex detected. A small amount of unbound HBD2 dimer is evident in the spectrum, in addition to a large amount of free monomer. The recent work of Seo *et al.* supports the observation of a 2:1 HBD2:fondaparinux complex: the diffusion coefficient of the peptide-GAG complex, as determined by NMR spectroscopy, suggests that HBD2 exists mostly as a dimer in this form.[22]

The 2:1 stoichiometry of the peptide:GAG complex observed for HBD2 is common among many chemokines.[1] Thus this result represents further evidence of the ability of a β-defensin to behave like a chemokine. Leary and co-workers discovered that fondaparinux preferentially binds dimers of the chemokine CCL2 rather than monomers,[15] a finding that is consistent with the specific binding observed in this experiment.

The absence of any 1:1 HBD2:fondaparinux complex implies that in solution GAG binding occurs *after* formation of the defensin dimer. The intensity of the unbound HBD2 dimer in the spectrum is the same (1.3% of base peak intensity) before and after the addition of GAG. However there is significantly more dimer present in the spectrum, in the form of the GAG-bound complex, upon the addition of fondaparinux. Crystallography revealed the presence of a proline residue along the dimer interface of HBD2 that sterically prohibits extensive hydrogen bonding between the β-strands of the two monomer units.[19] Consequently, the HBD2 dimer is weakly held together and (presumably) can be easily disrupted. It would appear that electrostatic interactions between the very negatively-charged fondaparinux molecule and the highly cationic peptides stabilise the HBD2 dimer. Moreover, the

GAG may help to drive the formation of HBD2 dimer by bringing two monomers in close proximity (although, as stated above, GAG binding must occur after dimer formation). Presumably the original amount of unbound HBD2 dimer is then restored by a shift in the equilibrium between monomeric and dimeric peptide according to Le Châtelier's principle.

A 2:1 peptide:GAG complex is also detected when an equimolar amount of a different GAG, dermatan sulfate dp6, is added to a solution of HBD2. However this species is of much weaker intensity than the HBD2-fondaparinux complex (Figure 5.3c and enlarged, Figure 5.4c). Again, no 1:1 peptide-GAG binding is observed. The difference in HBD2 binding affinity between fondapariunx and dermatan sulfate hexasaccharide is likely due to the relative sulfation of the polysaccharides. Fondaparinux has a higher net charge (10-) than the hexasaccharide (6-) and so would be expected to interact more strongly with the positively charged β-defensin. Although fondaparinux is a synthetic polysaccharide, the preference of HBD2 to bind one GAG more strongly than another is of interest because of the potential role of GAGs in cell signalling.

In contrast, Seo *et al.* did not observe a 2:1 complex by NMR upon the addition of dermatan sulfate dp6 to HBD2: the diffusion coefficient is consistent with a monomeric peptide.[22] A possible explanation is that the diffusion coefficient is a weighted average of more than one species and the dimeric complex is of very low abundance relative to the monomeric peptide, as indicated by the mass spectrum.

Upon addition of a different GAG, heparin dp4, a 2:1 peptide:GAG complex is observed also (Figure 5.3d and Figure 5.4d). In addition, a 1:1 complex is evident at the $[M+4H]^{4+}$ charge state. Others have shown that the size and flexibility of the oligosaccharide are important to the nature of the chemokine-GAG interaction.[35] For example, a heparin octasaccharide was found to bind CCL2 dimers exclusively, whereas fondaparinux gave a mixture of dimer-GAG and monomer-GAG complexes.[36] The authors attribute this lack of selectivity to the pentasaccharide being of insufficient length to bridge the GAG binding sites of the CCL2 dimer.[35] In the experiments described here, both the pentasaccharide fondaparinux and the dermatan sulfate hexasaccharide exhibit good selectivity for the HBD2 dimer. As

HBD2 (41 residues) is somewhat smaller than CCL2 (76 amino acids), it appears that the pentasaccharide is long enough to span both monomer units in the case of HBD2 but not CCL2. In contrast, heparin dp4 binds HBD2 monomers and dimers. This lack of selectivity suggests that the tetrasaccharide is too short to bridge the GAG binding site of the HBD2 dimer.

In the only other mass spectrometry-based investigation of β-defensins and GAG interactions to date, McCullough *et al.* did not observe GAG-induced dimerisation for several murine β-defensins and related peptides.[20] In addition to differences in the peptides studied, the lack of oligomerisation is probably due to the small chain length of the heparin-derived disaccharide used.

In an attempt to quantify the dissociation constant of the GAG-bound dimer, other ratios of HBD2 to fondaparinux were studied: solutions at 2:1, 10:1 and 20:1 HBD2:GAG were prepared and analysed by mass spectrometry (Appendix 7). Unfortunately, it was not possible to determine the K_d of the HBD2-fondaparinux complex due to fluctuations in the abundance of the GAG-bound dimer with increasing saccharide concentration. Jansma *et al.* recently reported a similar effect, in which in they observed fluctuations in the NMR diffusion co-efficient of the chemokine CCL2 in an assay with a heparin octasaccharide.[37] With increasing amounts of GAG, they observed an initial increase in the oligomerisation state of CCL2 from monomer to dimer and then to tetramer. Upon the addition of further GAG, the tetramer reversed to dimer. Although no higher order oligomers (beyond dimer) were observed in this experiment, it would appear that the GAG-induced oligomerisation of HBD2 is a complicated process. It is possible that higher order oligomers of HBD2 do occur on this pathway in solution but are not amenable to detection by mass spectrometry (see study of HBD3, below).

Human β-defensin 3

The effect of different glycosaminoglycans has been discussed above: now a different peptide, human β-defensin 3, is considered. Shown below is the mass spectrum of HBD3 in 20 mM ammonium acetate in the absence of GAG (Figure 5.5a and enlarged, Figure 5.6a). As with HBD2, the spectrum of HBD3 shows two

charge state distributions: the most intense belonging to the monomer and the other relating to the dimer.

HBD3 was found to exist as a dimer in solution-phase studies at 360 μM.[4] In this experiment, at 135 μM, the HBD3 monomer is the major species in the mass spectrum. At this somewhat lower concentration, the equilibrium in solution between the monomer and dimer would be expected to shift slightly towards the dissociated peptide. In addition, although some intact dimer is still observed, it is possible that the non-covalent interactions between the HBD3 monomer units are not strong enough to preserve all of the dimer ions in the gas-phase. This is supported by comparison of the charge state distributions of the monomer and dimer. The highest charge state observed for the monomer is at $z = 6+$, whereas it is $z = 7+$ for the dimer.

Figure 5.5 Mass spectra of HBD3 in the absence and presence of glycosaminoglycan

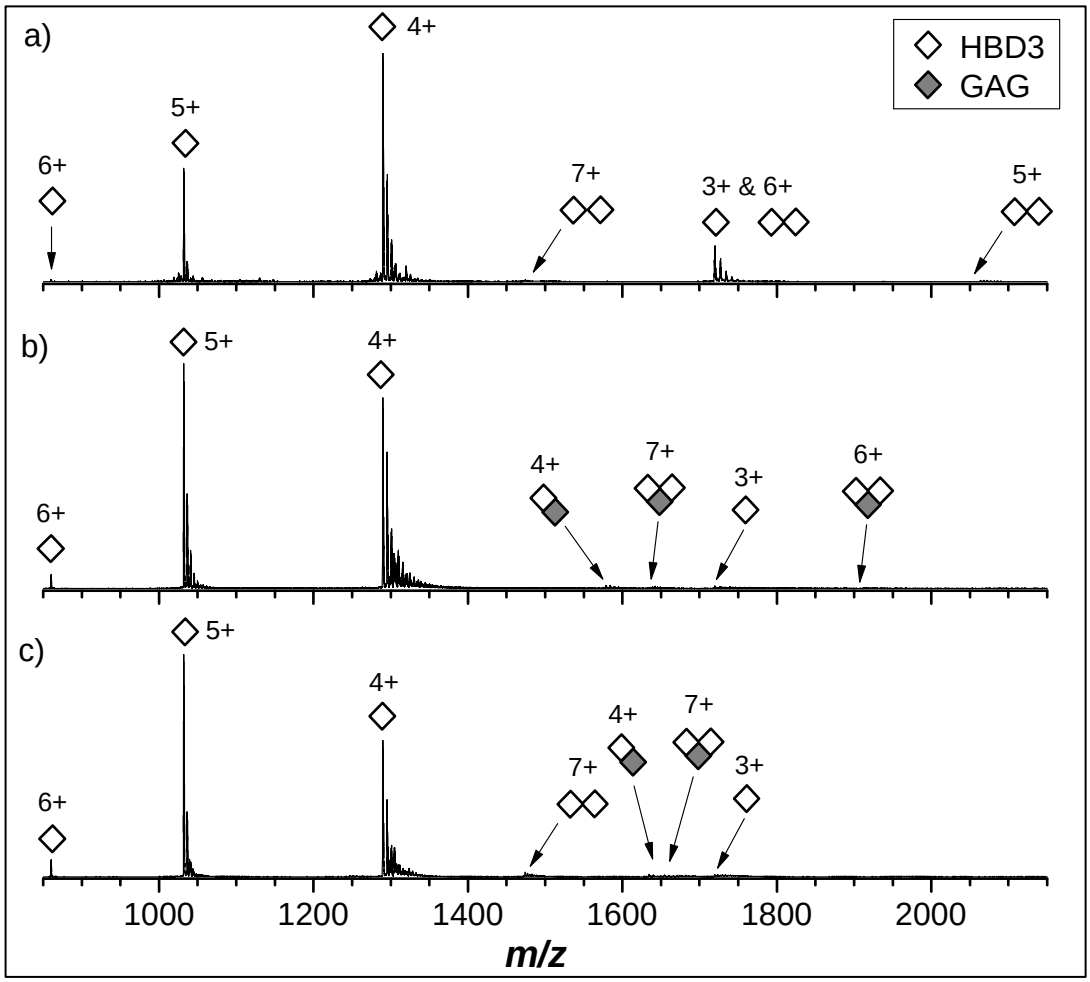

Mass spectra of: (a) HBD3 only; (b) HBD3 plus heparin dp4; (c) HBD2 plus dermatan sulfate dp6. GAGs present at 1:1 ratio in spectra (b) and (c). List of expected/observed masses given in Appendix 8.

Despite being double the mass of the monomer, the maximum number of protons carried by the dimer is just one greater. In part, this is due to the conformation of the peptides in solution: the dimer interface may obscure some basic residues that would otherwise readily accept a proton. Although the structure of the HBD3 dimer has yet to be solved, for comparison, only 18% of the HBD2 monomer unit is obscured upon forming a dimer.[19] Therefore this effect alone does not fully account for the relatively low charge carried by the HBD3 dimer. It is likely that those dimers that acquire a charge greater than $z = 7+$ in solution are overcome by Coulomb repulsion in the gas-phase and dissociate to monomers before they reach the detector.

Figure 5.6 Mass spectra of HBD3 in absence and presence of glycosaminoglycan, *m/z* region 1450 to 1700 enlarged

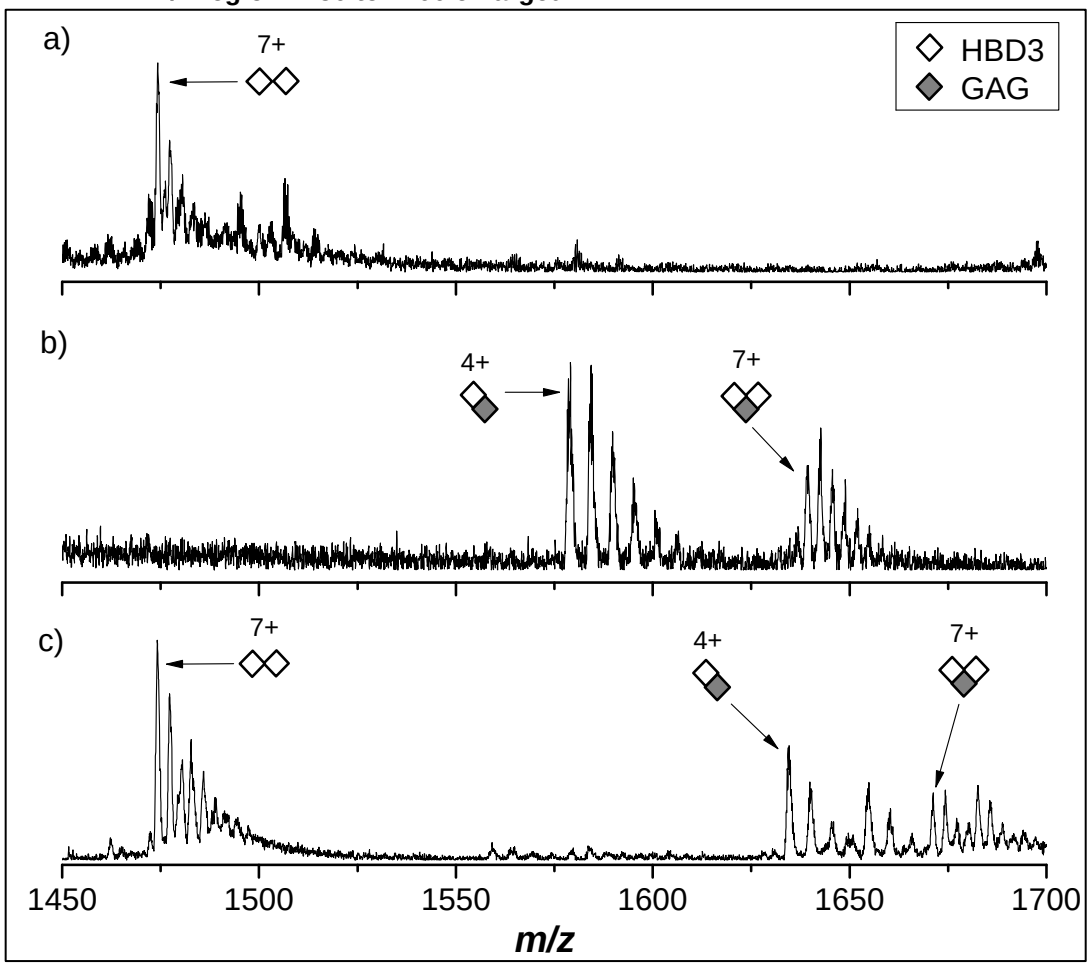

Mass spectra of: (a) HBD3 only; (b) HBD3 plus heparin dp4; (c) HBD2 plus dermatan sulfate dp6. GAGs present at 1:1 ratio in spectra (b) and (c).

Human β-defensin 3 plus glycosaminoglycan

Upon addition of an equimolar amount of fondaparinux to HBD3, a precipitate was observed to form in the nano-electrospray tip (Figure 5.7). No particulates were observed in the individual solutions of HBD3 or fondaparinux prior to mixing. This effect was reproducible and was observed upon the addition of heparin dp4 also (Appendix 9). The presence of insoluble matter in the spray solution resulted in clogging of the nano-electrospray tip and severely impeded ionisation of the sample.

Figure 5.7 Precipitation of HBD3 upon addition of fondaparinux

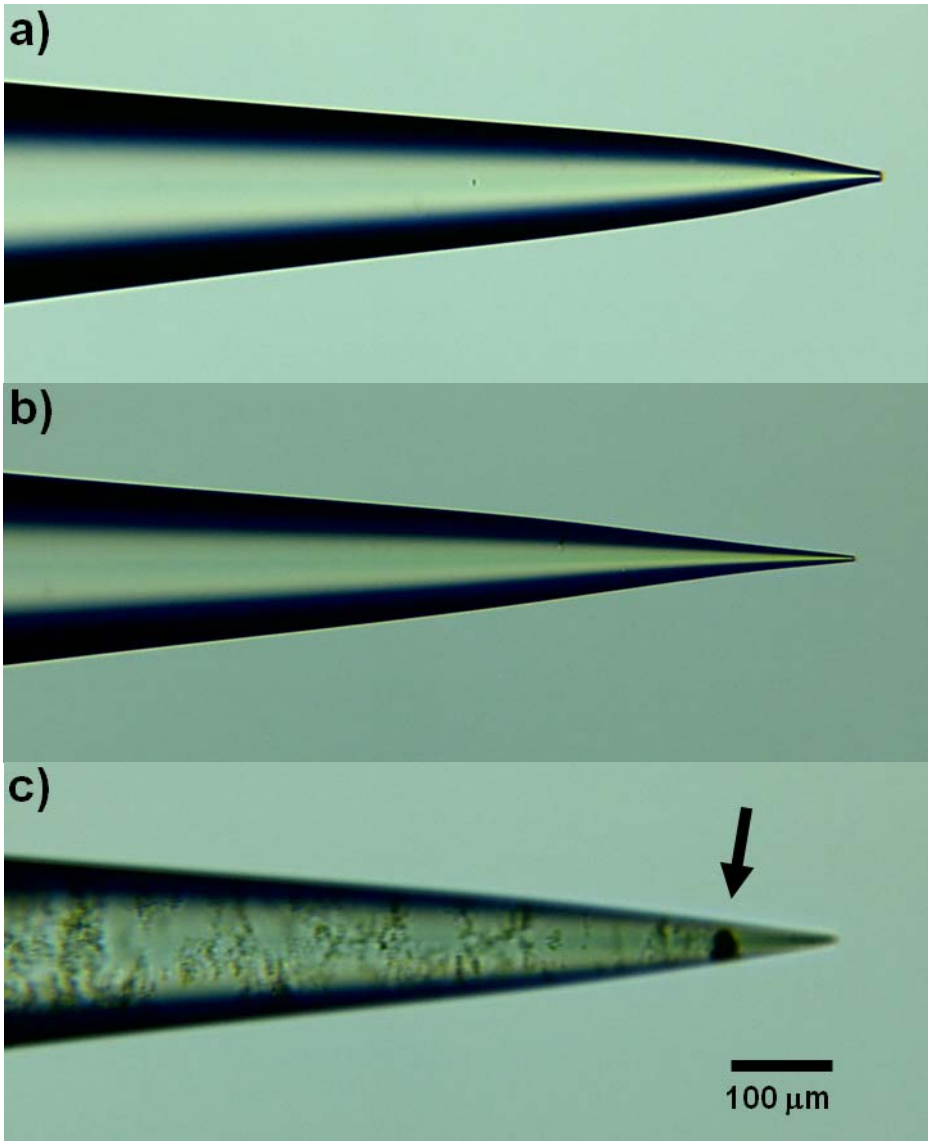

Photographs of nESI tips containing: (a) HBD3 only; (b) fondaparinux only; (c) HBD3 plus fondaparinux (1:1). The arrow indicates blockage of the capillary by a precipitate.

It was possible to obtain a steady spray by centrifuging the HBD3-GAG mixture and using only the supernatant for analysis. In the case of HBD3 plus fondaparinux, no protein or protein-GAG complex peaks were detected in the resultant mass spectrum (data not shown). For HBD3 plus heparin dp4, peaks corresponding to 1:1 and 2:1 peptide:GAG complexes were observed (Figure 5.5b and enlarged, 5.6b). No precipitation was observed upon the addition of dermatan sulfate dp6: this also formed both 1:1 and 2:1 peptide:GAG complexes. The observation of both 1:1 and 2:1 peptide GAG complexes indicates that heparin dp4 and dermatan sulfate dp6 do not bind either monomer or dimer selectively. This perhaps indicates that the distance between the two GAG binding sites is greater in the HBD3 dimer compared to the HBD2 dimer.

The observation of precipitate in the HBD3-fondaparinux solution could be attributable to higher order oligomers which, as insoluble aggregates, are not amenable to nESI mass spectrometry. This hypothesis is supported by the reports of others studying chemokine-GAG interactions: peptide precipitation upon the addition of GAGs can result in the attenuation of NMR signal and is believed to occur due to extensive oligomerisation of the peptide.[22, 37] It remains to be proven whether or not the monomer-GAG and dimer-GAG complexes observed by MS represent precursors to larger, insoluble oligomers in the aggregation process. Notably, GAGs also promote the formation of amyloid fibrils, which are insoluble protein aggregates.[38]

If this hypothesis is correct, it suggests that HBD3 binds fondaparinux most strongly (precipitates, no peptide observed in supernatant), followed by heparin dp4 (precipitates, some peptide in supernatant), then dermatan sulfate dp6 (no precipitation). Thus, the binding affinity increases with increasing sulfation of the GAG, as observed previously with HBD2. Work is currently underway to confirm the binding of GAGs to HBD3 by means of a gel mobility shift assay.

5.3.2 Ion mobility-mass spectrometry

Human β-defensin 2

The rotationally-averaged collision cross-sections measured for the HBD2 monomer, dimer and fondaparinux-bound complex are listed below (Table 5.1). As discussed

in previous chapters, the collision cross-section of each species increases with charge state as a result of increased Coulomb repulsion.[39, 40] It can be seen from the $[M+4H]^{4+}$ and $[M+5H]^{5+}$ charge states that the collision cross-sections of the unbound and GAG-bound HBD2 dimers are indistinguishable within experimental error. Thus it can be concluded that any change in peptide conformation that occurs upon binding the polysaccharide does not result in a drastic change in the overall size of the complex, implying that the HBD2 dimer contracts to accommodate the extra size of the GAG. When compared to the cross-sections of the monomer at the same charge state, both the free dimer and the GAG-bound complex are much more compact than might be expected. For example, the HBD2 dimer is only 20% larger than the monomer at the $[M+4H]^{4+}$ charge state. It would seem that the higher density of charge on the monomeric peptide results in greater gas-phase unfolding due to Coulomb repulsion.

Table 5.1 Mean collision cross-sections (Å^2) of HBD2 monomer, dimer and fondaparinux-bound complex

Charge state	HBD2 monomer	HBD2 dimer	HBD2 dimer + fondaparinux
$[M+3H]^{3+}$	598 ± 3	n.o.	n.o.
$[M+4H]^{4+}$	622 ± 4	760 ± 16	765 ± 10
$[M+5H]^{5+}$	675 ± 3	957 ± 6	919 ± 25
$[M+6H]^{6+}$	711 ± 11	n.o.	1072 ± 4
$[M+7H]^{7+}$	n.o.	n.o.	1142 ± 3

Errors are quoted as the standard error of the mean. Species marked n.o. were not observed in sufficient intensity to accurately determine collision cross-sections by IM-MS.

The collision cross-sections of HBD2 calculated from the PDB entries are shown in Table 5.2 and compared to experimental data in Figure 5.8. For the monomer, the cross-section of the lowest charge state observed by IM-MS is approximately 100 Å^2 smaller than that calculated for the NMR structure. As discussed previously, this more compact conformation results from a 'hydrophobic collapse' of the peptide structure upon transfer from solution to the gas-phase.[41] Thereafter, the peptide becomes more extended with increasing Coulomb repulsion, thus the $[M+6H]^{6+}$

charge state of HBD2 in the gas-phase has a collision cross-section similar to that of the monomer in solution.

Table 5.2 Collision cross-sections (Å^2) of HBD2 calculated from protein databank entries

	HDB2 monomer	HBD2 dimer
NMR spectroscopy	706	n/a
X-ray crystallography	717	1121

The above values were calculated using the trajectory method. The NMR value of the monomer is given as the mean collision cross-section of the twenty lowest energy structures in PDB 1FQQ. The crystallography values for the dimer and its monomer subunit were obtained from PDB 1FD3. NMR data for the HBD2 dimer is not available.

Figure 5.8 Collision cross-sections of HBD2: gas-phase data compared to calculated values from NMR and crystallography

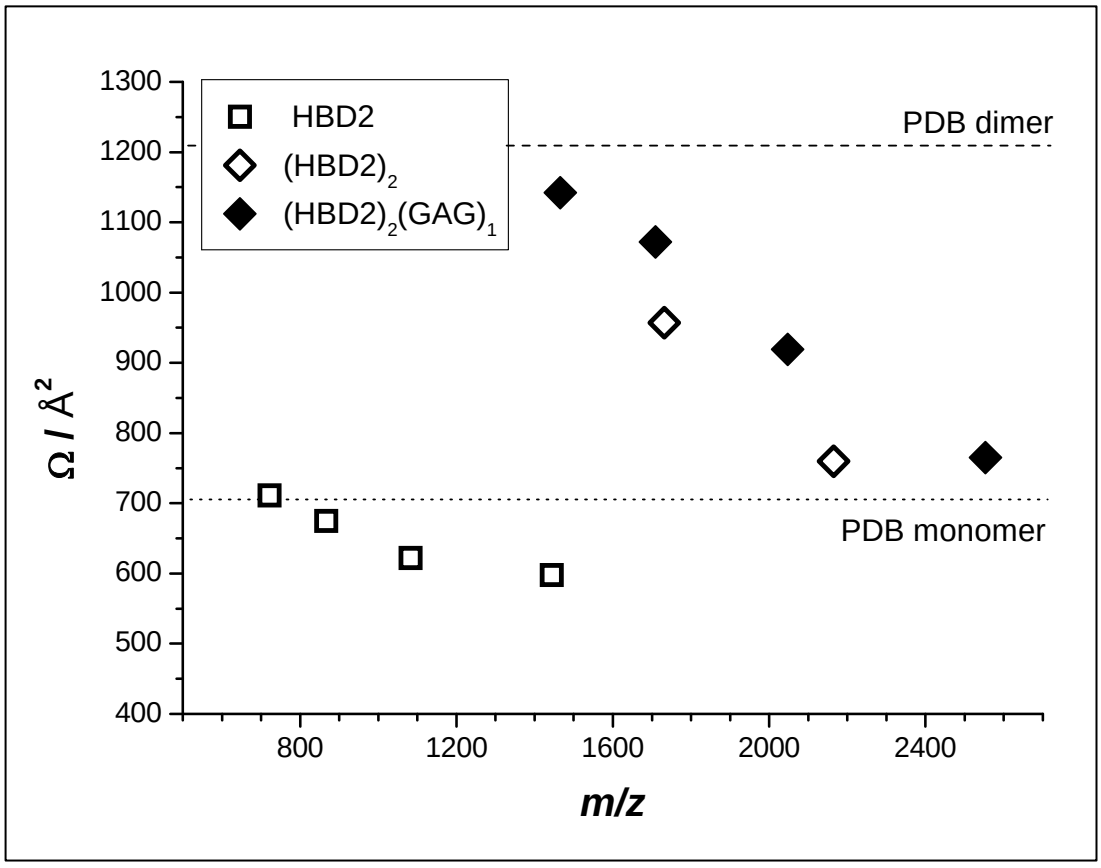

The dotted line indicates the mean collision cross-section calculated for the twenty lowest energy NMR structures of the HBD2 monomer. The dashed line indicates the collision cross-section calculated for the crystal structure of the HBD2 dimer. Experimental data are shown as squares or diamonds.

The gas-phase collapse of HBD2 is even more pronounced for the dimer, with the $[M+4H]^{4+}$ charge state being approximately 450 Å^2 more compact than the crystal form. It is striking that the lowest observed charge state of the HBD2 dimer is almost as compact as the monomer: there is only a 22% increase in size between monomer and dimer with $z = 4$. There are few documented examples of such a dramatic hydrophobic compression, although Faull *et al.* observed only a 15% difference in the collision cross-sections of cytochrome *c* monomer and dimer ions.[42]

Benesch *et al.* provide a relationship for estimating the collision cross-section of an ion, assuming a perfect sphere:[34]

{ 5.1 } $$\Omega = \pi\left(\sqrt[3]{\frac{3m}{4\pi\rho}} + r_g\right)^2$$

where Ω is the collision cross-section; m is mass; ρ is density (assumed to be 0.84 Da Å^{-3} for proteins) and r_g is the radius of the buffer gas (1.4 Å for helium). Using this relationship, the expected cross-section of the HBD2 monomer is 460 Å^2 and 700 Å^2 for the HBD2 dimer. Thus the measured cross-section of the HBD2 dimer is reasonable and consistent with a spherical shape of constant protein density. This gas-phase conformation must arise from the significant compression of two monomeric structures that are somewhat more extended than a theoretical sphere.

It was not possible to measure the cross-section of the HBD2-dermatan sulfate complex as a result of the very weak intensity of this species. With HBD2 in the presence of heparin dp4, only the $[M+4H]^{4+}$ charge state of the monomer-GAG complex and the $[M+6H]^{6+}$ charge state of the dimer-GAG complex were observed in sufficient abundance to allow measurement by IM-MS (Appendix 11). The cross-sections of these species are consistent with the measurements in Table 5.1.

Human β-defensin 3

As expected, the collision cross-sections of HBD3 (Table 5.3) are larger than those of HBD2 (Table 5.1), which is four amino acids shorter. The increase in size from $[M+3H]^{3+}$ to $[M+6H]^{6+}$ is similar (approximately 110 Å^2) for both HBD2 and HBD3 monomers. Comparison of the IM-MS data to the NMR structure of HBD3 (Ω =

883 Å^2), reveals once more that the peptide adopts a more compact geometry in the gas-phase (Figure 5.9).

Precipitation of the HBD3-fondaparinux complex prohibited analysis by IM-MS, whist it was not possible to measure the cross-sections of the HBD3-dermatan sulfate complexes on account of their low abundance. Only the $[M+5H]^{5+}$ charge state of the HBD3 monomer-heparin dp4 complex was observed in sufficient intensity for ion mobility measurements (Table 5.3). The cross-section of the GAG-bound monomer is slightly larger than the unbound monomer of the corresponding charge state (although within experimental uncertainty). This suggests that the defensin monomer may not contract as much as the dimer upon GAG binding.

Figure 5.9 Collision cross-sections of HBD3: gas-phase data compared to calculated values from NMR

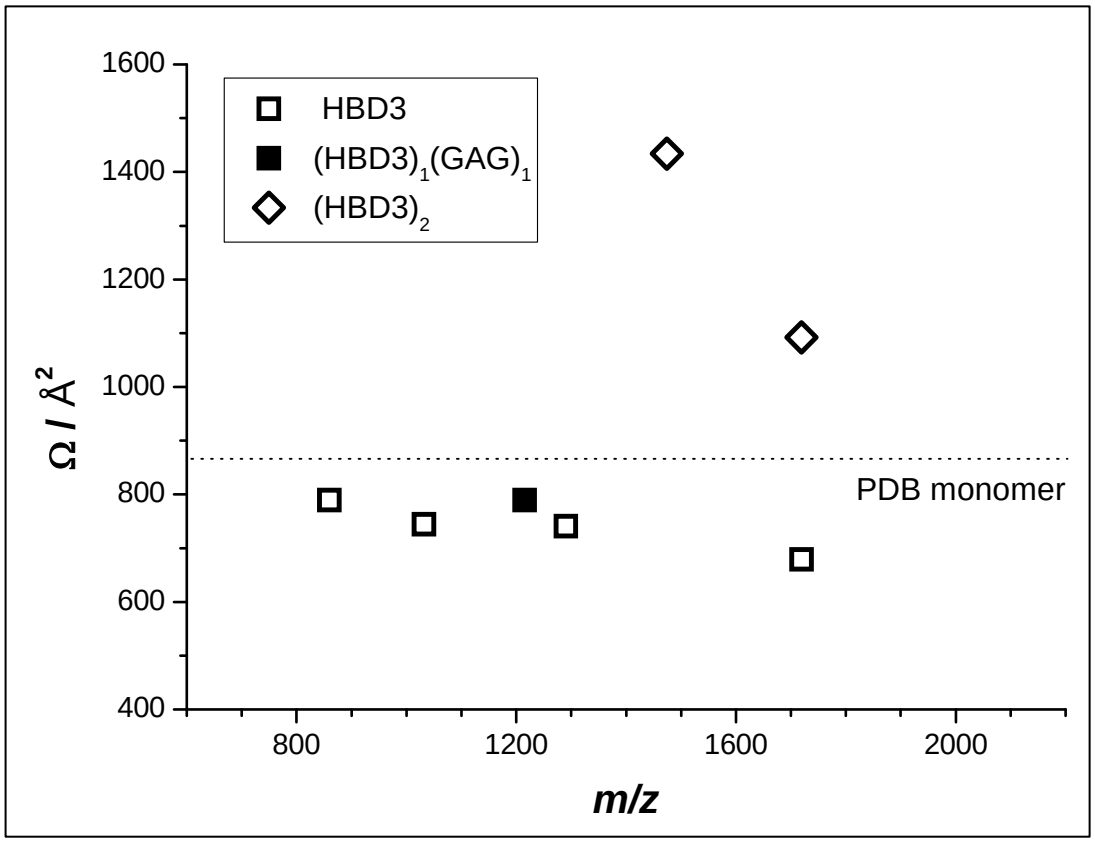

The above values were calculated using the trajectory method. The dotted line indicates the mean collision cross-section calculated for the twenty lowest energy NMR structures of the HBD3 monomer. No NMR or X-ray crystallography data is available for the HBD3 dimer.

Table 5.3 Collision cross-sections (Å^2) of HBD3 monomer and dimer

Charge state	HBD3 monomer	HBD3 monomer + heparin dp4	HBD3 dimer
$[M+3H]^{3+}$	679 ± 34	n.o.	n.o.
$[M+4H]^{4+}$	741 ± 37	n.o.	n.o.
$[M+5H]^{5+}$	745 ± 37	790 ± 40	n.o.
$[M+6H]^{6+}$	790 ± 40	n.o.	1092 ± 55
$[M+7H]^{7+}$	n.o.	n.o.	1434 ± 72

Species marked n.o. were not observed in sufficient intensity to accurately determine collision cross-sections by IM-MS. It was not possible to obtain replicate measurements for this data set: the experimental uncertainty is estimated at ± 5 %, based on the minimum precision of previous measurements.

5.3.3 Chemotaxis

It was observed that the presence or absence of fondaparinux did not significantly affect the chemotactic activity of HBD2 *in vitro* (Appendix 12). Thus, it can be concluded that fondaparinux does not inhibit the binding of HBD2 to CCR6 and so HBD2 must bind the GAG at a different site to that at which it interacts with the chemokine receptor.

For several proteins, GAG binding domains occur at 'BBXB' regions of the amino acid sequence (where 'B' denotes a basic residue and 'X' signifies a hydrophobic or other residue).[9] For example, the chemokine CCL5 binds heparin at a cluster of basic amino acids (RKNR) situated in the loop between the second and third β-strands.[43, 44] Inspection of the primary structure of HBD2 (Figure 5.10) reveals the presence of such a motif at residues 22-25 (RRYK). These amino acids are also located in the loop between two β-strands and may comprise the GAG binding domain of HBD2. The identification of this postulated binding site is supported by NMR data, which show the chemical shifts of these residues (and the C-terminal lysines at residues 39 and 40) change significantly upon GAG binding.[22] The 'BBXB' motif is not present in HBD3 and so it is difficult to predict the GAG binding site of this peptide. NMR spectroscopy and/or molecular modelling would be required to establish which residues are involved in GAG binding.

Figure 5.10 Primary structure of HBD2 and HBD3

HBD2:	GIGDPVTCLKSGAICHPVFCPRRYKQIGTCGLPGTKCCKKP
HBD3:	GIINTLQKYYCRVRGGRCAVLSCLPKEEQIGKCSTRGRKCCRRKK

Aligned amino acid sequences of HBD2 and HBD3. The 'BBXB' motif present in HBD2 is underlined.

5.4 Conclusions

β-defensins and chemokines have a number of structural features and functions in common. In this chapter the ability of β-defensins to form oligomers and to bind glycosaminoglycans has been demonstrated by mass spectrometry. Dimers of human β-defensins 2 and 3 were observed. For HBD2, the number of dimeric species was increased by the addition of GAG: a 2:1 peptide-GAG complex, commonly observed for chemokines, was formed in the presence of fondaparinux and dermatan sulfate. The specific stoichiometry of these complexes observed by mass spectrometry shed light on the mechanism of complex formation in solution. 1:1 and 2:1 HBD3-GAG complexes were also detected. In addition, the observation of precipitates may indicate that HBD3 forms higher order oligomers in the presence of some GAGs, although this could not be verified by mass spectrometry. Given that crystals are known to promote inflammation,[45] an extremely pro-inflammatory response could result if this precipitation was replicated *in vivo*.

The oligomerisation of β-defensins may be important *in vivo* for both chemotactic and antimicrobial activity. Whilst it is likely that the monomeric peptide interacts with the chemokine receptor to induce chemotaxis,[16] the oligomerisation of some chemokines is essential to their function *in vivo*.[10] By forming higher order oligomers, β-defensins may become more resistant to proteolytic enzymes.

As discussed in previous chapters, the mechanism by which β-defensins kill bacteria has yet to be fully resolved. Some antimicrobial peptides function by creating a pore in the bacterial membrane: this requires the formation of higher order oligomers.[46] Alternatively, β-defensins may act by disrupting the bacterial membrane in a 'carpet' mechanism,[47] or by passing through the membrane and then acting intracellularly.[48]

In either case, aggregation may enhance β-defensin activity by increasing the local peptide concentration.

The binding of GAGs to β-defensins also has implications for chemotactic and antimicrobial activity. It suggests that, like chemokines, β-defensins may attach to GAGs on the surfaces of cells so that a concentration gradient can be established *in vivo*. Immune cells would then be able to follow the increasing concentration of β-defensins to the appropriate site. Although no effect was observed in the *in vitro* assays described in this work, others have shown that the addition of GAGs can inhibit chemotaxis *in vivo*.[49] The GAG-binding site of chemokines can be blocked by binding the soluble GAG, thus preventing the chemokine from adhering to cell-surface GAGs. β-defensins are implicated in several inflammatory diseases, including psoriasis and mastitis.[50, 51] A possible therapeutic strategy could be to dampen the immune response by using a glycsoaminoglycan to antagonise the β-defensin.

Previous studies have shown that GAG-binding can negate the antimicrobial activity of defensins.[20, 21] Presumably this occurs as a result of the reduction of the defensin's positive charge, which weakens the electrostatic attraction of the cationic peptide to the negatively-charged lipopolysaccharide of the bacterial cell wall. Some bacteria have been reported to exploit this, enhancing their virulence by inducing the release of GAGs from host cells in order to counteract the antimicrobial peptides that form part of the host defense.[52]

In short, the interaction of β-defensins and GAGs have biological consequences. Here mass spectrometry and ion mobility mass spectrometry have been used to provide insights into these interactions. In addition, the substantial structural rearrangement of the HBD2 dimer observed by IM-MS represents further evidence of the possible collapse of peptide oligomers in the gas-phase.

5.5 References

1. S. J. Allen, S. E. Crown and T. M. Handel, *Annu. Rev. Immunol.*, 2007, **25**, 787-820.
2. E. J. Fernandez and E. Lolis, *Annu. Rev. Pharmacol. Toxicol.*, 2002, **42**, 469-499.
3. J. M. Perez-Canadillas, A. Zaballos, J. Gutierrez, R. Varona, F. Roncal, J. P. Albar, G. Marquez and M. Bruix, *J. Biol. Chem.*, 2001, **276**, 28372-28379.

4. D. J. Schibli, H. N. Hunter, V. Aseyev, T. D. Starner, J. M. Wiencek, P. B. McCray, B. F. Tack and H. J. Vogel, *J. Biol. Chem.*, 2002, **277**, 8279-8289.
5. D. Yang, O. Chertov, N. Bykovskaia, Q. Chen, M. J. Buffo, J. Shogan, M. Anderson, J. M. Schroder, J. M. Wang, O. M. Z. Howard and J. J. Oppenheim, *Science*, 1999, **286**, 525-528.
6. M. Baggiolini, *Nature*, 1998, **392**, 565-568.
7. M. Baba, T. Imai, M. Nishimura, M. Kakizaki, S. Takagi, K. Hieshima, H. Nomiyama and O. Yoshie, *J. Biol. Chem.*, 1997, **272**, 14893-14898.
8. Z. B. Wu, D. M. Hoover, D. Yang, C. Boulegue, F. Santamaria, J. J. Oppenheim, J. Lubkowski and W. Y. Lu, *Proc. Natl. Acad. Sci. U.S.A.*, 2003, **100**, 8880-8885.
9. H. Lortat-Jacob, *Curr. Opin. Struct. Biol.*, 2009, **19**, 543-548.
10. A. E. I. Proudfoot, T. M. Handel, Z. Johnson, E. K. Lau, P. LiWang, I. Clark-Lewis, F. Borlat, T. N. C. Wells and M. H. Kosco-Vilbois, *Proc. Natl. Acad. Sci. U.S.A.*, 2003, **100**, 1885-1890.
11. D. P. Witt and A. D. Lander, *Curr. Biol.*, 1994, **4**, 394-400.
12. T. M. Handel, Z. Johnson, S. E. Crown, E. K. Lau, M. Sweeney and A. E. Proudfoot, *Annu. Rev. Biochem.*, 2005, **74**, 385-410.
13. M. A. McCornack, D. M. Boren and P. J. LiWang, *Biochemistry*, 2004, **43**, 10090-10101.
14. S. E. Crown, Y. H. Yu, M. D. Sweeney, J. A. Leary and T. M. Handel, *J. Biol. Chem.*, 2006, **281**, 25438-25446.
15. M. R. Schenauer and J. A. Leary, *Int. J. Mass Spectrom.*, 2009, **287**, 70-76.
16. K. Rajarathnam, B. D. Sykes, C. M. Kay, B. Dewald, T. Geiser, M. Baggiolini and I. Clarklewis, *Science*, 1994, **264**, 90-92.
17. F. Bauer, K. Schweimer, E. Kluver, J. R. Conejo-Garcia, W. G. Forssmann, P. Rosch, K. Adermann and H. Sticht, *Protein Sci.*, 2001, **10**, 2470-2479.
18. M. V. Sawai, H. P. Jia, L. D. Liu, V. Aseyev, J. M. Wiencek, P. B. McCray, T. Ganz, W. R. Kearney and B. F. Tack, *Biochemistry*, 2001, **40**, 3810-3816.
19. D. M. Hoover, K. R. Rajashankar, R. Blumenthal, A. Puri, J. J. Oppenheim, O. Chertov and J. Lubkowski, *J. Biol. Chem.*, 2000, **275**, 32911-32918.
20. B. J. McCullough, J. M. Kalapothakis, W. Chin, K. Taylor, D. J. Clarke, H. Eastwood, D. Campopiano, D. MacMillan, J. Dorin and P. E. Barran, *Phys. Chem. Chem. Phys.*, 2010, **12**, 3589-3596.
21. A. Schmidtchen, I. M. Frick and L. Bjorck, *Mol. Microbiol.*, 2001, **39**, 708-713.
22. E. S. Seo, B. S. Blaum, T. Vargues, M. De Cecco, J. A. Deakin, M. Lyon, P. E. Barran, D. J. Campopiano and D. Uhrin, *Biochemistry*, 2010, **49**, 10486.
23. T. Vargues, G. J. Morrison, E. S. Seo, D. J. Clarke, H. L. Fielder, J. Bennani, U. Pathania, F. Kilanowski, J. R. Dorin, J. R. W. Govan, C. L. Mackay, D. Uhrin and D. J. Campopiano, *Protein Peptide Lett.*, 2009, **16**, 668-676.
24. R. V. Iozzo, *Annu. Rev. Biochem.*, 1998, **67**, 609-652.
25. J. M. Trowbridge and R. L. Gallo, *Glycobiology*, 2002, **12**, 117R-125R.
26. M. E. Selsted and A. J. Ouellette, *Nat. Immunol.*, 2005, **6**, 551-557.
27. M. Lyon, J. A. Deakin, D. Lietha, E. Gherardi and J. T. Gallagher, *J. Biol. Chem.*, 2004, **279**, 43560-43567.
28. B. J. McCullough, J. Kalapothakis, H. Eastwood, P. Kemper, D. MacMillan, K. Taylor, J. Dorin and P. E. Barran, *Anal. Chem.*, 2008, **80**, 6336-6344.
29. D. A. Case, T. A. Darden, T. E. Cheatham III, C. L. Simmerling, J. Wang, R. E. Duke, R. Luo, K. M. Merz, D. A. Pearlman, M. Crowley, R. C. Walker, W. Zhang, B. Wang, S. Hayik, A. Roitberg, G. Seabra, K. F. Wong, F. Paesani, X. Wu, S. Brozell, V. Tsui, H. Gohlke, L. Yang, C. Tan, J. Mongan, V. Hornak, G. Cui, P. Beroza, D. H. Mathews, C. Schafmeister, W. S. Ross and P. A. Kollman, *AMBER 9*, University of California, San Francisco, 2006.
30. M. F. Mesleh, J. M. Hunter, A. A. Shvartsburg, G. C. Schatz and M. F. Jarrold, *J. Phys. Chem.*, 1996, **100**, 16082-16086.
31. C. Tyrrell, M. De Cecco, N. L. Reynolds, F. Kilanowski, D. Campopiano, P. Barran, D. Macmillan and J. R. Dorin, *Molecular Immunology*, 2010, **47**, 1378-1382.
32. J. F. de la Mora, *Anal. Chim. Acta*, 2000, **406**, 93-104.
33. M. Dole, L. L. Mack and R. L. Hines, *J. Chem. Phys.*, 1968, **49**, 2240-&.

34. J. L. P. Benesch, B. T. Ruotolo, D. A. Simmons and C. V. Robinson, *Chem. Rev.*, 2007, **107**, 3544-3567.
35. Y. H. Yu, M. D. Sweeney, O. M. Saad, S. E. Crown, T. M. Handel and J. A. Leary, *J. Biol. Chem.*, 2005, **280**, 32200-32208.
36. Y. H. Yu, M. D. Sweeney, O. M. Saad and J. A. Leary, *J. Am. Soc. Mass Spectrom.*, 2006, **17**, 524-535.
37. A. L. Jansma, J. P. Kirkpatrick, A. R. Hsu, T. M. Handel and D. Nietlispach, *J. Biol. Chem.*, 2010, **285**, 14424-14437.
38. R. Kisilevsky and P. E. Fraser, *Crit. Rev. Biochem. Mol. Biol.*, 1997, **32**, 361-404.
39. S. J. Valentine, J. G. Anderson, A. D. Ellington and D. E. Clemmer, *J. Phys. Chem. B*, 1997, **101**, 3891-3900.
40. D. E. Clemmer and M. F. Jarrold, *J. Mass Spectrom.*, 1997, **32**, 577-592.
41. E. Jurneczko and P. E. Barran, *Analyst*, 2011, **136**, 20-28.
42. P. A. Faull, K. E. Korkeila, J. M. Kalapothakis, A. Gray, B. J. McCullough and P. E. Barran, *Int. J. Mass Spectrom.*, 2009, **283**, 140-148.
43. A. E. I. Proudfoot, S. Fritchley, F. d. r. Borlat, J. P. Shaw, F. Vilbois, C. Zwahlen, A. Trkola, D. Marchant, P. R. Clapham and T. N. C. Wells, *J. Biol. Chem.*, 2001, **276**, 10620-10626.
44. H. Lortat-Jacob, A. Grosdidier and A. Imberty, *Proc. Natl. Acad. Sci. U.S.A.*, 2002, **99**, 1229-1234.
45. P. Platt and W. C. Dick, *Ann. Rheum. Dis.*, 1983, **42**, 4-7.
46. W. C. Wimley, M. E. Selsted and S. H. White, *Protein Sci.*, 1994, **3**, 1362-1373.
47. Y. Shai, *Biochim. Biophys. Acta*, 1999, **1462**, 55-70.
48. V. Sass, U. Pag, A. Tossi, G. Bierbaum and H. G. Sahl, *Int. J. Med. Microbiol.*, 2008, **298**, 619-633.
49. Z. Johnson, M. H. Kosco-Vilbois, S. Herren, R. Cirillo, V. Muzio, P. Zaratin, M. Carbonatto, M. Mack, A. Smailbegovic, M. Rose, R. Lever, C. Page, T. N. C. Wells and A. E. I. Proudfoot, *J. Immunol.*, 2004, **173**, 5776-5785.
50. J. Harder and J. M. Schroder, *J. Leukocyte Biol.*, 2005, **77**, 476-486.
51. L. Liu, L. N. Wang, H. P. Jia, C. Q. Zhao, H. H. Q. Heng, B. C. Schutte, P. B. McCray and T. Ganz, *Gene*, 1998, **222**, 237-244.
52. F. D. Menozzi, K. Pethe, P. Bifani, F. Soncin, M. J. Brennan and C. Locht, *Mol. Microbiol.*, 2002, **43**, 1379-1386.

6 Conclusions and outlook

As bacteria continue to find new ways to evade antibiotics,[1] so too must the human race find new ways to overcome bacteria. Drugs based on β-defensins and other antimicrobial peptides could form part of our arsenal against infection in future. With a defensin derivative currently in preclinical development,[2] that future may not be too far away. A more thorough understanding of how the activities of β-defensins are related to their structures will lead to a more informed search for other clinically useful antimicrobial peptides. This thesis attempts to explain the variation in biological activities observed for a range of β-defensin analogues using biophysical techniques.

Previous work revealed that a cysteine near the C-terminus of the murine defensin Defb14 was crucial to its chemotactic activity.[3] In this thesis, ion mobility-mass spectrometry was used to evaluate the unfolding behaviour of the peptide upon chemical modification of this residue. In cases where modification was deleterious to biological activity, an expansion in gas-phase structure was observed under denaturing conditions. This suggests that the altering cysteine residue affects the overall conformational preferences of the peptide.

At the N-terminus of this peptide, mutation of the second amino acid (leucine) affected the chemotactic activity but IM-MS revealed no significant changes in tertiary structure. Taken together with the results described above, it is proposed here that the C-terminal cysteine orientates the peptide so that the N-terminal leucine can interact directly with the receptor.

Analysis of a series of N-terminal truncations revealed that antimicrobial activity was diminished upon the deletion of more than eleven amino acids from Defb14-1Cys^{V}. Using reversed-phase HPLC it was established that this variation in activity did not correlate with a change in hydrophobicity and so it is likely that a balance between both charge and hydrophobicity is required. Furthermore, CD spectroscopy revealed that the removal of amino acids from the N-terminus resulted in a decrease in the propensity of the peptide to form an α-helix. To determine if this affects the peptide's ability to kill bacteria, it would be interesting to investigate the mechanism

of antimicrobial action. It would be possible to establish if the peptide forms pores in bacterial membrane by monitoring the electrical conductivity of membrane bilayers or measuring the permeabilisation of fluorescent dyes.[4]

The ability of β-defensins to bind GAGs could be essential for their chemotactic activity *in vivo*. In the final chapter of this thesis, the interaction of human β-defensins 2 and 3 with glycosaminoglycans was studied. Oligomerisation of both HBD2 and HBD3 in the presence of GAG was observed by MS. Of particular interest was the identification of a 2:1 defensin-GAG complex that is characteristic of chemokines. By establishing the stoichiometry of this complex, mass spectrometry was used to elucidate the mechanism of binding in solution. In addition, by measuring the differences in intensities of defensin-GAG complexes in the mass spectrum, the relative affinity of various GAGs for defensins could be assessed.

This research exploited the three main advantages of mass spectrometry for studying peptides: sensitivity, speed and specificity. The sensitivity and speed of the technique made the synthesis and analysis of a large number of modified peptides feasible. By studying a range of different mutations in various regions of the molecule, it was possible to assess the structure-activity relationships of Defb14. The specificity of MS allowed for the unambiguous characterisation of defensin-GAG complexes on the basis of their mass. By combining mass spectrometry with ion mobility mass spectrometry, information on the tertiary structure of the peptides was obtained.

The disadvantage of ion mobility spectrometry is that it is intrinsically a low-resolution technique, providing only a measure of the overall size of an ion. In this thesis it is hypothesised that GAGs bind to HBD2 *via* a 'BBXB' motif: to verify this experimentally, other methods of analysis would be required. Another concern is the extent to which a gas-phase conformation resembles the structure of a peptide in solution. Since defensins interact with either a bacterial membrane or a cell receptor, it may be helpful to create a 'membrane-like' environment prior to ionisation by using surfactants. This approach has been used to great success by the group of Robinson for the analysis of membrane-bound proteins by mass spectrometry.[5]

In conclusion, the work presented in this thesis elucidates structure-activity relationships for the peptide Defb14 and provides new insights into the structural and functional overlap between β-defensins and chemokines. Yet, since every peptide and every organism behaves differently, the relationship between the structure and activity of antimicrobial peptides is complex and much more research is required before this is fully understood.

References

1. J. D. D. Pitout, *Lancet Infect. Dis.*, 2010, **10**, 578-579.
2. P. H. Mygind, R. L. Fischer, K. M. Schnorr, M. T. Hansen, C. P. Sonksen, S. Ludvigsen, D. Raventos, S. Buskov, B. Christensen, L. De Maria, O. Taboureau, D. Yaver, S. G. Elvig-Jorgensen, M. V. Sorensen, B. E. Christensen, S. Kjaerulff, N. Frimodt-Moller, R. I. Lehrer, M. Zasloff and H. H. Kristensen, *Nature*, 2005, **437**, 975-980.
3. K. Taylor, D. J. Clarke, B. McCullough, W. Chin, E. Seo, D. Yang, J. Oppenheim, D. Uhrin, J. R. W. Govan, D. J. Campopiano, D. MacMillan, P. Barran and J. R. Dorin, *J. Biol. Chem.*, 2008, **283**, 6631-6639.
4. K. A. Brogden, *Nat. Rev. Microbiol.*, 2005, **3**, 238-250.
5. N. P. Barrera, N. Di Bartolo, P. J. Booth and C. V. Robinson, *Science*, 2008, **321**, 243-246.

Appendices

Appendix 1 Collision cross-sections (Å^2) of Defb14, Defb14-1Cys^V and Defb14-0Cys under denaturing conditions

	Defb14	Defb14-1Cys^V	Defb14-0Cys
$[M+3H]^{3+}$	n.o.	n.o.	n.o.
$[M+4H]^{4+}$	709	n.o.	n.o.
$[M+5H]^{5+}$	751	916	n.o.
$[M+6H]^{6+}$	881	962	979
$[M+7H]^{7+}$	1008	1018	1070
$[M+8H]^{8+}$	n.o.	1105	1170
$[M+9H]^{9+}$	n.o.	n.o.	n.o.

Species marked n.o. were not observed from IM-MS.

*The above data is taken from: B. J. McCullough, J. Kalapothakis, H. Eastwood, P. Kemper, D. MacMillan, K. Taylor, J. Dorin and P. E. Barran, Anal. Chem., 2008, **80**, 6336-6344.*

Appendix 2 Collision cross-sections (Å^2) of Defb14, Defb14-1Cys^V and Defb14-0Cys under buffered conditions

	Defb14	Defb14-1Cys^V	Defb14-0Cys
$[M+3H]^{3+}$	-	n.o.	659 ± 3
$[M+4H]^{4+}$	-	740 ± 12	798 ± 9
$[M+5H]^{5+}$	-	888 ± 23	1008 ± 7
$[M+6H]^{6+}$	-	986 ± 19	1076 ± 15
$[M+7H]^{7+}$	-	1053 ± 15	1086 ± 11
$[M+8H]^{8+}$	-	1125 ± 15	1116 ± 7
$[M+9H]^{9+}$	-	1216 ± 9	1185 ± 2

Cross-sections of Defb14 were not determined. Species marked n.o. were not observed by IM-MS.

Appendix 3 HPLC retention times of Defb14-1Cys^{V} and N-terminal truncations, relative to melittin

	Monomer	Dimer
Defb14-1Cys^{V}	0.630	0.705
Δ(1-2)	0.639	0.728
Δ(1-5)	0.633	0.719
Δ(1-8)	0.599	0.688
Δ(1-11)	0.377	0.459
Δ(1-14)	0.407	0.493
Δ(1-17)	0.500	0.627

Increasing relative retention time indicates increasing hydrophobicity.

Appendix 4 Wimley White scores hydrophobicity scores for Defb14-1Cys^{V} and N-terminal truncations

	Monomer	Dimer
Defb14-1Cys^{V}	-13.56	-27.12
Δ(1-2)	-15.25	-30.50
Δ(1-5)	-13.67	-27.34
Δ(1-8)	-12.43	-24.86
Δ(1-11)	-14.52	-29.04
Δ(1-14)	-13.21	-26.42
Δ(1-17)	-12.38	-24.76

A less negative score indicates increasing hydrophobicity.

Using the scale described in: W. C. Wimley and S. H. White, *Nat. Struct. Biol.*, 1996, **3**, 842-848.

Appendix 5 CDSSTR analysis of Deb14-1Cys^{V}, N-terminal truncation and N-terminal substitution peptides

All of the peptides analysed contained the following secondary structural elements in 10 mM ammonium acetate buffer.

	Basis set 4	Basis set 7
Helix (%)	7 ± 1	4 ± 1
Strand (%)	35 ± 2	30 ± 2
Turn (%)	23 ± 1	16 ± 1
Unordered (%)	33 ± 1	49 ± 2

Analysis was performed using two different basis sets: basis set 7 includes denatured proteins and so gives a higher estimate of unordered structure. The algorithm is only applicable to peptides/proteins in aqueous solution and so analysis was not performed for the peptides in 50% water, 50% trifluoroethanol.

Appendix 6 Expected/observed masses of HBD2-GAG complexes

Spectrum	Species	Expected mass (Da)	Observed mass (Da)
(a)	HBD2 monomer	4328.23	4328.21
	HBD2 dimer	8656.46	8656.30
(b)	HBD2 monomer	4328.23	4328.16
	HBD2 dimer	8656.46	8656.20
	HBD2 dimer + fondaparinux	10164.65	10164.84
(c)	HBD2 monomer	4328.23	4328.10
	HBD2 dimer	8656.46	8656.38
	HBD2 dimer + DS dp 6	10034.60	10034.70
(d)	HBD2 monomer	4328.23	4329.09
	HBD2 monomer + heparin dp4	5483.17	5484.40
	HBD2 dimer	8656.46	8656.84
	HBD2 dimer + heparin dp4	9811.40	9813.75

The expected masses of fully de-salted, protonated GAGs are: fondaparinux 1508.19; dermatan sulfate dp6 1378.14; heparin dp4 1154.94.

Observed masses were obtained by deconvolution of the corresponding charge states in the ESI mass spectra using the transform algorithm in MassLynx v4.1 (Waters).

All masses are quoted as the average molecular weight.

Appendix 7 HBD2 plus fondaparinux at various ratios

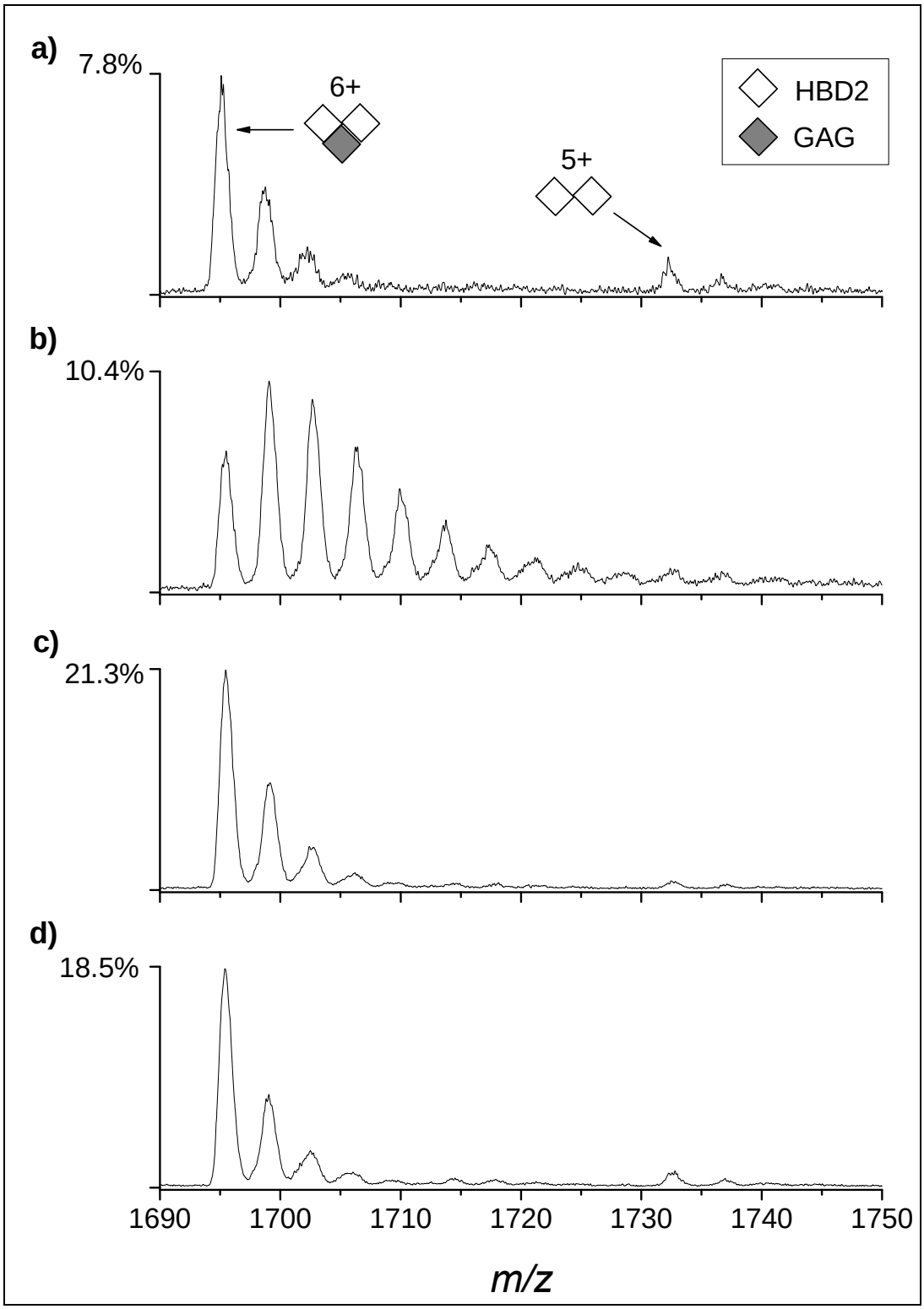

Ratios of HBD2 to fondaparinux: (a) 1:1; (b) 2:1; (c) 10:1; (d) 20:1 HBD2:GAG. The number given on the y-axis corresponds to the relative intensity of the $[M+6H]^{6+}$ complex peak, with respect to the most intense peak in the spectrum (the $[M+4H]^{4+}$ HBD2 monomer).

Appendix 8 Expected/observed masses of HBD3-GAG complexes

Spectrum	Species	Expected mass (Da)	Observed mass (Da)
(a)	HBD3 monomer	5155.19	5155.39
	HBD3 dimer	10310.38	10310.93
(b)	HBD3 monomer	5155.19	5155.82
	HBD3 monomer + heparin dp4	6310.13	6311.33
	HBD3 dimer	10310.38	10312.06
	HBD3 dimer + heparin dp4	11465.32	11467.46
(c)	HBD3 monomer	5155.19	5155.75
	HBD3 monomer + DS dp 6	6533.33	6534.31
	HBD3 dimer	10310.38	10312.21
	HBD3 dimer + DS dp 6	11688.52	11691.37

The expected masses of fully de-salted, protonated GAGs are: heparin dp4 1154.94; dermatan sulfate dp6 1378.14.

Observed masses were obtained by deconvolution of the corresponding charge states in the ESI mass spectra using the transform algorithm in MassLynx v4.1 (Waters).

All masses are quoted as the average molecular weight.

Appendix 9 Precipitation of HBD3 in the presence of heparin dp4

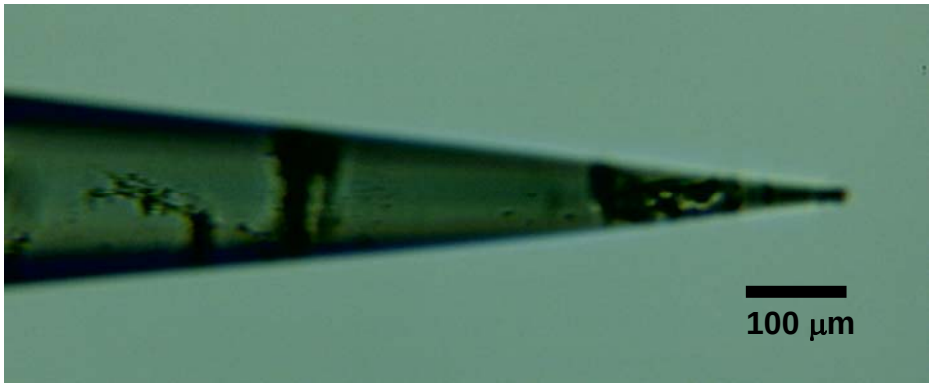

Photograph of nESI tip containing HBD3 plus heparin dp4 at 1:1 ratio (135 μM).

Appendix 10 Mass spectrum of HBD2 in presence and absence of fondaparinux, acquired on the MoQToF instrument

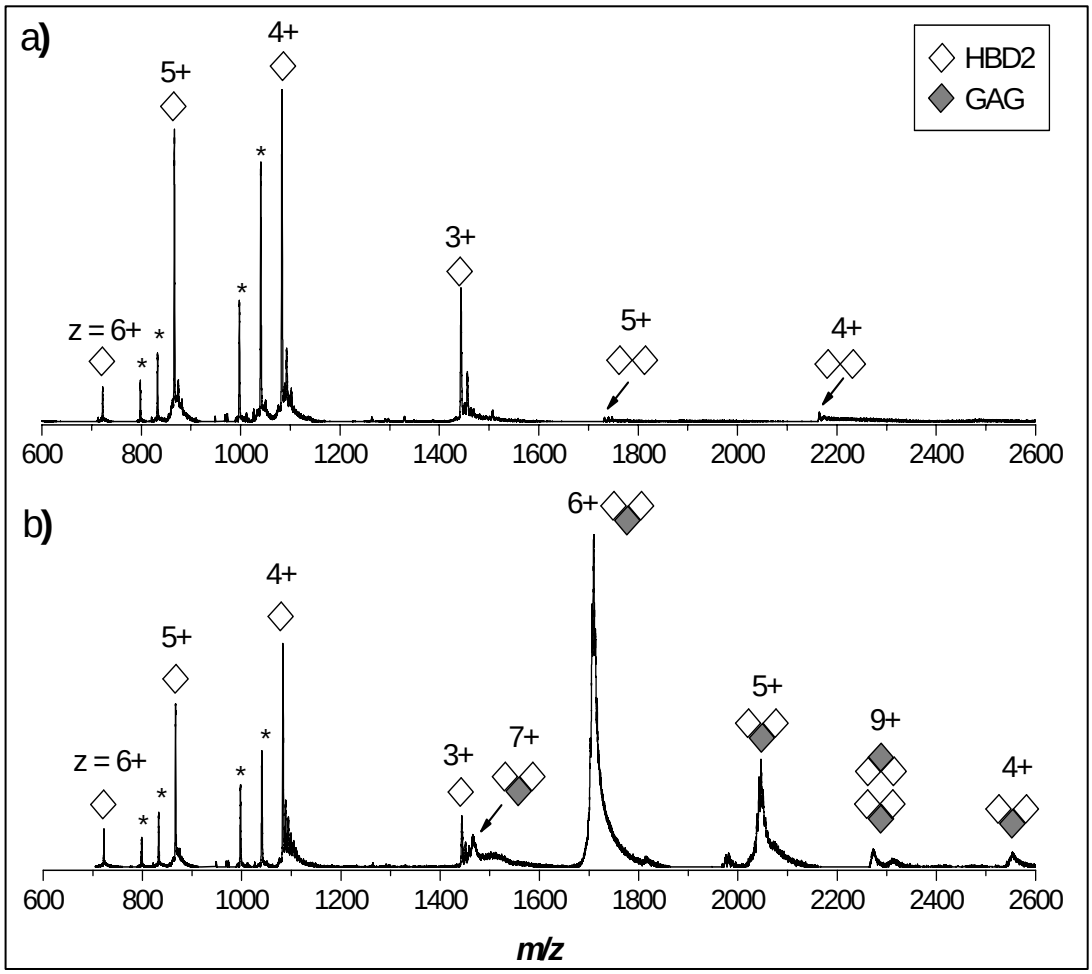

Mass spectra of: (a) HBD2 only; (b) HBD2 plus fondaparinux at 1:1 ratio. Peaks marked with an asterisk (*) correspond to peptide fragments formed in source. Note the elevated levels of the 2:1 HBD2:GAG complex. A tetrameric (4:2) HBD2:GAG complex is also observed. The collision cross-section of the 4:2 complex was measured as 1654 ± 34 Å^2.

Appendix 11 Collision cross-sections (Å^2) of HBD2 complexes with heparin dp4

Charge state	HBD2 monomer + heparin dp4	HBD2 dimer + heparin dp4
$[M+4H]^{4+}$	654 ± 33	n.o.
$[M+5H]^{5+}$	n.o.	n.o.
$[M+6H]^{6+}$	n.o.	1022 ± 51

Species marked n.o. were not observed in sufficient intensity to accurately determine collision cross-sections by IM-MS. It was not possible to obtain replicate measurements for this data set: the experimental uncertainty is estimated at ± 5 %, based on the minimum precision of previous measurements.

Appendix 12 ***In vitro*** **chemotactic activity of HBD2 in absence and presence of fondaparinux**

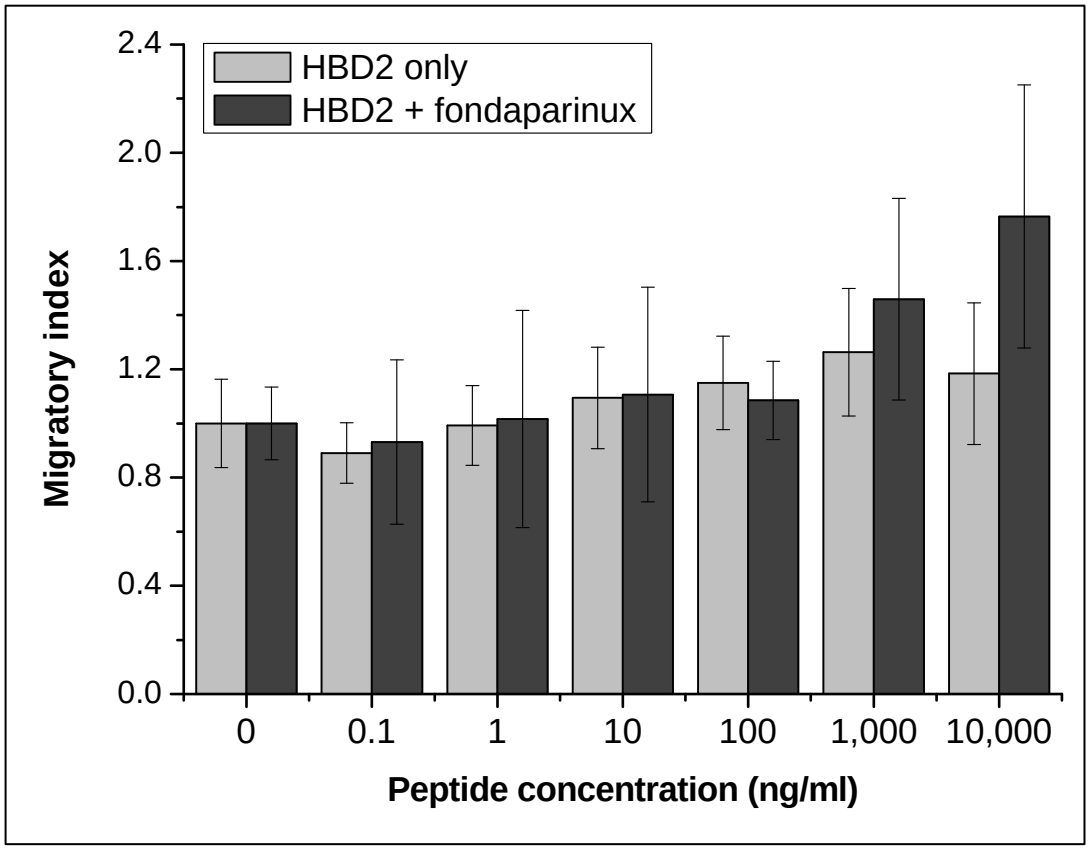

The migratory index (ratio of the number of cells per high power field with peptide to number of cells media alone) is quoted as the mean ± the standard deviation. In all cases the migratory index of the HBD2 in the presence and absence of fondaparinux is the same within experimental uncertainty.

Appendix 13 Publications arising from this thesis

'Conformational preferences of linear β-defensins are revealed by ion mobility-mass spectrometry'

M. De Cecco, E. S. Seo, D. J. Clarke, B. J. McCullough, K. Taylor, D Macmillan, J. R. Dorin, D. J. Campopiano and P. E. Barran, *J. Phys. Chem. B*, 2010, **114**, 2312.

'Isoleucine/leucine-2 is essential for chemoattractant activity of β-defensin Defb14 through chemokine receptor 6'

C. Tyrrell, M. De Cecco, N. L. Reynolds, F. Kilanowski, D. Campopiano, P. Barran, D. Macmillan and J. R. Dorin, *Mol. Immunol.*, 2010, **47**, 1378.

'Peptide fragments of a β-defensin derivative with potent bactericidal activity'

N. L. Reynolds, M. De Cecco, K. Taylor, C. Stanton, F. Kilanowski, J. Kalapothakis, E. Seo, D. Uhrin, D. Campopiano, J. Govan, D. Macmillan, P. Barran and J. R. Dorin, *Antimicrob. Agents Chemother.*, 2010, **54**, 1922.

'Interaction of human β-defensin 2 (HBD2) with glycosaminoglycans'

E. S. Seo, B. S. Blaum, T. Vargues, M. De Cecco, J. A. Deakin, M. Lyon, P. E. Barran, D. J. Campopiano and D. Uhrin, *Biochemistry*, 2010, **49**, 10486.